JOURNAL OF APPLIED PHYSICS

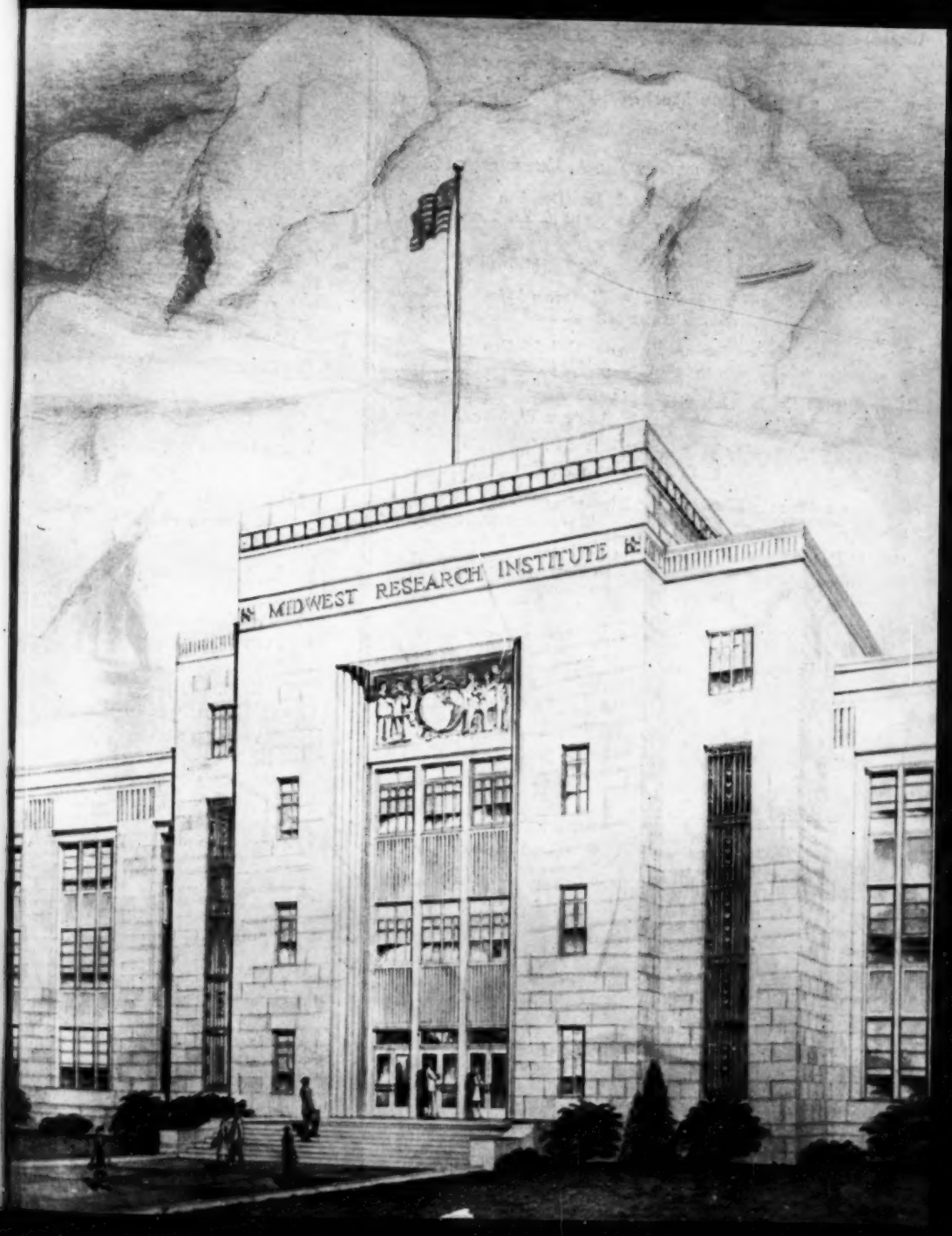

JOURNAL OF APPLIED PHYSICS

Vol. 17, No. 8 AUGUST, 1946

In This Issue

Page

Oxide Coated Cathode Literature, 1940–1945 JOHN P. BLEWETT 643

Pulsed Properties of Oxide Cathodes EDWARD A. COOMES 647

Study of Oxide Cathodes by X-Ray Diffraction Methods. Part II. Oxide Coating Composition A. EISENSTEIN 654

Studies of the Interface of Oxide Coated Cathodes A. FINEMAN AND A. EISENSTEIN 663

Midwest Research Institute—A New Scientific Research Institution GEORGE E. ZIEGLER 669

Contributed Original Research

Method for Preparing Rubber Latex Specimens for the Electron Microscope R. H. KELSEY AND E. E. HANSON 675

Perturbation Theory of the Normal Modes for an Exponential *M*-Curve in Non-Standard Propagation of Microwaves C. L. PEKERIS 678

Stresses in Cylindrical Glass-Metal Seals with Glass Inside ALBERT W. HULL 685

Particle Size Determination from X-Ray Line Broadening L. S. BIRKS AND H. FRIEDMAN 687

Effect of Hydrostatic Pressure on Plastic Flow under Shearing Stress P. W. BRIDGMAN 692

Hysteresis and Related Elastic Properties of Tire Cords HELMUT WAKEHAM AND EDITH HONOLD 698

Letters to the Editor:

On the "Power Function" FIDEL ALSINA FUERTES 712

In Every Issue

Here and There 673

Calendar of Meetings 674

Index to Advertisers xxvi

BOARD OF EDITORS

ELMER HUTCHISSON, *Editor*

Associate Editors

R. BOWLING BARNES
OTTO BEECK
W. F. BUSSE
S. H. CALDWELL
CLARK GOODMAN
SELIG HECHT
W. JAMES LYONS
PAUL E. SABINE
FREDERICK SEITZ
J. R. TOWNSEND

Publication of the American Institute of Physics

ADMINISTRATIVE STAFF

HENRY A. BARTON, *Director*

MARGARET S. GRIFFIN *Publications Manager*

THEODORE VORBURGER, *Business Manager*

JOHN T. TATE, *Adviser on Publications*

GOVERNING BOARD

PAUL E. KLOPSTEG, *Chairman*

WALLACE WATERFALL, *Secretary*

GEORGE B. PEGRAM, *Treasurer*

R. B. DOW
L. A. DUBRIDGE
W. F. FAIR, JR.
FLOYD A. FIRESTONE
HARVEY FLETCHER
R. C. GIBBS
K. S. GIBSON
W. H. MARKWOOD, JR.
A. H. PFUND
JOHN T. TATE
L. W. TAYLOR
A. G. WORTHING

The JOURNAL OF APPLIED PHYSICS, published monthly at Prince and Lemon Sts., Lancaster, Pa., is devoted to physics in its role as the science basic to other natural sciences and to the arts and industries. Previous to 1937 this publication was known as PHYSICS. The JOURNAL OF APPLIED PHYSICS publishes editorials, news of physicists, and reviews, as well as technical papers of applied physics.

Manuscripts should be submitted to Elmer Hutchisson, Editor, Case School of Applied Science, Cleveland 6, Ohio.

Subscriptions and orders for back numbers should be addressed to Prince and Lemon Streets, Lancaster, Pa. or to the American Institute of Physics, 57 East 55 Street, New York 22, N. Y.

Subscription Price

	U.S. AND CANADA	ELSEWHERE
To members of scientific societies	$5.00	$5.70
To all others	7.00	7.70

Back Number Prices

Complete set: Vol. 1, July, 1931–Vol. 16, 1945 – $101.50
Yearly back number rate: $7.70
Single copies: $0.70 each.

Changes of address and proofs should be addressed to the Publications Manager.

Advertising rates supplied on request. Orders, advertising copy, and cuts should be sent to the American Institute of Physics.

Entered as second class matter January 22, 1937, at the Post Office at Lancaster, Pennsylvania, under the Act of March 3, 1879.
Accepted for mailing at the special rate of postage provided for in the Act of February 28, 1925, authorized May 2, 1932.

Copyright 1946, by the American Institute of Physics.

Journal
of
Applied Physics

Volume 17, Number 8 August, 1946

Oxide Coated Cathode Literature, 1940-1945

JOHN P. BLEWETT

Research Laboratory, General Electric Company, Schenectady, New York

1. INTRODUCTION

BEFORE the war, it appeared that the mechanism of the oxide coated cathode was becoming fairly clear. The impurity semiconductor picture developed by the authorities on the theory of the solid state seemed to be a good representation of the behavior of an oxide coated cathode. Many phenomena which were well authenticated experimentally and which had been mysteries as far as interpretation was concerned, dropped neatly into place and numerical agreement was achieved between experiment and theory within the rather wide limits of experimental error. It began to appear that sufficiently careful control over such parameters as particle size, packing density, and so forth would lead to accurately reproducible results predictable from theory.

The situation fifteen years ago was somewhat different. At that time it was felt by such authorities as Reimann, Lowry, and others that the interface between oxide and core metal played an important part in the oxide cathode mechanism. Proponents of this view were silenced by the work of Becker and Sears and others around 1931, who seemed to have demonstrated that the outer surface of the oxide and the body of the oxide were the only regions which required consideration.

In the light of this history, it is particularly interesting that experiments performed during the war and reported elsewhere in this issue, lead not only to reconsideration of the oxide-core interface, but also to a possible re-evaluation of the whole oxide cathode theory. The high pulsed currents which have been drawn from oxide cathodes during the war must have resulted in conditions within the cathode which were far removed from equilibrium. It therefore becomes increasingly doubtful that correct results can be deduced from statistical mechanics which is a discipline related only to matter in equilibrium. The late Professor Fowler in the treatment of semiconductors in his monograph, *Statistical Mechanics*, emphasized this fact as follows: "It should be remembered that all these formulae are only valid so long as the rate of emission of electrons is very slow compared with the rate of readjustment of the internal equilibrium. The process creating the free electrons and free holes must be able to maintain the normal equilibrium supply. This is an essential assumption and there is no simple means of investigating its validity—nor any *a priori* reason why it should be true."

Mr. Hahn of our laboratory has suggested that future theoretical work should include the concept of mass motion and has pointed out that the basic mathematical techniques are already available in Chapman and Cowling's book[1] on the dynamics of gases.

[1] S. Chapman and T. G. Cowling, *The Mathematical Theory of Non-Uniform Gases* (Cambridge University Press, New York, 1939).

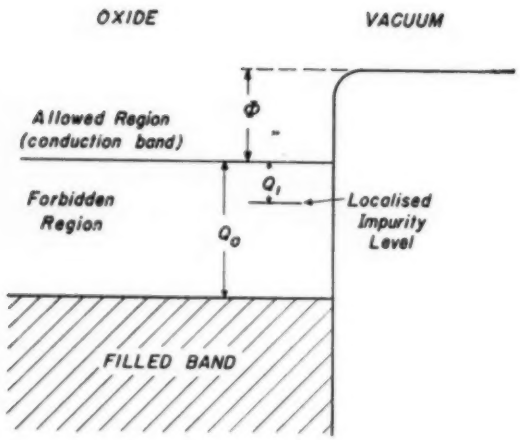

FIG. 1. Energy level distribution for an impurity semiconductor.

Most of the recent work on oxide coated cathodes has been performed under the veil of secrecy imposed by necessary wartime restrictions. A literature survey will thus be, at best, of secondary interest. Several important papers have appeared in the literature, however, and are worthy of mention by way of introduction to the survey of wartime research presented in this issue of the *Journal of Applied Physics*. The bibliography presented herewith is intended to be a supplement to the bibliography included in the author's 1939 review paper.

2. PROPERTIES OF BARIUM

The disagreement between Becker and Moore and Benjamin and Jenkins as to whether or not barium migrates over the surface of tungsten was resolved in 1940 by Becker and Moore who obtained one of Benjamin and Jenkins' experimental tubes and showed that Benjamin and Jenkins' tungsten surface had been slightly contaminated with oxygen. When this contamination was removed, Becker and Moore demonstrated that barium migration does take place in the temperature range above 970°K. They showed also that the migration is predominantly toward the negative end of the filament, so that the barium must have been at least partly ionized.

Timofeev and Aranovich (1940) studied the secondary emission from O–Ba and O–Mg surfaces and pointed out that the stability of such surfaces up to temperatures of the order of 600°C makes them interesting for practical secondary emitter applications.

Brüning (1940) pointed out that an alloy of copper and barium, when coated on tungsten, possesses a temperature stability much greater than that of a coating of pure barium on tungsten. His experiments indicated that barium evaporates from such a surface at 1300°K at a rate slower than the rate of evaporation of barium from tungsten at 1000°K. Since the alloy has thermionic characteristics which are comparable with those of pure barium on tungsten, such an alloy cathode may have considerable practical interest.

3. PHYSICAL PROPERTIES OF OXIDE COATED CATHODES

A method for determining the true surface area of an oxide cathode was devised by Wooten and Brown in 1943. They pointed out that this area is deducible from the form of adsorption isotherms and measured the areas of a number of cathodes using ethylene at −183°C and −196°C and butane at −116°C. The results were self-consistent and had the form predicted by theory. The measured surface areas of supposedly identical cathodes, however, varied between fifteen and fifty times the apparent surface areas. Wooten and Brown concluded that this scattering was caused by inadequate control of the process of conversion of barium carbonate to oxide.

Measurements of the thermal emissivities of standard uncombined oxide cathode types were reported in 1941 by Moore and Allison. True temperatures were measured by Worthing's method and the results were checked against reflectometer measurements obtained by the method of Prescott and Morrison. Both the spectral and total emissivities were found to lie between 0.23 and 0.51 depending on the method of preparation of the cathode, and, in some cases, on the temperature.

The crystal structures of a variety of two component mixtures of alkaline earth oxides were investigated by x-ray and electron diffraction by Huber and Wagener in 1942. They verified earlier results which had demonstrated the formation of mixed crystals, and studied variations

in lattice parameter with component concentration. By electron diffraction they showed that barium oxide was absent in the outer few hundred atom layers of an active barium oxide-strontium oxide cathode.

4. ELECTRICAL AND THERMIONIC PROPERTIES OF OXIDE COATED CATHODES

An interesting study of the energy levels in oxide coated cathodes was published in 1940 and 1941 by Nishibori and his associates. By mounting a probe in the coating of an oxide cathode they were able to make simultaneous measurements of the conductivity and thermionic emission of the oxide. Since the conductivity depends exponentially on $eQ_1/(2kT)$(cf. Fig. 1 or Fig. 6 of the author's 1939 review paper) and the thermionic emission depends exponentially on $e(Q_1/2+\varphi)/(kT)$, it was possible from these measurements to deduce the values of Q_1 and φ. Typical results obtained were as follows:

Before activation	After activation
$Q_1=1.68$ ev	$Q_1=1.40$ ev
$\varphi=0.27$ ev	$\varphi=0.28$ ev.

Since φ remained effectively constant, it is evident that activation of the cathode was caused by changes in the body of the oxide and not to any surface changes. Nishibori and his associates then proceeded to measure the photoelectric work function which should be given by $(Q_1+\varphi)$.[2] For an activated cathode they obtained a value of 1.66 ev in good agreement with the value of 1.68 ev deducible from the thermionic results.

Several other studies of oxide cathode work functions have appeared since 1940. Fan (1943) studied the variation of the A factor of a cathode with work function during activation over a range of work functions from 1.5 to 1.8 ev and obtained a more or less linear relation as did the classical authorities. Sproull (1945) measured work functions for impulse operation about 0.2 ev higher than the work functions observed for the same cathodes during steady operation. Sano (1941) described an ingenious method for measuring the work function of a cathode under zero field conditions, by studying the plate current of a diode in the retarding field range. This method was checked for metallic cathodes and proposed for use on oxide cathodes, but no oxide cathode results were reported.

The Schottky effect for oxide cathodes was investigated by Fan (1943) and Sproull (1945). Schottky lines with slopes 3.7 and 2.5 times the theoretical slope were obtained by these two investigators, respectively. Presumably their cathode surfaces differed in roughness.

Early work on determination of oxide cathode temperatures from the shape of retarding field-emission current curves led to temperatures which were too high by as much as fifty percent. The errors possible in such measurements were rather carefully investigated by Heinze and Hass (1938) who showed that temperatures of oxide cathodes can be determined by this method with errors of the order of one percent if the major sources of error are eliminated. Fan (1943) checked this conclusion by deductions of oxide cathode temperature which agreed within five percent with thermocouple measurements over the temperature range from 582°K to 951°K.

Generally qualitative electron microscope studies of the surface distribution of emission from oxide cathodes were reported by Fox and Bailey (1941) and Mecklenburg (1942). The surface distribution was found to be very non-uniform, an observation already well-authenticated by previous work on oxide cathodes. Mecklenburg noted that some of the emission centers were very small, in some cases of the order of 400 Angstrom units in diameter.

The emission of negative ions from oxide cathodes which plagues operators of magnetically controlled cathode-ray tubes received further attention from Bachman (1940) and Schaefer and Walcher (1943). Bachman explained some of the anomalous effects associated with magnetic resolution of negative ions in an oscilloscope tube as due to secondary effects at accelerating or focusing electrodes. Schaefer and Walcher performed a refined mass spectrometer analysis of the negative ions and reported a formidable list of ion masses. Unfortunately, their tube was not sealed off and some of the ions which they detected may not appear in

[2] Because of an unfortunate error in the author's 1939 review paper the photoelectric work function was said to be given by $(Q_1/2+\varphi)$. It is evident from Fig. 1 that the correct value is $(Q_1+\varphi)$.

conventional tubes. They made further observations relating negative ion emission, particularly of oxygen, to cathode activity.

Knowles and McNall (1941) described extensive experiments on cathode sparking when high currents were drawn from oxide cathodes in the presence of mercury vapor. They made careful measurements of tube drop before breakdown of time elapsed before breakdown occurred, and of breakdown current.

5. TIME EFFECTS

Johnson (1944) observed that bombardment of an oxide cathode by electrons from an external source produced changes in the electron emission from the cathode which decayed rather slowly after the bombarding current was turned off. The anomalous current was not attributable to temperature changes but may have its explanation in the electrolytic transport of barium which is considered to be responsible for the normal decay effect.

The normal decay effect was noted by Andrianov (1944) who was able to draw currents as high as 30 amperes per sq. cm for periods of a few microseconds from oxide coated cathodes. Fan (1943) was unable to detect any decay effect whatever. This interesting observation is, perhaps, to be associated with the fact that his cathode, from his account, appears to have been incompletely activated. A detailed study of the normal decay effect was published by Sproull in 1945 who outlined and expanded a theory of the effect. He showed that the effect was independent of cathode thickness and concluded that it depended, rather, on crystallite size. Also he discussed the "flicker" effect observed by J. B. Johnson and others and suggested that this effect might be associated with the decay effect since the time constants involved were of the same order of magnitude.

6. BIBLIOGRAPHY

The parentheses after each paper listed below indicate the feature of the paper of particular interest in connection with oxide coated cathodes.

1938.

J. Ewles, Proc. Roy. Soc. **A167**, 34 (1938) (Luminescence of alkaline earth oxides).

W. Heinze and W. Hass, Zeits. f. tech. Physik **19**, 166 (1938) (Determination of oxide cathode temperature from retarding field emission characteristics).

1939.

J. P. Blewett, J. App. Phys. **10**, 668 and 831 (1939) (Review articie).

N. D. Morgulis, Tech. Phys. (USSR) **9**, 853 (1939) (in Russian) (Theory of secondary emission from composite cathodes).

1940.

C. H. Bachman, J. App. Phys. **11**, 83 (1940) (Formation and focusing of negative ions in cathode-ray tubes).

J. A. Becker and G. E. Moore, Phil. Mag. **29**, 129 (1940) (Thermionic emission, migration, and evaporation of barium on tungsten).

K. Brüning, Physik. Zeits. **41**, 285 (1940) (Thermionic properties of barium-copper alloy coatings on tungsten).

B. Gysae and S. Wagener, Zeits. f. Physik **115**, 296 (1940) (Work functions of cathodes with non-uniform emitting surfaces).

E. Nishibori and H. Kawamura, Phys. Math. Soc. Japan Proc. **22**, 378 (1940) (Conductivity and thermionic emission of oxide coated cathodes).

B. N. Srivastava, Proc. Roy. Soc. **A175**, 26 (1940) (Thermal ionization of barium vapor).

P. V. Timofeev and R. M. Aranovich, J. Tech. Phys. (USSR) **10**, 32 (1940) (in Russian) (Oxygen-barium and oxygen-magnesium surfaces for secondary emitter applications).

Y. Uehara and M. Takahasi, Bull. Chem. Soc. Japan **15**, 15 (1940) (Quantum mechanical theory of electron emission from oxide coated cathodes).

1941.

G. W. Fox and F. M. Bailey, Phys. Rev. **59**, 174 (1941) (Electron microscope study of oxide coated cathode emission).

D. D. Knowles and J. W. McNall, J. App. Phys. **12**, 149 (1941) (Sparking of oxide coated cathodes in mercury vapor).

G. E. Moore and H. W. Allison, J. App. Phys. **12**, 431 (1941) (Spectral and total thermal emissivities of oxide coated cathodes).

N. D. Morgulis, Bull. Acad. Sci. (USSR) (Ser. Phys.) (in Russian) (Izvestia Akademia nauk SSSR, Seria fizicheskaya) **5**, 536 (1941) (Nine-page review of oxide coated cathode fundamentals).

E. Nishibori, H. Kawamura, and K. Hirano, Phys. Math. Soc. Japan Proc. **23**, 37 (1941) (Photoelectric work functions of oxide coated cathodes).

C. H. Prescott, Jr., "The pyrometry of oxide coated cathodes" in *Temperature, its Measurement and Control in Science and Industry* (Reinhold Publishing Corporation, New York, 1941), p. 1199.

S. Sano, Electrotech. J. (Japanese) **5**, 78 (1941) (A new method for measuring work functions of oxide coated cathodes).

1942.

K. H. Geyer, Ann. d. Physik, **42**, 241 (1942) (Secondary emission from alkaline earth oxides).

H. Huber and S. Wagener, Zeits. f. tech. Physik **23**, 1 (1942) (X-ray and electron diffraction studies of oxide coated cathodes).

W. Mecklenburg, Zeits. f. Physik **120**, 21 (1942) (Electron microscope study of oxide coated cathode emission).

1943.

H. Y. Fan, J. App. Phys. **14**, 552 (1943) (Thermionic emission from oxide coated cathodes).

G. Herrmann and S. Wagener, *Die Oxydkathode*, Physikalische Grundlagen (J. A. Barth, Leipzig, 1943), Vol. I (124 pages) (This book is not yet available in the United States).

H. Schaefer and W. Walcher, Zeits. f. Physik **121**, 679 (1943) (Mass spectrometer analysis of negative ions emitted from oxide cathodes).

C. F. Veenemans, Ned. Tijd. Naturkunde. **10**, 1 (1943) (in Flemish) (Sixteen-page review on oxide coated cathodes).

L. A. Wooten and C. Brown, J. Am. Chem. Soc. **65**, 113 (1943) (Surface area of oxide coated cathodes by adsorption of gas at low pressures).

1944.

M. Andrianov, Bull. Acad. Sci. (USSR) (Ser. Phys.) (in (Russian) (Izvestia Akademia nauk SSSR, Seria fizicheskaya) **8**, 290 (1944) (One-page discussion of impulse emission from oxide coated cathodes).

J. B. Johnson, Phys. Rev. **66**, 352 (1944) (Anomalous emission from oxide coated cathode bombarded by electrons).

1945.

R. L. Sproull, Phys. Rev. **67**, 166 (1945) (Short time emission from oxide coated cathodes).

The Pulsed Properties of Oxide Cathodes*

EDWARD A. COOMES†

Radiation Laboratory, Massachusetts Institute of Technology, Cambridge, Massachusetts

A survey of the results obtained in an experimental study of the pulsed properties of oxide cathodes is presented. Pulsed measurements reveal that unusually large electron currents are available in microsecond pulses, and that several other phenomena are modifications of the d.c. properties, namely (a) sparking and (b) pulse temperature rise. Sparking may be either current limited or voltage limited, depending upon cathode materials and life. The pulse temperature rise also depends upon materials and life and is indicative of the nature of the cathode resistance. Evidence for a layer structure of the oxide cathode can be drawn from pulsed data.

I. INTRODUCTION

THE fact that oxide cathodes have interesting time-dependent properties was clear before the war. J. Blewett pointed this out in his 1939 paper[1] on the time changes in oxide cathodes. O. Schade, in his discussion of rectifier analysis,[2] stated that transient peak currents of 25 amp./cm^2 had been observed from well-activated oxide cathodes. A good phenomenological picture of cathode sparking was also given, with a clear distinction between the two types.

The extensive use of pulsed electron tubes during the war invoked interest in the properties of oxide cathodes under pulsed conditions, since it appeared that unusually large electron currents were available in short pulses. Before 1942 at Radiation Laboratory, J. McNall[3] had obtained microsecond pulses of emission of more than 1 amp./cm^2 at 850 deg. C, under space charge limited conditions. He used a diode having an internal anode, and his measurements were taken at a relatively high pulse recurrence frequency (p.r.f.), so that currents were limited by anode dissipation.

Ramsay at Bartol, using single pulses, observed two types of decay in the pulsed emission from oxide cathodes, the first type having a decay time of about 10^{-5} second, and the second, a decay time of the order of milliseconds. The short time decay, which is of interest for microsecond pulse phenomena, was observed in aged cathodes

* This paper is based on work done for the Office of Scientific Research and Development under contract OEMsr-262 with the Massachusetts Institute of Technology.

† Now at Department of Physics, University of Notre Dame, Notre Dame, Indiana.

[1] J. P. Blewett, Phys. Rev. **55**, 713 (1939).

[2] O. Schade, Proc. I.R.E. **31**, 341 (1943).

[3] J. W. McNall, M.I.T. Doctor's Thesis (1942).

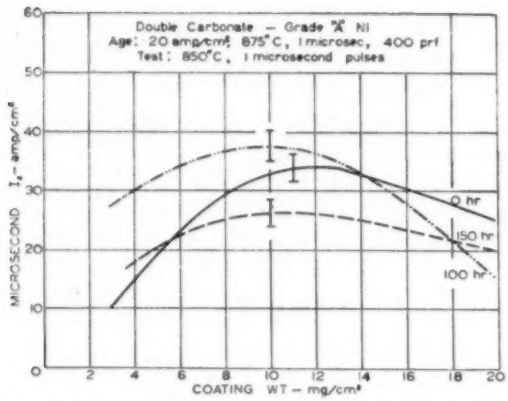
Double Carbonate – Grade "A" Ni
Age: 20 amp/cm² 875°C, 1 microsec, 400 prf
Test: 850°C, 1 microsecond pulses
MICROSECOND I_p – amp/cm²
COATING WT – mg/cm²
0 hr
150 hr
100 hr

FIG. 1. The dependence of microsecond pulsed emission on coating weight for plain oxide cathodes. The maximum spread of experimental points is indicated.

but could not be found in very active cathodes. R. Sproull,[4] using pulse widths in the range 0.2 to 300 microseconds, observed experimentally that the rate of decay of emission was independent of cathode coating thickness.

In the experiments that followed the work of McNall at Radiation Laboratory, microsecond pulses of emission space-charge-limited[5] up to about 5 amp./cm² at 850°C were obtained from oxide cathodes of the prewar commercial variety, using an early design of test diode with an external water cooled anode. About this time the screen cathode[6] emerged from the technological developments of oxide cathodes for pulsed transmitter tubes, and with this type of structure microsecond emissions of at least 35 amp./cm² at 850°C were consistently obtained in test diodes. Apparently there was nothing very fundamental in the screen structure that could account for the difference in emission between the two types of cathodes, and in making a comparison only two significant differences were noted at the time: (a) the coating weight per unit area was much larger on screen cathodes, having a value of about 20 mg/cm² compared with about 6 mg/cm² for the plain type and (b) because of the unique preparation technique for screen cathodes, the density of coating was about twice that ordinarily obtained with plain coatings. Tests were run on a series of grade "A" nickel plain sleeves coated with a double-carbonate suspension, and a good dependence of pulsed emission on weight was obtained, with the highest value of microsecond pulsed emission at about 10–12 mg/cm². The results obtained by J. Buck in his studies during the life of a series of plain cathodes is given in Fig. 1. This shows that the dependence of emission on coating weight is maintained for at least 150 hours of operation at 850°C. The result is also significant in that it was not found to apply in the case of d.c. emissions; no systematic dependence of d.c. emission on coating weight was observed.

From the time that pulsed oxide cathodes became technologically important there was hope that correlations could be made between the d.c. and pulsed properties. It appeared from early diode experiments that definite correlations of a simple nature did not exist. About all that could be inferred from correlation experiments was that usually good pulsed cathodes were also good d.c. cathodes, but the reverse need not be true. For example, in a certain life test three groups of cathodes (a), (b), and (c) with selected structural differences all gave ½ amp./cm², d.c. emission at 800°C for over 500 hours of life. Group (a) gave a microsecond pulsed emission of 60 amp./cm², group (b) 20 amp./cm², and group (c) ½ amp./cm², for the same life test conditions.

II. PARAMETERS FOR DESCRIBING THE PULSED PROPERTIES OF OXIDE CATHODES

Tests designed to give extensive information on the pulsed properties of oxide cathodes reveal phenomena and limitations which are usually not found by d.c. methods. Two effects are particularly serious in tending to limit and confuse the interpretation of pulse data.

(a) The Temperature Rise

When large currents are drawn in pulses with a relatively high pulse recurrence frequency from an oxide cathode, there is a large rise in the average temperature of the cathode, as illustrated in Fig. 2. This effect may be minimized by going to lower duty cycles; with microsecond pulses at 60 p.r.f. the effect is not observable by ordinary methods of optical pyrometry on usual oxide cathodes.

[4] R. Sproull, Phys. Rev. **67**, 166 (1945).

[5] The maximum value of space-charge-limited emission is taken at the point where the cathode emission characteristic plotted on ⅔-power paper deviates from the computed Langmuir-Child line.

[6] The screen cathode is made by firmly bonding nickel mesh to a supporting nickel sleeve and impregnating the interstices of the mesh with cathode coating.

(b) Sparking

The second, and probably most serious, limitation encountered in the pulsed observations on oxide cathodes is the phenomenon of sparking. In this case the electron current from the cathode is limited by the physical transfer of particles of oxide coating from the cathode sleeve to the anode, accompanied by a large increase in electron current with an extremely steep wave front. The sparking value of current on pulsing usually occurs before temperature saturation of emission is reached, and for the most active cathodes it will occur before the cathode emission deviates from space charge limitation. An example of this case is given in Fig. 3. With this situation the problem of improving the pulsed thermionic emission immediately transforms to the problem of improving sparking properties. Experiment indicates that the space charge limited value of pulsed sparking current is higher for shorter pulse widths; for example, during the normal life of an active oxide cathode the sparking current for 10 microsecond pulses is about $\frac{1}{3}$ the value obtained for 1-microsecond pulses, at a low pulse recurrence frequency. This means that to measure the highest instantaneous value of electron current available from an oxide cathode well-defined voltage pulses below a microsecond in width must be used.

While sparking and temperature rise place limitations on the pulsing of oxide cathodes, the phenomena related with these two effects have good reproducibility and may be used to define parameters of measurements for different cathode types.

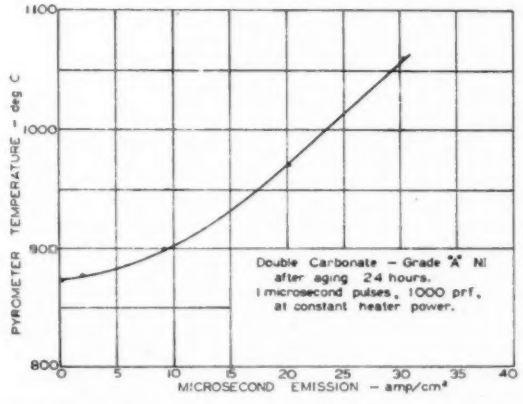

FIG. 2. The rise in temperature with increase of magnitude of pulse current for an oxide cathode.

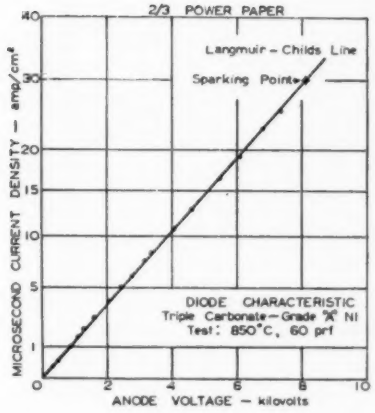

FIG. 3. Space charge limited sparking.

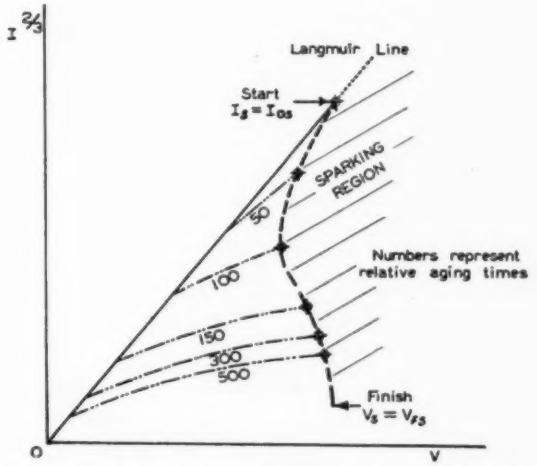

FIG. 4. Sparking diagram for a pulsed oxide cathode.

1. The Sparking Points

These are defined by the $I-V$ diode values at which the electron current from the cathode is limited by sparking. Data of this type cannot be taken on d.c., but with short pulses at a low recurrence rate not only can the data be reproducibly obtained but important connections with the chemical and physical details of the cathode structure seem to exist. A comprehensive representation of the sparking phenomena may be arrived at by drawing $I^{\frac{3}{2}}$ *versus* V curves at various stages in the life of the cathode as illustrated in Fig. 4. This diagram represents the probable life cycle of a well-aged, well-activated oxide cathode for 1-microsecond pulsed emission at a low recurrence rate. While it has been recognized before[2] that there are two types of sparking, this is brought out clearly in the study of the pulsed sparking currents. Differentiation

between the two types may be made in the manner stated below.

(*a*) *Space-charge limited sparking* occurs early in the life of the cathode when the current is limited to a value $I_s = I_{0s}$ on the space charge line (see Fig. 4). As a result of experiment, an I_{0s} value of at least 50 amp./cm² at 800°C and 1 microsecond may be assigned to cathodes prepared with a good double carbonate coating on grade "A" nickel, while values as high as 130 amp./cm² have been obtained under pulsed conditions with purer nickels as base metals. The space-charge limited sparking current is an important parameter for pulsed oxide cathodes because it is the highest value of electron current that can be taken from the cathode, and because it seems to bear a definite relation to the material system which comprises the cathode.

(*b*) *Voltage limited sparking* takes place late in the life of an oxide cathode when the diode sparking occurs at a value of anode voltage $V_s = V_{fs}$ (see Fig. 4). This may mean that sparking takes place at a critical value of field at the cathode surface, and, therefore, it is an important parameter since it may depend in a fundamental way upon the nature of the oxide at the cathode surface. In experiments on cathodes prepared with strontium carbonate or double carbonates, the computed field corresponding to V_{fs} was found to be 40–60 kv/cm, while for cathodes prepared with pure barium carbonate the field was in the range 100–125 kv/cm. Using cathode coating prepared with alternate layers of the single carbonates, results for sparking field checked the above ranges, giving the low value of sparking field when strontium oxide was formed on the surface, and the higher value when barium oxide was on the surface.

While sparking of the two types may usually be distinguished for oxide cathodes during a life test, there is experimental evidence to indicate that in some cases sparking may be dependent on the state of the anode, which would prevent the observation of either one or both of the two fundamental types already described.

2. The Maximum Space-Charge-Limited Emission

If the cathode does not spark on the space charge line, then the point I_0 at which the plotted experimental data first deviate from the theoretical Langmuir-Child line is the maximum electron current obtained from the cathode under space charge limited conditions. If this point is interpreted as the maximum thermionic emission current that can be obtained at a constant temperature with zero field at the cathode surface then this is an important parameter since it corresponds to the value of current given by Richardson's equation.[7] Figure 5 illustrates the manner in which I_0 is obtained. This figure also illustrates the general trends of pulsed data above the space charge limited value. At a given time in life, there will be observed one of two types of behavior: cathodes will either have $I-V$ characteristics that follow the normal Schottky equation but possibly with a temperature different than the observed value, or there will be an anomalous behavior which is much more pro-

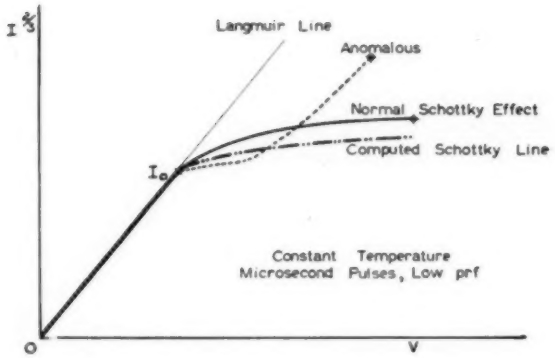

FIG. 5. Typical emission characteristics of an oxide cathode pulsed at a constant temperature.

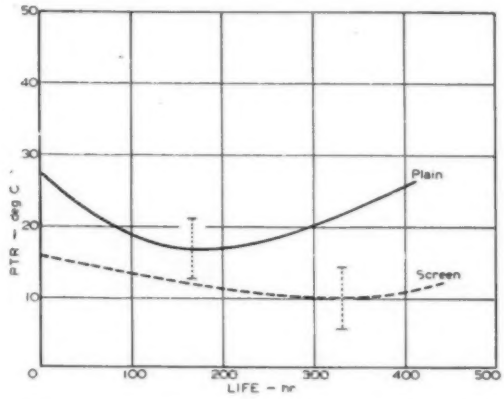

FIG. 6. Pulse temperature rise as a function of life.

[7] A series of values of I_0 at various temperatures for average good cathodes prepared from double-carbonate coating on grade "A" nickel, gave a computed value of about 1 volt for the work function.

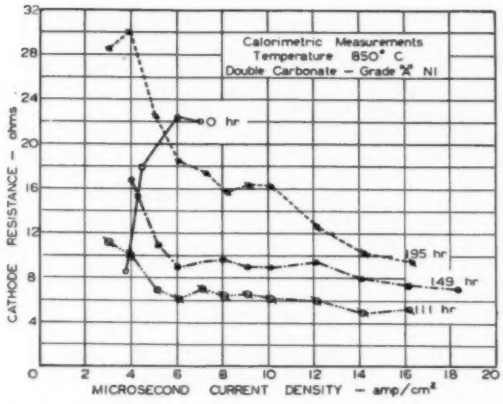

FIG. 7. Oxide cathode resistance measured under pulsed conditions. (Data taken by J. Buck.)

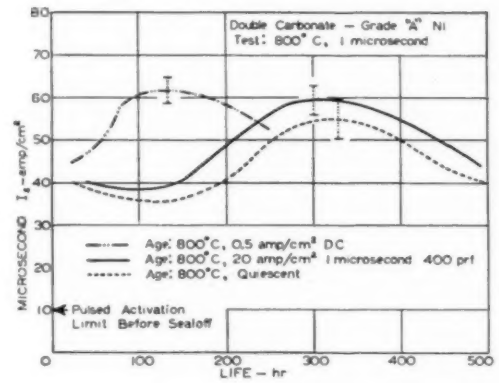
Double Carbonate – Grade "A" Ni
Test: 800° C, 1 microsecond
Age: 800°C, 0.5 amp/cm² D.C.
Age: 800°C, 20 amp/cm² 1 microsecond 400 prf
Age: 800°C, Quiescent
Pulsed Activation Limit Before Sealoff
MICROSECOND Ia – amp/cm²
LIFE – hr

FIG. 8. The effect of duty cycle on the life of a pulsed oxide cathode.

nounced than in the case of the well-known d.c. effect.[8]

3. *The Pulse Temperature Rise*

The average temperature rise which occurs on pulsing at higher recurrence rates may be used as a parameter, when measured in a standard way. This pulse temperature rise (ptr) may be specified at a given current level and duty cycle. For example, when an average oxide cathode is pulsed at 10 amp./cm², 1-microsecond pulses, 1000 p.r.f., the pyrometer temperature may show an increase of from about 5 to 60°C above the initial quiescent temperature at zero current. This ptr may be studied over the life of the cathode, or it may be compared for different cathode systems. Experiment indicates that, in general, during the life of a cathode the ptr falls to a minimum and then increases for later times. Figure 6 shows that the ptr for an average good screen cathode is always lower than the ptr for an average good plain oxide cathode. If the extra cathode heat which causes the ptr is attributed to the RI^2 loss resulting from the passage of current through the resistance of the cathode, then the ptr is an indication of the cathode resistance, and the resistance R may be determined experimentally by a caloremetric method, based on the equation

$$W_H + RI^2bf - \phi Ibf = e\sigma T^4 + \Sigma,$$

where

W_H = cathode heater power input,
I = pulsed current,
bf = duty cycle, which is pulse width times p.r.f.,
ϕ = thermionic work function,
e = total emissivity,
σ = Stefan's constant, and
Σ = conduction and convection heat losses.

In this method at a chosen current I, and for two different values of duty cycle, values of W_H are alternately set to give the same temperature. Substituting these data in the equation (neglecting ϕI and Σ) gives two simultaneous equations from which a value of R corresponding to a given I may be computed. A typical plot of resistance *versus* current obtained in this manner during the life of a cathode is given in Fig. 7. Since there is a striking resemblance between the R *versus* I curve for an oxide cathode and this same characteristic curve for a blocking layer rectifier in the high resistance direction, the hypothesis first suggested by Reimann,[9] that a high resistance contact between coating and the base metal might be responsible for the observed variations of cathode resistance with current, deserves consideration. Measurements were made using probes embedded in the coating at various distances from the base metal,[10] and it was found that at least in the case of cathodes prepared with double carbonates on pure and Cr plated nickel, the resistance by probe measurements had the same type of current dependence as found by calorimetric measurements, and that the resistance at zero life at the metal-to-coating interface

[8] See A. L. Reimann, *Thermionic Emission* (John Wiley and Sons, New York, 1934), Chapter VI.

[9] A. L. Reimann and R. Murgoci, Phil. Mag. **9**, 440 (1930).

[10] A. Fineman and A. Eisenstein, "Studies of the interface of oxide cathodes," J. App. Phys. **17**, 663 (1946).

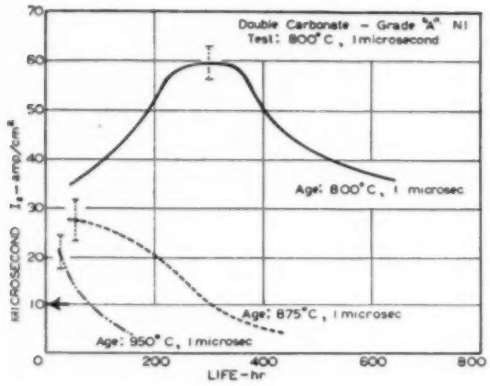
Double Carbonate – Grade "A" Ni
Test: 800°C, 1 microsecond
Age: 800°C, 1 microsec
Age: 875°C, 1 microsec
Age: 950°C, 1 microsec
MICROSECOND I_s – amp/cm²
LIFE – hr

FIG. 9. The effect of operating temperature on the life of a pulsed oxide cathode.

at operating temperature of 850°C was in some cases an order of magnitude greater than the resistance of the coating.

III. LIFE PROPERTIES AND THE EFFECTS OF MATERIALS

Interesting phenomena in the pulsed studies of oxide cathodes come out of life testing, and it becomes evident that before any comparison of the pulsed properties of various oxide cathodes can be made one must realize just how these properties vary during the life of a single cathode. As an example, some life studies of the cathode sparking current are given. Figure 8 is an average plot of the microsecond sparking current I_s as a function of life on cathodes prepared with double carbonate coatings on grade "A" nickel, each cathode having a weight of 12 mg/cm² and having undergone a good standard processing schedule. While this diagram shows particularly the effect of duty cycle, the nature of the curves is general for life test data taken under pulsed conditions. Each curve has an initial rise, a relatively flat portion, and then a definite falling off with life, the trends defining three different regions of activity in the life of the cathode.

Region I: The cathode is still apparently undergoing aging so that the activity is not constant. In the experiment from which these data were taken the activation was purposely stopped at 10 amp./cm² to allow the observation of this effect.

Region II: This might be defined as the normal life of the cathode, since in this region the activity is at its highest measurable value and remains practically constant throughout the period. Usually, the sparking current density over this period of life remains near its space charge limited value I_{0s}.

Region III: This is the region of constant sparking voltage, since over this period of life sparking takes place at practically the same value of voltage, V_s equal to V_{fs}. As the cathode activity falls with life, the sparking current density will show a decline, since it is measured at a constant anode voltage.

The effect of operating temperature on the sparking properties of a pulsed oxide cathode is shown in Fig. 9. When compared with Fig. 8 this illustrates particularly that under pulsed conditions operating temperature exerts a much stronger influence on the obtainable level of cathode activity than does the duty cycle.

Life tests have consistently indicated that the effect of cathode base metal on the pulsed properties of oxide cathodes is a very strong one, and to date the nickels of higher purity than grade "A" have given higher values of pulsed emission. Figure 10 gives a comparison of results with a good electrolytic nickel[11] base metal against the results obtained with a good grade "A" nickel.

IV. THE LAYER STRUCTURE OF OXIDE CATHODES

Several types of evidence come out of pulsed measurements that might indicate a layer structure for an oxide cathode as suggested by Fig. 11. There are the probe measurements of cathode resistance which show a comparatively high resistance in the interface region. The variation of

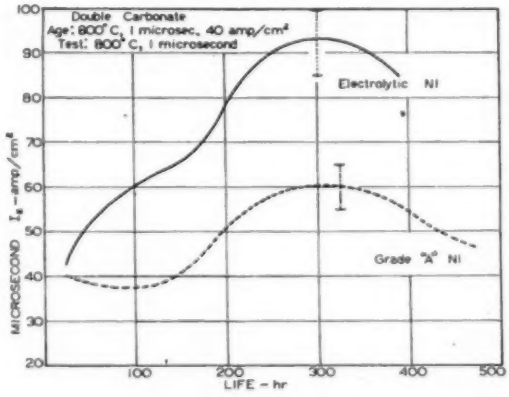

FIG. 10. A comparison of pulse emissions with pure and grade "A" nickel cathode base metals.

[11] The electrolytic nickel used in these tests was supplied by Mr. E. M. Wise of International Nickel Company.

this resistance with current, and the temperature dependence of this relation are those that would be expected[12] if the oxide cathode had a structure similar to a blocking layer rectifier. This model also lends itself to a straightforward explanation of high pulsed emissions when microsecond voltages pulses are appliéd. The conduction band of the semiconducting oxide, which is filled by the thermally excited electrons from the impurity levels, might act as a reservoir of electrons from which large transient currents could be taken at the oxide-vacuum surface. The emission limitations of the high resistance blocking layer at the interface may be overcome by the production of high fields in this blocking layer which in turn cause a copious emission of electrons at the base metal surface by means of the Schottky effect or even by field emission. Although theoretically a blocking layer that could withstand such a field can be formed by simply placing a semiconductor in contact with a metal, it has been observed that metal-oxide interfaces both in the case of copper oxide rectifiers[13] and in oxide cathodes are usually compounds that are different than the main body of the semiconductor. For example, A. Eisenstein,[10] by the use of x-rays has found complicated barium compounds at the interfaces of cathodes made on nickels containing small amounts of selected metallic impurities.

There are other experimental facts that indicate the cathode interface as a possible important factor in any consideration of electron emission mechanisms from oxide cathodes. Extensive life tests have indicated that for pulsed emission the selection and treatment of the base metal before coating and the details of the subsequent breakdown schedule are more important than the choice of carbonate coating. During processing, not only can impurities initially contained in the base metal reduce the oxide coating to produce free alkaline earth metal, but it is possible that they also effect the rate, type, and extent of the compound formation at the interface. For example, it was observed that ordinarily very thin coatings never produce good pulsed emissions; however in an experiment performed by A. Fineman, coatings of the order of 1 mg/cm^2 were converted in an atmosphere of several microns

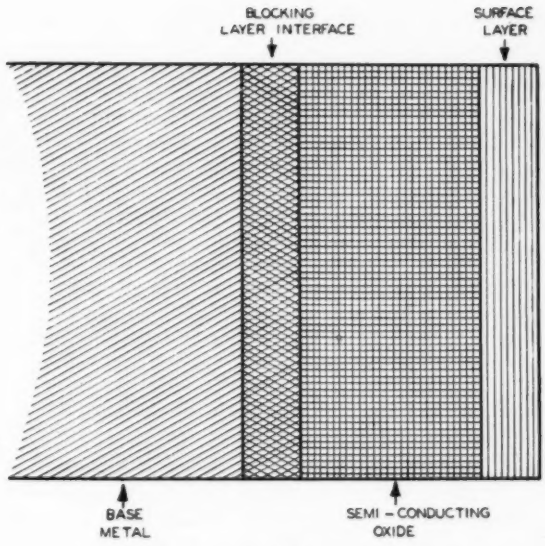

FIG. 11. A layer model for oxide cathodes.

pressure of the breakdown gases from a larger cathode heated simultaneously, and pulsed emissions of 25 amp./cm^2 were obtained. Details such as sharpness and completeness of conversion entering as an essential requirement for obtaining high pulsed currents, may point to a critical pressure-temperature value at the base metal surface during conversion as being important in the cathode forming process. There is also the direct experimental evidence obtained by J. Buck, that preoxidation of certain nickel base metals produces cathodes that give higher pulsed emissions than the same base metal in an unoxidized condition.

Rather good evidence has been obtained for the existence of the surface layer of an oxide cathode. While experiments that have been carried out to give direct evidence for a monolayer of barium have not been conclusive,[14,15] these same experiments did reveal that during the life of a barium-strontium oxide cathode there is formed on the cathode surface a thin layer of pure strontium oxide. Life test experiments in conjunction with x-ray measurements by A. Eisenstein[16] indicate that this layer reaches a thickness of about 10^{-5} cm roughly at the time the sparking current becomes voltage limited, or at the beginning of Region III of the life diagram. It has been noted

[12] N. F. Mott, Proc. Roy. Soc. **A171**, 27 (1939).
[13] L. O. Grondahl, Rev. Mod. Phys. **5** (1933).
[14] J. A. Darbyshire, Proc. Phys. Soc. **50**, 635 (1938).
[15] H. Huber and S. Wagener, Zeits. f. tech. Physik **23**, 1 (1942).
[16] A. S. Eisenstein, J. App. Phys. **17**, 654 (1946).

that this is also the same time at which the ptr reaches its minimum value during life. It is thus apparent that the available pulsed emission can be limited either by conditions at the surface or at the interface, and the nature of this limitation can only be ascertained by a careful consideration of the effect of the operating temperature and the thermochemistry of the cathode structure as a whole at this temperature.

The author wishes to thank the members of the Cathode Research Group of Radiation Laboratory for their cooperation in this wartime research. James Buck, Abe Fineman, and Albert Eisenstein were the staff members on whom fell the burden of the experimental program, and Earnest Parsons managed the test program that produced the enormous amount of data needed to complete the work.

A Study of Oxide Cathodes by X-Ray Diffraction Methods*

Part II. Oxide Coating Composition

A. EISENSTEIN†

Radiation Laboratory, Massachusetts Institute of Technology, Cambridge, Massachusetts

X-ray diffraction methods were used to investigate time changes which occur in the composition of oxide cathode coatings, initially equal molar (BaSr)O. Changes which occur in the composition of the bulk of the coating were detected by means of lattice constant measurements. A new method of analysis was developed to permit a determination of the variation of composition with depth below the surface. The bulk loss of BaO is primarily a function of the base metal used and the surface loss from the oxide is effected to a lesser extent. Possible correlations with thermionic emission are discussed.

PART I of this paper described in detail the x-ray diffraction method as applied to the study of oxide coated cathodes. This technique is particularly suited to the analysis of time changes in composition which occur in oxide cathode coatings. Because of the non-destructive nature of this method extensive studies can be made of single cathodes. As a tool, x-ray diffraction measurements reveal only the crystal structure and the crystallographic lattice constants of the sample, hence some *a priori* knowledge is required of the relationship between crystal structure and molar composition. The oxides BaO and SrO, which have the same crystal structure, are reported[1,2] to form true solid solutions, the lattice constant of which varies continuously and linearly with composition.

By means of x-ray diffraction analyses, Benjamin and Rooksby[3] found that the compositions of several different (BaSr)O oxide solid solutions changed by a few percent during the thermal activation of the cathode because of the preferential evaporation loss of the BaO component. They also report a considerable bulk loss of BaO at the "end of life" of a group oxide coated cathodes.

Gaertner,[4] Darbyshire,[5] and Huber and Wagener,[2] using electron diffraction analyses, agree that in activated cathodes the bulk composition of the oxide solid solution, is not homogeneous throughout but that the surface usually consists of pure SrO. Burgers[1] has shown that a cathode "flashed" at 1225°C will develop a relatively thick BaO deficient surface layer in 30 minutes, this layer being detected by an asymmetry in the shape of the diffracted x-ray lines.

In this paper, variations in coating composition which are detected by changes in the crystal lattice constant are presumed to be a character-

* This paper is based on work done for the Office of Scientific Research and Development under Contract OEMsr-262 with the Massachusetts Institute of Technology.

† Now at the Research Laboratory of Electronics, Massachusetts Institute of Technology.

[1] W. G. Burgers, Zeits. f. Physik **80**, 352 (1933).

[2] H. Huber and S. Wagener, Zeits. f. tech. Physik **23**, 1 (1942).

[3] M. Benjamin and H. P. Rooksby, Phil. Mag. **15**, 810 (1933).

[4] H. Gaertner, Phil. Mag. **19**, 82 (1935).

[5] J. A. Darbyshire, Proc. Phys. Soc. **50**, 635 (1938).

istic of the bulk of the coating and are termed bulk changes. Surface changes refer to those variations in composition which occur near the external surface of the coating and which are detected by asymmetries in the shape of the diffraction lines.

EXPERIMENTAL

The experimental techniques used to obtain x-ray diffraction patterns of the chemically unstable oxides of barium and strontium have been described in detail.[6] X-ray diffraction patterns were taken of the oxide cathode coatings in a 4.70-cm radius camera using filtered Cu$K\alpha$- or Co$K\alpha$-radiation. The following groups of cathodes were studied.

Group 1

In a preliminary survey, a group of 16 cathodes which had reached the "end of life" were examined to determine, if possible, what physical changes in the oxide coating could be correlated with the decline in thermionic activity. This group consisted of standard[7] test cathodes run in the laboratory diode.[8] For the 11 cathodes which were operated and tested[9] under pulsed conditions of 1 μsec., 400 and 50 p.r.f., respectively, the "end of life" was defined as that time at which the sparking current[7] fell below 10 amp./cm². For the 5 cathodes operated under d.c. conditions the "end of life" state was reached when the emission current fell below 0.1 amp./cm² at an anode voltage capable of giving initially, 1 amp./cm² space charge limited emission. Life tests were carried out at constant, uncorrected, pyrometered temperatures in the range 800°C to 950°C at which the initial pulsed cathode emission currents at sparking were in excess of 50 amp./cm² and the d.c. cathode emission levels were 1 amp./cm².

[6] A. Eisenstein, "A study of oxide cathodes by x-ray diffraction methods," J. App. Phys. **17**, 434 (1946).

[7] The cathodes were coated approximately 10 mg/cm², with an equal molar solid solution carbonate $(BaSr)CO_3$, (Ratheon C51–2); 8-mm coated length on 3-mm×14-mm indirectly heated sleeves. Pure nickel, grade A nickel, and nickels containing added amounts of chromium and silicon were used as base metals.

[8] A 9.5-mm external Kovar anode tube. Anode outgassed by electron bombardment in a pre-processing treatment prior to mounting the test oxide cathode. Anode water cooled during test and life run periods.

[9] E. A. Coomes, "The pulsed properties of oxide cathodes," J. App. Phys. **17**, 647 (1946).

Group 2

To investigate the effect of temperature, time, and base metal, on coating composition, twelve monodes containing standard cathodes were processed and life tested. Eight of these had as a base metal, electronic grade A nickel and four a pure nickel, RCA N-81. These monodes were evacuated using a three-stage oil diffusion pump and baked for one hour at 450°C. The cathodes were processed and the tubes sealed off at a pressure of less than 10^{-7} mm. These cathodes were operated quiescent, i.e., glowed without emission current at either 800°C or 875°C for periods of from 50 hours to 1200 hours. At the end of this time interval the tubes were opened and x-ray diffraction patterns were taken of the cathode coating.

Group 3

Eight standard cathodes, prepared on the pure nickel, N-81, were processed in the laboratory diode. Five of these were operated for 40 hours in a quiescent state at a temperature in excess of 950°C and three were operated at a d.c. emission current of 0.5 amp./cm² at the same temperature and for the same time interval. X-ray patterns were then taken of these cathodes to determine the effect of a thermionic emission current on the change of oxide composition with time.

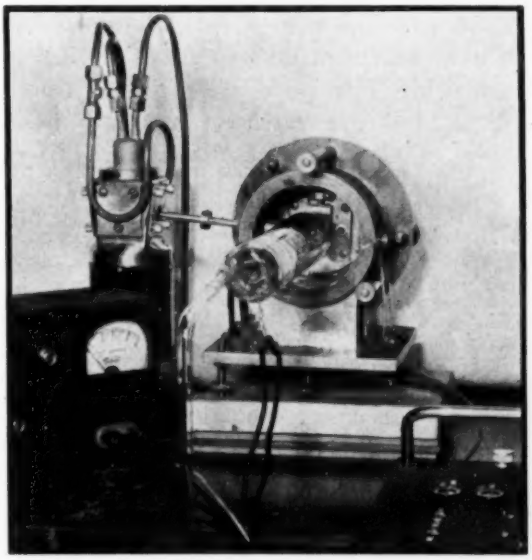

FIG. 1. Beryllium windowed, continuously pumped diode mounted at center of an x-ray camera.

Group 4

Three standard cathodes were operated in continuously pumped, beryllium windowed diodes.[6] Figure 1 shows a diode of this type

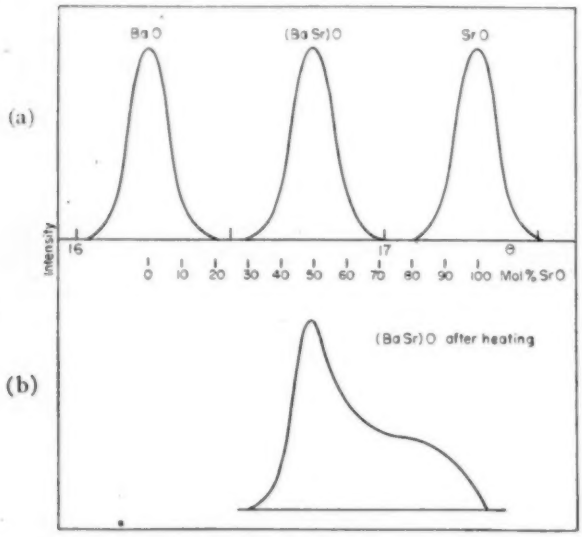

FIG. 2. Idealized 200 diffraction lines from (a) homogeneous phases BaO, (BaSr)O, and SrO and (b) an inhomogeneous solid solution, see text.

mounted at the center of the x-ray camera which is rigidly mounted with respect to the x-ray source. A pressure of less than 5×10^{-7} mm could be maintained in the vacuum system throughout the life test period. Diffraction patterns were taken at time intervals during the quiescent life test periods of these cathodes which in one case extended for 1200 hours. Analyses of the series of diffraction patterns thus obtained permitted evaluations of (1) bulk changes in the oxide coating composition and (2) surface changes in composition.

To check the results obtained in the continuously pumped diodes, one standard cathode was life tested in a sealed-off, beryllium windowed diode.[6] The copper anode block of this tube was outgassed by electron bombardment in a preprocessing treatment. Following a baking period of one hour at 450°C the cathode was converted and activated, and the diode sealed off at a pressure of less than 10^{-7} mm. The diode was mounted in the x-ray camera and life tested at a quiescent temperature of 875°C.

METHODS OF ANALYSIS

In the absence of a detectable surface layer, the oxide solid solution was always homogenous throughout and produced relatively sharp diffraction lines. Figure 2a shows an idealized representation of the 200 diffraction lines of (1) BaO, (2) equal molar (BaSr)O, and (3) SrO. The intensities are plotted both as a function of half the scattering angle 2θ and the molar composition. The breadth of the curves has been adjusted to correspond to an average value observed experimentally. If an oxide coating, initially equal molar (BaSr)O is heated at a high temperature, a preferential loss of BaO will occur near the surface and the shape of the intensity curve will change from that of (BaSr)O of Fig. 2a to the asymmetrical form as indicated in Fig. 2b. The peak of the curve represents the bulk composition of the coating while the asymmetry corresponds to scattering from BaO deficient coating layers near the surface.

The lattice constant, determined from the peak positions, was used to evaluate the bulk molar composition of the oxide solid solution which was assumed to vary linearly[2] between 5.523A for BaO and 5.143A for SrO. An experimentally determined correction was required[6] to compensate for line displacements due to absorption and to the large sample diameter. In spite of this correction it was occasionally observed that measurements of the lattice constant made from the diffraction lines of 2θ near 90° were not in agreement with measurements from the smaller 2θ lines, 111, 200, and 220. This discrepency was believed to be caused by a variation of bulk composition with depth since in these patterns the large 2θ lines always gave slightly lower compositions of SrO than did the smaller 2θ lines. Only the 111, 200, and 220 diffraction lines were used in these analyses in order that the bulk composition always be determined in the same manner. The accuracy with which the bulk molar composition could thus be determined varied with the crystal size of the oxide and with its resulting effect on the "graininess" of the diffraction lines but was in general between two and five percent.

A method of analysis has been devised which allows a calculation of the composition *vs.* depth

function to be made from the experimental intensity *vs.* composition curves. It is assumed that the variation of composition with depth below the surface is a monotonic function between the limits 100 percent SrO at zero depth and a known concentration (50 percent SrO in Fig. 2b) at the maximum depth from which x-ray scattering is observed.

For purposes of analysis, the oxide is assumed to possess a layered structure, in any layer of which the oxide is homogeneous in composition. Figure 3 shows a structure of this type consisting of layers A, B, C, $-$, $-$, having respective thicknesses l_A, l_B, l_C, $-$. An x-ray beam of total power P_0 incident upon the structure gives rise to sets of diffracted beams of power P_A, P_B, P_C, $-$, $-$. Each set corresponds to one of the allowed *hkl* diffraction lines of the oxide solid solution. Since the composition and hence the lattice constant of each layer was assumed to have a unique value the diffracted beams P_A, P_B, P_C, $-$, $-$, will each be scattered at slightly different angles with respect to the incident beam, P_0. The superposition of scattering from all layers gives rise to the asymmetrical diffraction line, Fig. 2b. When the composition increments distinguishing adjacent layers are sufficiently small, the experimentally observed diffraction lines can

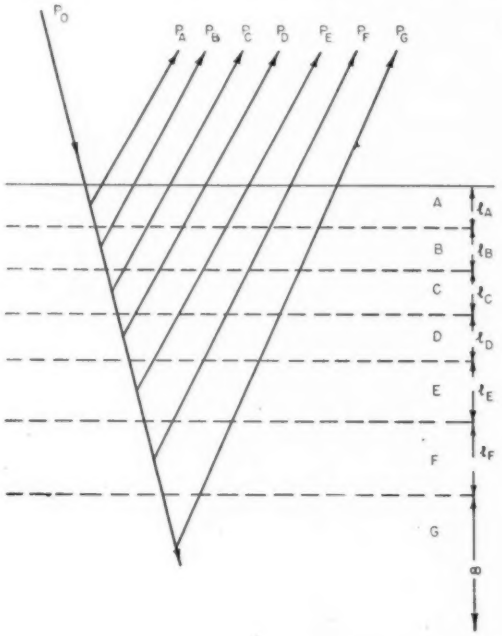

FIG. 3. Assumed layered structure of oxide coating at the external surface (see text).

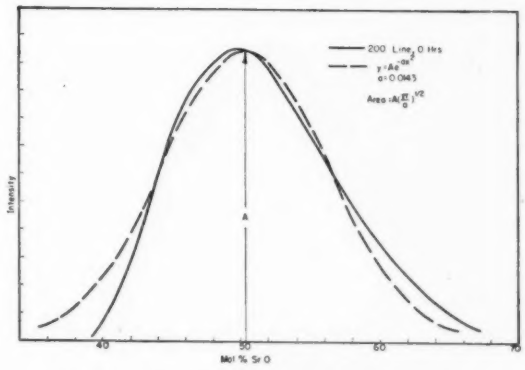

FIG. 4. Error curve fitted to experimental 200 diffraction line.

be synthesized by the summation of increments of power scattered by the various layers. Composition increments of five percent were found adequate to give a reasonable agreement with the experimental curves. These curves were synthesized by two methods which differed only in the form chosen to describe the angular distribution of intensity of the diffracted power increments. In one, the increments of diffracted power P_A, P_B, P_C, $-$, $-$, were represented by a set of Gaussian error curves, each having the same coefficient in the exponent as the original diffraction line from the completely homogeneous oxide (see Fig. 4). Error curves were of the form,

$$y = \mathbf{A} \exp(-ax^2), \qquad (1)$$

where **A**, the amplitude factor, is the height of the curve and a is the constant coefficient determined from the original diffraction line. Figure 4 shows an error curve fitted to the 200 diffraction line obtained from a homogeneous equal molar solid solution oxide. The obvious asymmetry of the diffraction line is caused[10,11] primarily by absorption in the sample. The coefficient a is a function of oxide crystal size, beam divergence, and sample dimensions. When once determined for the cathode at zero hours life, this factor should be applicable to diffraction lines from the same cathode taken later in life but under identical experimental conditions, assuming that crystal growth does not occur during the life test period.[6] With a knowledge of the coefficient a, the amplitudes $\mathbf{A}_i$ of the diffracted power

[10] A. Taylor and H. Sinclair, Proc. Phys. Soc. **57**, 108 (1945).
[11] B. E. Warren, J. App. Phys. **16**, 614 (1945).

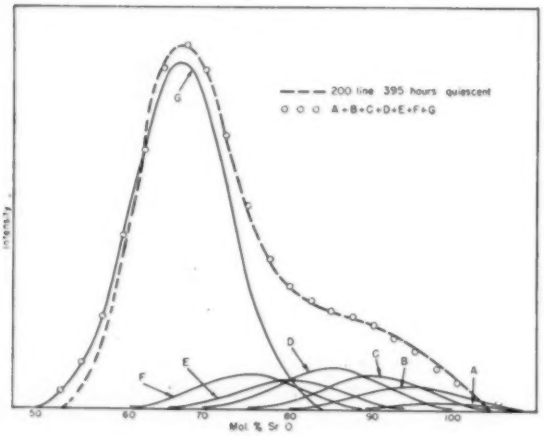

FIG. 5. 200 diffraction line shape synthesized from diffracted power increments A, B, C, $-$, $-$.

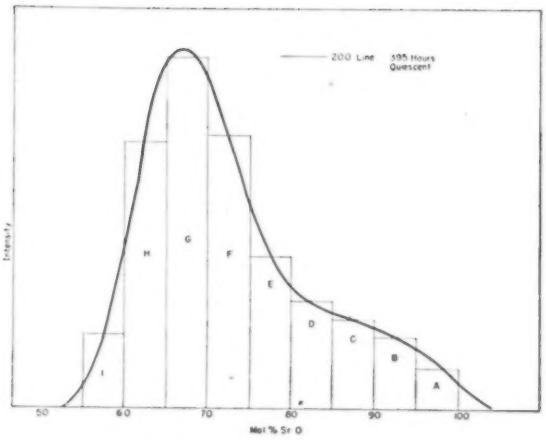

FIG. 6. 200 diffraction line shape synthesized from diffracted power increments A, B, C, $-$, $-$.

increments P_i are adjusted by successive approximations such that the sum of the ordinates at any point along the abscissae gives the best fit to the experimental intensity curve. In Fig. 5 the sum of these increments taken at intervals of $2\frac{1}{2}$ percent in composition are seen to be in good agreement with the observed experimental curve. The diffracted power increments are simply the areas under the separate curves labeled A, B, C, $-$, and,

$$P_i = \mathbf{A}_i(\pi/a)^{\frac{1}{2}}. \tag{2}$$

As we shall be interested only in the ratio of diffracted power increments from layers having similar a coefficients, the power increments are simply the amplitude factors $\mathbf{A}_i$.

A considerably simpler method of snythesis is illustrated in Fig. 6. In this, a step function is fitted to the experimental curve and the areas of blocks A, B, C, $-$, represent increments of power scattered by the corresponding layers of Fig. 3. As the 5 percent breadth of these blocks is considerably less than the *true* line breadth, little significance can be attached to blocks at the extremities of the curve, e.g., H and I of Fig. 6. A first-order correction can be made however by fitting blocks to the zero-hour curve, Fig. 4, and using the results of a similar analysis on this as a subtractive correction to be applied to subsequent curves. These two methods of synthesis will be referred to as the error function method and the step function method of fitting.

The total diffracted power which is recorded on the photographic film is

$$P_{\text{total}} = \sum_1^n P_i(\theta), \tag{3}$$

where

$$P_i(\theta) = A_i(\theta) P_i'(\theta), \tag{4}$$

and $P_i(\theta)$ is the total power arriving at the film, scattered by layer i into the diffraction cone of semi-apex angle 2θ; $P_i'(\theta)$ represents a similar increment of scattered power neglecting absorption and $A_i(\theta)$ is an appropriate correction for absorption in both the incident and diffracted beams. The form of this correction has been discussed[12] for the cylindrical sample case of a thin layer of unknown thickness overlying a second layer having a considerably greater thickness. The thickness of this surface layer can be computed if the ratio of power diffracted from the two layers is known.

In the present treatment, increments of *effective* scattered power P_i are treated in turn starting with P_A from the surface layer. Making use of the relationship[12] between the surface layer thickness and the scattered power ratio, there results,

$$\frac{P_A}{P_{\text{total}}-P_A} = \frac{N_A^2(F_A^2/\mu_A)}{N_K^2(F_K^2/\mu_K)} \times \frac{\int_0^{2\theta} \frac{1}{y}(1-\exp\{-\mu_A l_A y\})d\alpha}{\int_0^{2\theta} \frac{1}{y}\exp\{-\mu_A l_A y\}d\alpha}, \tag{5}$$

[12] A. Eisenstein, Bull. Am. Phys. Soc. **21**, No. 1, A-12, (1946); Phys. Rev. **69**, 252 (1946).

where

N = number of unit cells per unit volume,
F = molecular structure factor,
μ = linear absorption coefficient,
$y = (1/\sin\alpha) + (1/\sin[2\theta - \alpha])$,
2θ = scattering angle,
α = angle of incidence between primary beam and the tangent to the cylindrical surface, and
l_A = thickness of layer A.

The subscript A denotes properties of the surface layer and K represents an average of the properties of all underlying layers. A numerical evaluation was made[12] of the integrals of (5), as a function of $\mu_A l$ for the particular values of 2θ which are of interest in this analysis. Designating the ratio of integrals as S_1/S_2, then,

$$\frac{S_1}{S_2} = \frac{P_A}{P_{\text{total}} - P_A} \frac{N_K^2(F_K^2/\mu_K)}{N_A^2(F_A^2/\mu_A)}. \qquad (6)$$

A comparison of the power increment P_A from layer A with the power diffracted by all underlying layers, $P_{\text{total}} - P_A$, allows a determination of the layer thickness l_A. The diffracted powers P_B, P_C, P_D, $-$, can be lumped together as in (5) and (6) only if their $N^2(F^2/\mu)$ values are similar. As shown in Fig. 7b, this quantity varies by as much as 60 percent in the composition range 50 percent–100 percent SrO; however an error considerably less than this is introduced by selecting a weighted average value of $N^2(F^2/\mu)$.

Similarly P_B is compared with $P_{\text{total}} - P_A - P_B$ to obtain l_B or, as is usually done, P_A and P_B are lumped together $(P_A + P_B)$ and with an average $N^2(F^2/\mu)$ are compared with $P_{\text{total}} - P_A - P_B$ to obtain $(l_A + l_B)$. This process is repeated until the thickness of each layer has been evaluated.

TABLE I. Monode cathodes coated with C51-2 and operated quiescent.

Base Metal	Coating temperature °C	Hours	Bulk % SrO	Surf.
Gr. A Ni	800	300	51±2	none
Gr. A Ni	800	600	54±2	thin
Gr. A Ni	875	50	49±5	med. thin
Gr. A Ni	875	75	52±5	med. thick
Gr. A Ni	875	75	50±2	thick
Gr. A Ni	875	300	56±2	med. thick
Gr. A Ni	875	600	62±2	med. thick
Gr. A Ni	875	1200	62±1	very thick
N-81 Ni	875	280	52±1	med. thin
N-81 Ni	875	280	51±2	med. thin
N-81 Ni	875	600	56±3	med. thin
N-81 Ni	875	1200	58±1	medium

Finally l_A, $l_A + l_B$, $l_A + l_B + l_C$, $-$ are plotted as a function of composition to obtain the composition distribution curves.

RESULTS

An analysis of the diffraction patterns of the 16 cathodes of Group 1 which had reached the "end of life" showed that with one exception all oxide coatings had lost nearly all of the initial BaO content. These 15 coatings whose life test periods varied from 500 to 1000 hours had an average final bulk composition of 95±4 percent SrO. The one exception was a cathode prepared on a 5 percent Si-nickel base which had reached the "end of life" in 650 hours at 800°C under d.c. life test conditions. In this cathode a bulk composition of 52 percent SrO was found as well as a surface layer containing up to 95 percent SrO.

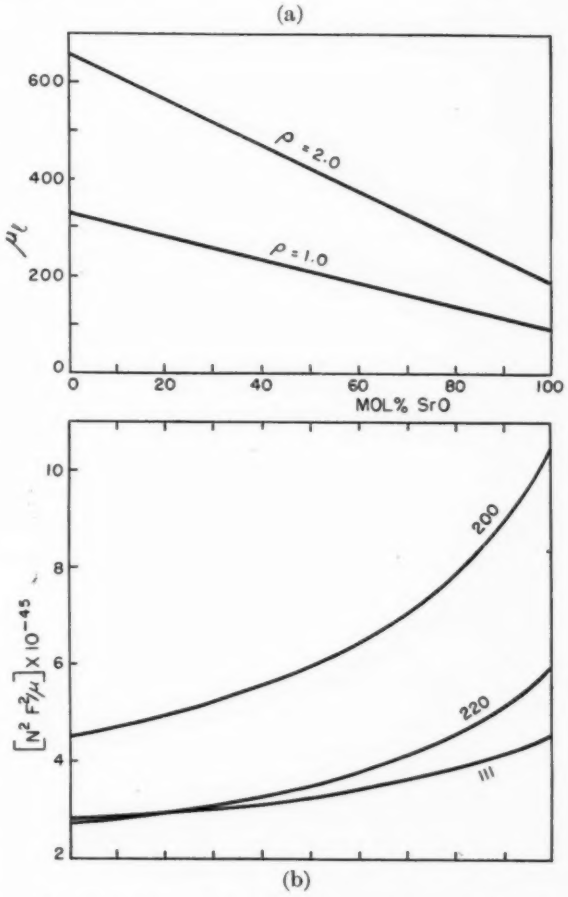

FIG. 7. (a) Computed linear absorption coefficient *vs.* composition for apparent densities ρ, of 1.0 and 2.0 g/cm³, and (b) computed N^2f^2/μ *vs.* composition for 111, 200, and 220 diffraction lines.

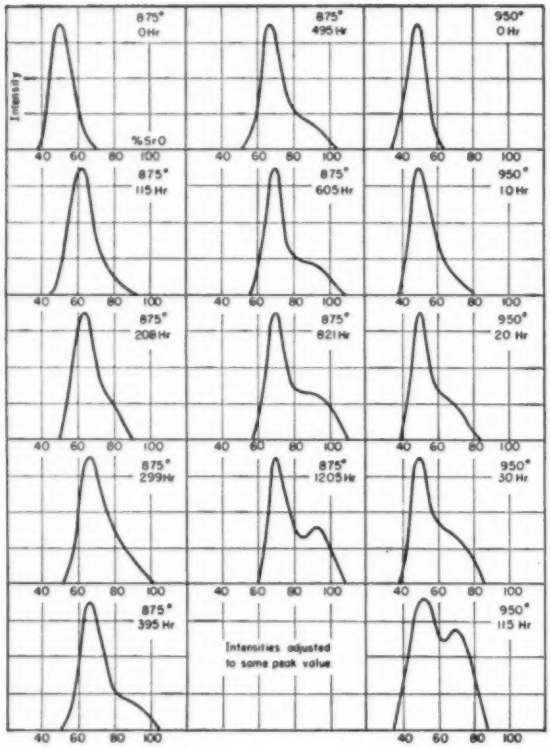

FIG. 8. 200 diffraction lines from cathodes 1 and 2 of Table II.

TABLE II. Diode cathode coated with C51–2 and operated quiescent.

Grade A nickel base (1) 875°C—pumped Bulk % SrO		Grade A nickel base (2) 870°C—pumped Bulk % SrO		Vacuum fired Grade A Ni base (3) 950°C—pumped Bulk % SrO		Vacuum fired Grade A Ni base (4) 875°—sealed off Bulk % SrO	
Hours	SrO	Hours	SrO	Hours	SrO	Hours	SrO
0	50	0	50	0	50	0	50
13	50±1	27	50	10	51±1	34	47±1
33	54±1	115	61±3	20	50±2	75	50±1
64	59±3	260	64±1	30	54±4	147	48±2
115	62±4			40	52±1		
208	65±3			50	52±1		
299	67±3			72	52±1		
395	67±3			115	49±2		
495	67±4						
605	69±4						
821	68±2						
1205	70±1						

Table I shows the results obtained from an analysis of the diffraction patterns taken of the cathodes from the twelve monodes of Group 2 which were life tested in a quiescent state. In those patterns which showed a marked asymmetry in the shape of the diffraction lines, measurements of the peak positions were used to determine the bulk composition. The indicated ± error represents the average deviation of the measured 111, 200, and 220 lines of the diffraction pattern and does not represent the absolute accuracy of the determination.

In general, it appears that the bulk loss of BaO as well as the surface loss is slightly less for the cathodes prepared on the purer nickel base. This is consistent with the presence of larger amounts of the reducing impurities Mn, Mg, and Si in the grade A nickel than in N-81 which were detected in a spectroscopic analysis. The effect of the operating temperature on the bulk loss of BaO is indicated by comparing the molar compositions of the grade A cathodes operated 600 hours at 800°C and at 875°C. A thicker BaO deficient surface layer is found on the cathodes operated at 875°C than on those at 800°C.

In the experiment designed to investigate the effect of a d.c. emission current density of 0.5 amp./cm² on the loss of BaO, Group 3, the following results were obtained. In 40 hours at a temperature in excess[13] of 950°C, a thick surface layer was observed on all of the seven cathodes. The four which were operated quiescent had a final average bulk composition of 63±4 percent SrO and the three life tested at 0.5 amp./cm² showed a bulk composition of 61±3 percent SrO. It is evident that the effect of the d.c. emission current is less than the experimental error involved in the composition determination. The error introduced into both the bulk and surface layer determinations could be reduced by using a lower operation temperature thus avoiding excessive crystal growth in the oxide coating and the resulting "graininess" in the diffraction patterns.

Time changes which occur in the bulk composition of the oxide coating are shown in Table II and were obtained from diffraction patterns of cathodes operated in the pumped and sealed off beryllium windowed diodes, Group 4. The effect of the base metal on the bulk loss of BaO is seen by comparing the three diodes operated at about 875°C. The vacuum fired grade A base cathode shows no loss of BaO in 147 hours at which time the regular grade A cathodes have increased to over 60 percent SrO. The second vacuum fired grade A base cathode shows no

[13] All cathodes were initially set at 950°C but line voltage fluctuations in an overnight life test caused all cathode temperatures to increase by an unknown amount.

detectable BaO bulk loss in 115 hours at 950°C. All four cathode sleeves were chemically cleaned and hydrogen fired prior to coating. Two of these were heated to 1050°C for 30 minutes in the additional vacuum firing treatment. The effect of this process is to evaporate possible reducing agents from the surface of the base metal. A spectroscopic analysis of the evaporated material shows it to contain major quantities of Mg, Mn, Cu, and Ni. All cathodes of this group showed asymmetrical diffraction lines indicating some surface loss of BaO as well. Cathodes 1 and 2 of Table II, Group 4, showed a more rapid loss of BaO than similar cathodes of Table I, Group 2. No completely satisfactory explanation was found for this difference.

The effect of time and temperature on the shape of the 200 diffraction line from initially equal molar BaSr(O) may be seen in Fig. 8. Microphotometer tracings converted to units of intensity and adjusted to the same maximum value are shown plotted as a function of the molar percent SrO composition. The grade A nickel base cathode operated at 875°C shows a progressive asymmetry change with time as well as a shift in the position of the peak (see Table II). The vacuum fired grade A nickel base cathode at 950°C shows only the progressive asymmetry which develops at a rapid rate.

By means of the analysis method previously described, the intensity *vs.* composition functions of Fig. 8 have been transposed to the composition *vs.* depth functions of Fig. 9. The error function method of synthesizing the 875°C curves results in the composition distributions of Fig. 9a. In 115 hours a layer containing less than 10 percent BaO is found to cover the surface to a depth of 10^{-5} cm while in 1205 hours this layer has reached a thickness of 3×10^{-4} cm. At this period a layer of pure SrO covers the surface to a depth of about 5×10^{-5} cm. The simpler step function method of analysis when applied to the same curves gives the distributions of Fig. 9b. Applying the zero hour, fortuitous curve as a subtractive correction to each of the other curves brings the results into fair agreement with the distributions obtained using the more laborious error function method. An analysis of the 950°C intensity curves using the step function method may be seen in Fig. 9c. The bulk composition remains equal molar as the BaO deficient surface layers take form.

As a check on the validity of this method of composition determination, analyses were per-

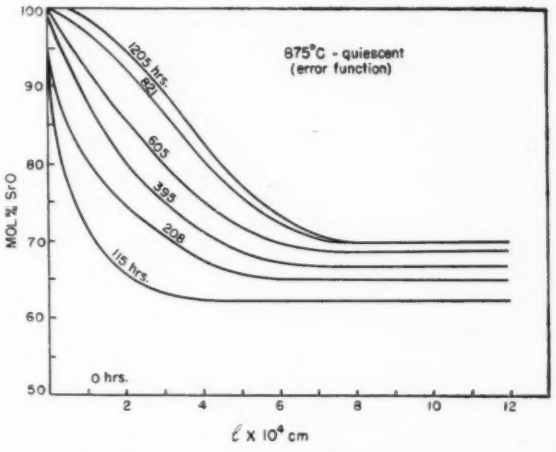

FIG. 9a. Composition *vs.* depth function, determined using error function method of fitting, 875°C.

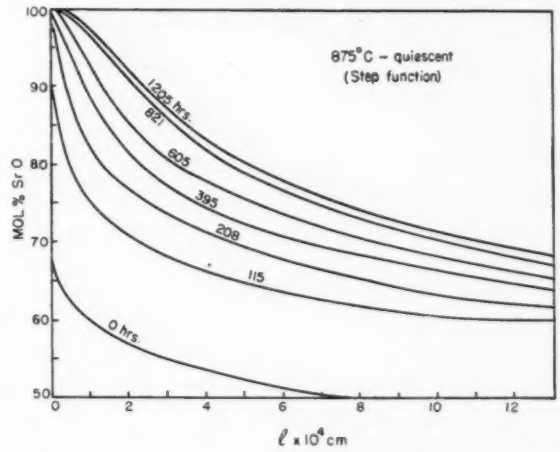

FIG. 9b. Composition *vs.* depth function, step function method of fitting, 875°C.

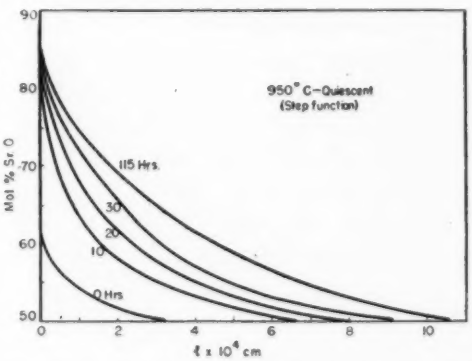

FIG. 9c. Composition *vs.* depth function, step function method of fitting, 950°C.

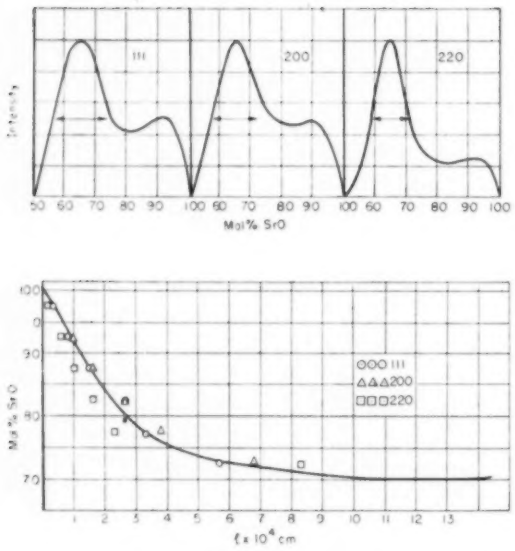

FIG. 10. (a) 111, 200, and 220 diffraction lines from cathode after 1225 hours quiescent at 875°C. (b) Composition *vs.* depth functions computed from these lines.

formed on three different diffraction lines of the same pattern. Figure 10a shows the intensity *vs.* composition traces of the 111, 200, and 220 diffraction lines from a cathode, initially equal molar BaSr(O), after 1225 hours at 875°C, quiescent. The marked effect of the scattering angle and the particular *hkl* reflection on the line shape is readily evident. Arrows at the half-maximum position indicate the true line breadth extrapolated from the measured breadth of nearby[6] large crystal tungsten lines. The principal peak of these curves corresponds therefore to a single homogeneous phase in accord with the initial assumption regarding this structure. Analyses performed on these three curves using the step function method result in the distributions of Fig. 10b. The agreement between the computed distributions indicates the self-consistency to be expected from this method of analysis using different diffraction lines. This agreement serves also as a reasonable confirmation of the assumed monotonic distribution function. Actually, the BaO content of the coating may be very low[14] in the oxide layers adjacent to be base metal because of the chemical affinity of Ba and certain base metal components.[15] In general, these layers contribute very little to the observed diffracted intensity as evidenced by the weak scattering from the adjacent base metal.

[14] L. A. Wooten, Bull. Am. Phys. Soc. **21**, D-3 (1945).
[15] A. Fineman and A. Eisenstein, "Studies of the interface of oxide coated cathodes," J. App. Phys. **17**, 663 (1946).

DISCUSSION

The loss of the BaO component of an oxide cathode coating initially equal molar (BaSr)O manifests itself as (1) a surface deficiency and (2) a bulk deficiency. It appears that, given sufficient time, all cathodes will develop a surface deficiency which is detectable using x-ray techniques. In this time interval the bulk loss may or may not be sufficient to permit its detection, depending upon the base metal used and the operating temperature (see Table I). The loss of BaO may occur as an evaporation of Ba or BaO. In either case the loss is presumably from the surface; hence, unless the temperature is sufficiently high to permit rapid diffusion of BaO or SrO, changes in the surface composition should be very sensitive to this evaporation loss. The results of Table II would seem to indicate that the removal of certain surface constituents from the base metal by the vacuum firing treatment eliminates the bulk loss without seriously impairing the loss from the surface. A comparison of the cathodes of Table I made on grade A nickel and run at 875°C with those made on the purer nickel, N-81, shows the effect of the base metal on the bulk loss and a lesser effect on the surface loss. This would seem to indicate that the bulk loss arises largely from a chemical reaction between the coating and reducing agents in the base metal, giving rise to free barium which diffuses to the surface and is lost through evaporation. Although a surface deficiency is found in cathodes made on the pure nickel, the observation that it is less than in cathodes made on grade A nickel indicates that at least part of the surface loss in the grade A cathode is caused by evaporation of Ba. Reducing impurities present initially in the coating may be responsible for this surface loss. The exact mechanism of the respective surface and bulk losses cannot be specified completely until more information is available regarding the diffusion rates of Ba, Sr, BaO, and SrO at these temperatures as well as the thermochemistry of the reactions involved. It is interesting to note that the surface deficiencies extend to depths of about 10^{-3} cm or

roughly 0.1 of the total coating thickness. In the case of cathodes "flashed" at a high temperature to promote crystal growth,[6] the observed composition variation probably occurs in single crystals on the cathodes surface. It should be noted that an experimental upper limit exists on the composition *vs.* depth function that can be determined using this method. This is reached when scattering from the surface layers obscures the prominent peak from the bulk composition. This condition is nearly reached in the 115 hour, 950°C curve of Fig. 8. A lower limit of about 10^{-5} cm is indicated.

The effect of changes in the BaO-SrO composition during life on the thermionic emission properties of the cathode remains problematical. No direct evidence has yet been obtained to prove the existence of such an effect although several indirect experimental observations would seem to substantiate it. The experiments of Benjamin and Rooksby[4] using d.c. thermionic emission cathodes, and Widell,[16] using pulsed cathodes, indicate an optimum coating composition of near equal molar proportions. However, through the use of a high current density aging treatment, Fineman[17] has been able to obtain a pulsed emission at 850°C to 900°C of 30 amp./cm² from a pure SrO coating and 60 amp./cm² from pure BaO, the latter value being in substantial agreement with that reported[10] from (BaSr)O. Recent measurements of Nishibori and Kawamura[18] give for the thermionic work functions of BaO and (BaSr)O about 1.0 ev and SrO 1.5 ev and for the conductivity activation energies (BaSr)O, 0.7 ev and SrO, 1.2 ev. The presence of a surface layer, deficient in BaO, *may* have an electronic conductivity somewhat lower than that of the bulk and, under certain conditions of operation, actually limit the thermionic emission.

The author is indebted to members of the Cathode Research Group for valuable assistance during the course of this investigation, particularly to Mr. A. Fineman who contributed most of the standard diode cathodes used in this study.

[16] E. G. Widell, Bull. Am. Phys. Soc. **21**, E2 (1946).

[17] A. Fineman, private communication.

[18] E. Nishibori and H. Kawamura, Proc. Phys. Math. Soc. Japan **22**, 378 (1940).

Studies of the Interface of Oxide Coated Cathodes*

A. FINEMAN AND A. EISENSTEIN

Radiation Laboratory, Massachusetts Institute of Technology, Cambridge, Massachusetts

X-ray diffraction patterns are presented as evidence for the existence of a crystalline "interface" compound between the base metal and the coating of the oxide coated cathode. Measurements of the coating resistance to microsecond pulse currents, made with imbedded probes, indicate the presence of an anomalous "interface" resistance between the metal and coating. The relative magnitude of the coating and interface resistances are shown as a function of current for various operating temperatures.

I. INTRODUCTION

WHEN a system consisting of a metal coated with alkaline earth carbonates is heated in a vacuum, some combination of the metal and alkaline earth element takes place. The nature of the interface compound formed in the case of the oxide coated cathode has been postulated by various workers[1] to be of the Type ABO_n where A is the alkaline earth element and B, the base metal (e.g., $BaPtO_n$, $BaNiO_n$, $BaTiO_n$). Arnold states that $BaPtO_3$ was identified on a Pt wire cathode but gives no indication of the method by which it was identified. The other estimates were based upon chemical or spectrographic determinations of the presence of the base metal in the coating layers close to the metal. Direct evidence, in the form of x-ray diffraction patterns, is presented in this paper to show that specific crystalline compounds are formed at the metal-coating interface of oxide-coated cathodes. The coating resistance to pulsed microsecond

* This paper is based on work done for the Office of Scientific Research and Development under contract OEMsr-262 with the Radiation Laboratory, Massachusetts Institute of Technology.

[1] H. D. Arnold, Phys. Rev. **16**, 70 (1920). A. Gehrts, Zeits. f. tech. Physik **11**, 246 (1930). L. A. Wooten, Bell Telephone Laboratory, private communication.

currents is shown to be anomalous in the region of the coating close to the metal. This anomalous resistance, which is termed interface resistance, greatly exceeds the coating resistance in most of the cases examined.

II. EXPERIMENTAL METHODS

A. X-Ray Diffraction Studies

The method used in obtaining x-ray diffraction patterns of oxide coated cylindrical cathodes has been described in detail.[2] The vacuum diode containing the cathode to be examined was opened in an atmosphere of dry nitrogen because of the chemical instability of certain of the interface compounds. The cathode coating was scraped off until the interface became exposed, and the cathode was coated with a protective wax. The specimen was mounted in a 4.70-cm radius x-ray camera and the exposure made using filtered Cu$K\alpha$-radiation. In some cases only half of the cathode was dipped into the wax, and patterns were then taken of the waxed and non-waxed portions in order to check the stability of the interface compound to oxidation by air or water vapor.

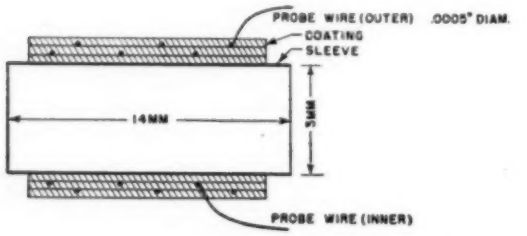

FIG. 1. Construction of double probe cathode.

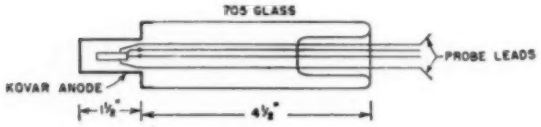

FIG. 2. Experimental diode.

B. Resistance Measurements

Coating and interface resistance measurements were made by the use of embedded probes.[3] Figure 1 illustrates the construction of the double probe cathode. The cylindrical sleeve was weighed, mounted in a rotatable chuck, sprayed with carbonate coating, and re-weighed. Several turns of probe wire were tightly wound around the coating and a second layer of carbonate coating was sprayed on. The cathode was again weighed and the process repeated with a second probe wire.

Figure 2 illustrates the test diode in which measurements were made, and Fig. 3 shows the electrical circuit. Determinations of pulsed anode voltage V_A, microsecond pulse current I, and probe pulse potentials (V_{P1}, V_{P2}) were made as indicated. The total resistance from the sleeve

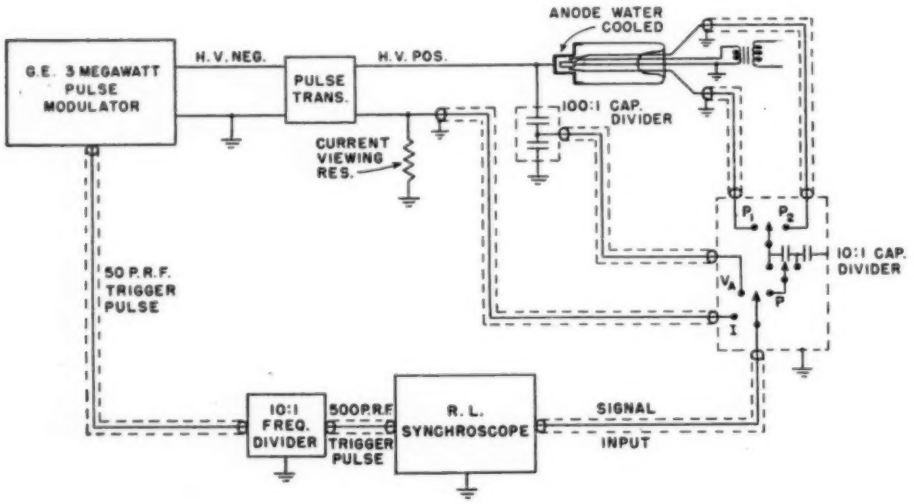

FIG. 3. Measuring circuit.

[2] A. S. Eisenstein, "A study of oxide cathodes by x-ray diffraction methods" (preceding article, this issue).
[3] E. Nishiburo and H. Kawamura, Proc. Phys. Math. Soc. Japan **22**, 378 (1940). W. E. Danforth, Bartol Research Foundation, private communication.

to each probe was obtained by dividing the corresponding probe potential by the current. The difference between these two resistances was taken as the resistance of the amount of coating lying between the probes. The resistance of the coating between the sleeve and first probe was then computed on the basis of simple weight proportion, and the substraction of this amount of coating resistance from the total resistance between sleeve and first probe gave the quantity which was termed interface resistance, R_i. The quantity $R_{c(10)}$ was defined as the resistance of 10 mg of coating. All cathodes were prepared with an area of 1 sq. cm.

III. RESULTS

Interface patterns were found on all coating, base-metal systems examined. These included base metals of copper, pure and Grade "A" nickels, chromium plated nickel, and alloys of Si-nickel and Cr-nickel.

A. Grade "A" and Pure Nickel Base Metals

The interfaces formed on Grade "A" nickel were light grey in color and usually too thin to give analyzable patterns with the x-ray technique used. In the case of the pure nickels a consistent pattern was obtained. However, because of the difficulty of obtaining good diffraction patterns of the interfaces on the pure and Grade "A" nickels, and since the interfaces observed on

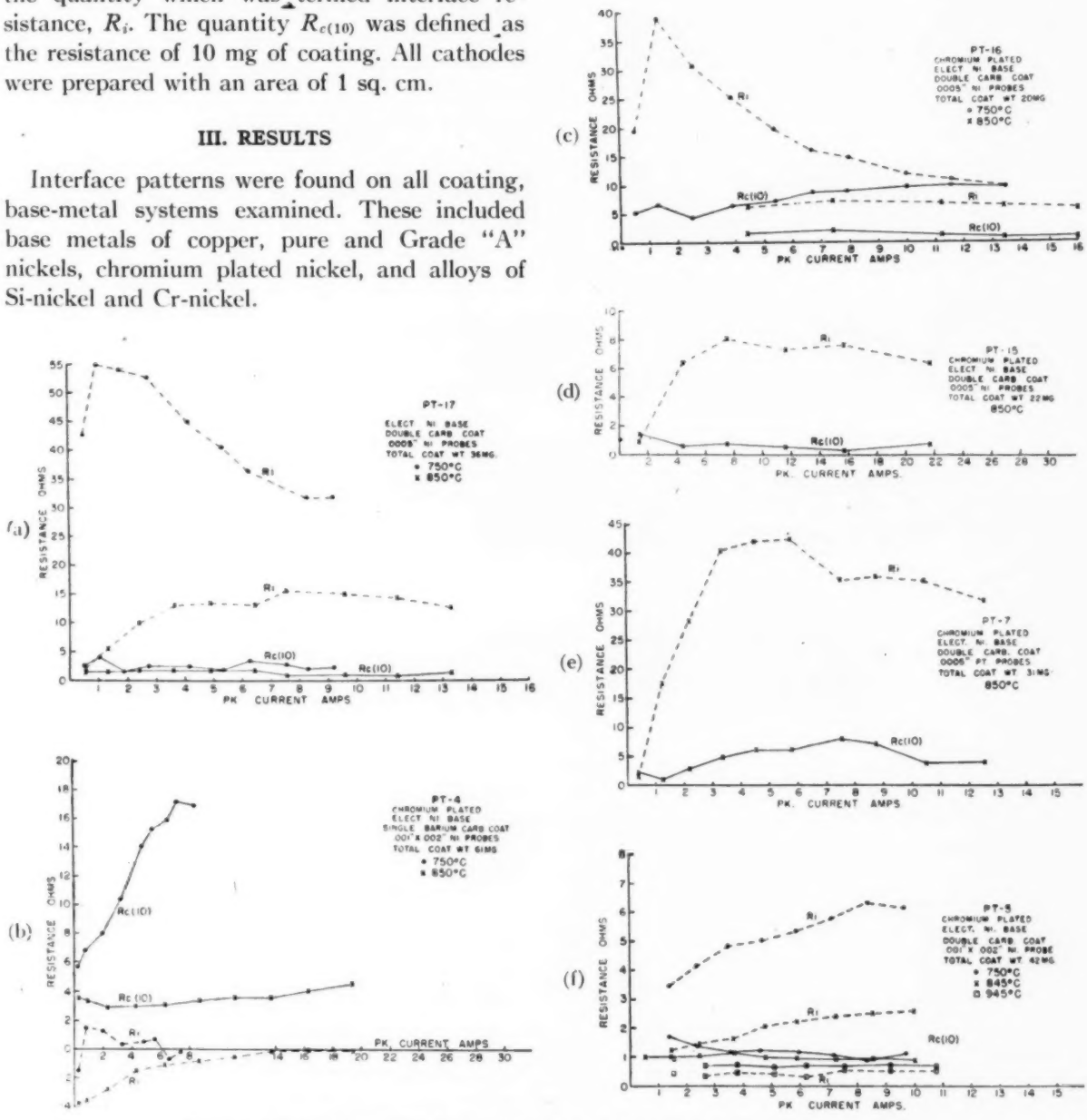

FIG. 4. Coating resistance $R_{c(10)}$ and interface resistance R_i *versus* peak current I.

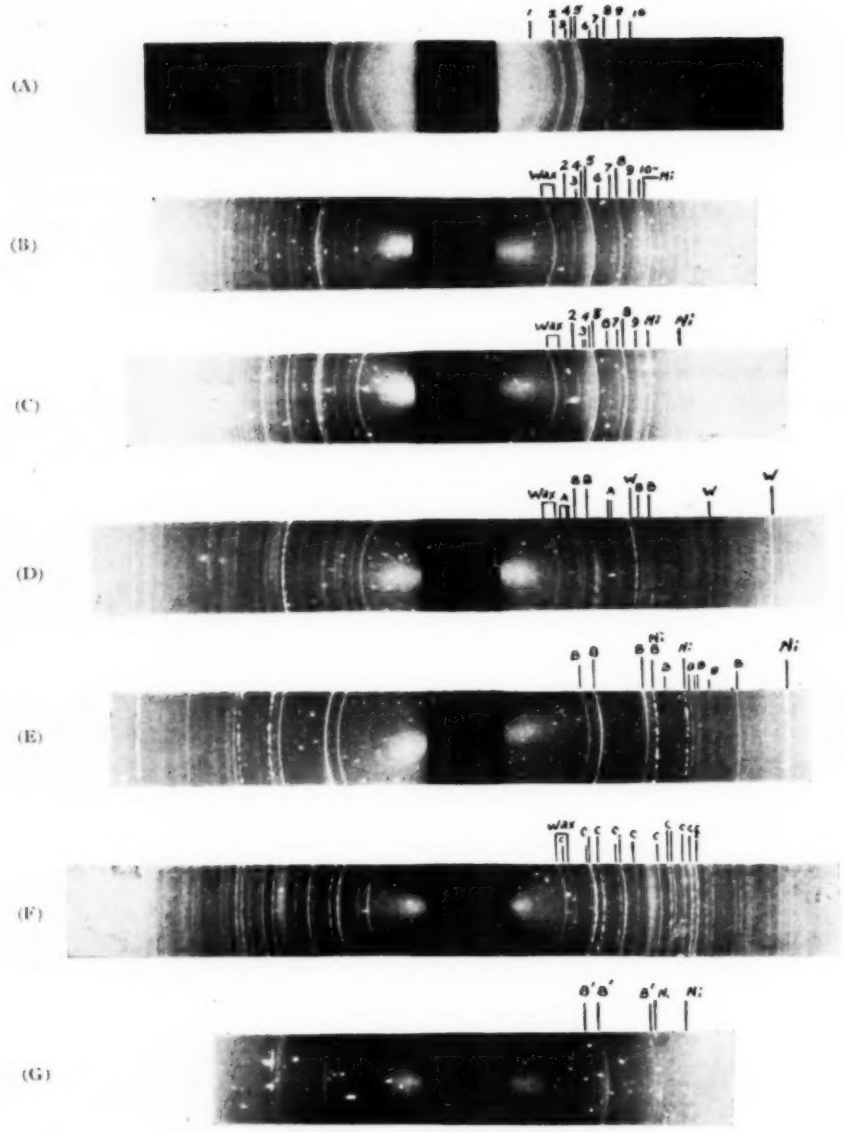

FIG. 5. X-ray diffraction patterns of interfaces:

(A) Synthetic "$BaSiO_3$" prepared by heating $BaCO_3$ and SiO_2 in air, ½ hour at 1000°C (0.5 mm sample diameter);
(B) "$BaSiO_3$" found at interface of cathode made from $(BaSr)CO_3$ on 5 percent Si-Ni base;
(C) Compound found at interface of cathode made from $SrCO_3$ on 5 percent Si-Ni base;
(D) Interface compounds "*A*" and "*B*" from cathode of $BaCO_3$ on Cr plated Ni;
(E) Interface compound "*B*" from cathode of either $BaCO_3$ or $(BaSr)CO_3$ on Cr plated Ni;
(F) Interface compound "C" from cathode of $BaCO_3$ on Cr plated Ni;
(G) Interface compound from cathode of $SrCO_3$ on Cr plated Ni.

cathodes made of Cr and Si nickel alloys[4] were consistent and more easily identified, these latter systems were chosen in preference to Grade "A" and pure nickels for the more extensive studies of the interface. Figure 4a shows a plot of the interface and coating resistances as a function of microsecond pulse current for a pure nickel cathode coated with $(BaSr)CO_3$.[5] The data given are for pyrometer temperatures of 750°C and 850°C. It is noted that the coating resistance is essentially ohmic, and that the interface resistance which greatly exceeds the coating resistance has a decided maximum which shifts to lower currents as the temperature is decreased. The dependence of resistance upon temperature is seen to be more pronounced in the case of the interface than in that of the coating.

B. Interface Compounds Formed on Si-Ni Alloy Base Metal

Cathodes prepared from double carbonate $(BaSr)CO_3$ on 2 percent or 5 percent SiNi alloy showed an interface pattern identifiable with

[4] All pure nickels and alloys used in this work were obtained through the kind cooperation of Mr. E. M. Wise of the International Nickel Company.

[5] Coating C51–2 obtained from the Raytheon Manufacturing Company, Newton, Massachusetts.

that of synthetically prepared $BaSiO_3$[6] (see Figs. 5A and 5B). The *d* values of the interface and synthetic compounds are compared in Table I. The synthetic $BaSiO_3$ was white while the interface "$BaSiO_3$" showed varying shades of grey, probably because of the interspersion of finely divided nickel. Although $(BaSr)CO_3$ coated cathodes at different states of activity and at d.c. and microsecond pulsed life from 0 to 500 hours were examined for interface patterns, the "$BaSiO_3$" pattern alone was observed in every case. This interface compound was stable to both air or water exposure.

One cathode was prepared with pure $SrCO_3$[7] substituted for $(BaSr)CO_3$ on the 5 percent Si-Ni alloy. The interface compound here was similar in crystal structure to "$BaSiO_3$" but had consistently smaller *d* values, caused probably by the direct replacement of Ba with Sr in the compound. See Fig. 5C. No resistance measurements were taken on these systems.

C. Interface Compounds Formed on Cr Plated Nickel

In the case of cathodes prepared of $BaCO_3$ on Cr plated pure nickel three separate interface compounds were identified. Their diffraction patterns did not correspond to any compounds of Ba and Cr listed in the ASTM x-ray diffraction card file. These compounds which are here arbitrarily designated as "*A*," "*B*," and "*C*" made their appearance at various levels of cathode activity and life (see Figs. 5D, E, and F).[8] The interface compounds were all clearly visible and colored. Those interfaces in which only "*B*" was detected showed homogeneous light or dark browns and in some cases brown mottled with green. "*A*" was never found alone, and "*C*" in the one case in which it was found alone showed dark brown. Both "*A*" and "*C*" were converted to "*B*" upon exposure to air. "*B*" was stable to both air and water at room temperature and was not affected by heating in air at 850°C for 15 minutes. Analyses of the "*B*" compound with the Davey-Hull charts indicated a possible close packed hexagonal structure with the *d* values given in Table II.

Cathodes prepared with $SrCO_3$ on Cr plated nickel showed an interface compound having a crystal structure similar to that of "*B*" but with somewhat smaller lattice constants. (See Fig. 5G.)

In the case of cathodes prepared of $(BaSr)CO_3$ on Cr plated nickel, only the "*B*" compound was identified. It is to be noted that as in the Si series, where both Ba and Sr were present in the coating, the Ba, alone, took part in the formation

TABLE I. Observed *d* values and line intensities of the interface and synthetic $BaSiO_3$ compounds.

Interface		Synthetic $BaSiO_3$	
d	*I*	*d*	*I*
4.14	*M*	4.11	*M*
3.38	*S*	3.36	*S*
3.11	*M*	4.09	*MW*
2.97	*VS*	3.97	*VS*
2.89	*VS*	2.87	*VS*
2.67	*VW*	2.66	*W*
2.47	*W*	2.48	*VW*
2.38	*MW*	2.38	*M*
2.21	*MW*	2.20	*M*
2.06	*M*	2.07	*M*
1.865	*W*	1.875	*MW*
1.82	*W*		
1.73	*W*	1.725	*M*
1.67	*M*	1.66	*W*
1.43	*W*		
1.41	*W*		

TABLE II. Compound "*B*" indices from Davy-Hull chart for simple hexagonal system.

Computed values		Compound "B"	
Indices	*d*	*d*	*I*
101	3.19	3.21	*VS*
110	2.89	2.91	*S*
200	2.50	2.50	*VW*
201	2.14	2.16	*S*
002	2.08	2.08	*M*
102	1.92	1.92	*M*
121	1.72	1.725	*M*
112	1.69	1.690	*M*
202	1.60	1.615	*MW*
122	1.46	1.415	*W*
003	1.385	1.340	*M*

Computed *d* values for $a_0 = 5.77$, $c/a = 0.72$.

[6] Finely powdered SiO_2 and $BaCO_3$ mixed in bulk and heated in air or vacuum to 850° to 1000°C. See W. Jander, Zeits. anorg. allgen. Chemie **163**, 8 (1927).

[7] Contained less than 0.01 percent Ba. Prepared by C. D. Prater, Bartol Research Foundation, Swarthmore, Pennsylvania.

[8] Bulk synthesis of the barium-chromium interface compounds, *A*, *B*, and *C*, was attempted by heating the following combinations: (*a*) 150-mesh chromium powder and barium carbonate, (*b*) chromium powder and barium chromate, and (*c*) chromium oxide (Cr_2O_3) and barium carbonate. Samples were heated in vacuum and in the air, at temperatures of 850°C and 1050°C, for times varying between 30 minutes to several hours. None of the interface compounds, *A*, *B*, or *C*, were observed in any case.

of the interface compound. The "*B*" compound was also identified in cathodes prepared with $(BaSr)CO_3$ on 5 percent CrNi alloy.

Plots of $R_{c(10)}$ and R_i *vs.* I for a cathode composed of $BaCO_3$ on Cr plated nickel are shown in Fig. 4b. Here, the coating resistance exceeded the interface resistance, and showed more dependence on temperature. Figures 4c, d, e, and f show resistance *vs.* current curves for four cathodes made of $(BaSr)CO_3$ on Cr plated nickel. Each of these tubes showed the Type "*B*" interface. It may be noted that usually the interface exceeds the coating resistance and is more temperature dependent than is the coating resistance in the range studied. Figure 4f shows, however, that the interface resistance may drop below the coating resistance at elevated temperatures. Variations in coating resistance from tube to tube are seen to be much smaller than corresponding variations in interface resistance.[9]

IV. DISCUSSION

The plots of coating and interface resistance shown above suggest that the interface may be a factor which enters into the limitation of pulsed emission in oxide coated cathodes.

The interface resistance curves of Fig. 4 when plotted against the voltage drop across the interface (IR_i), are similar in shape and in variation with temperature to those exhibited by multiple

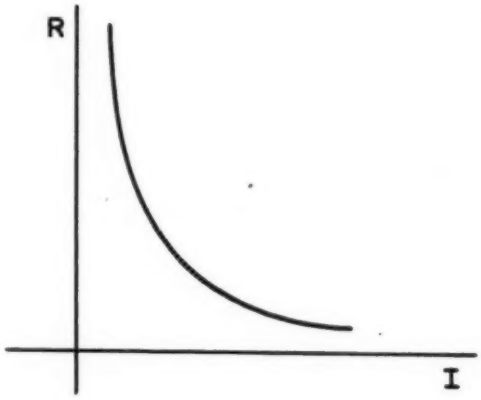

FIG. 6.

layer oxide rectifiers.[10] Since, in addition to this fact the x-ray data show the presence of a definite crystalline compound between the coating and the base metal, it is suggested that the oxide coated cathode is dependent for its operation upon the same physical structure (metal +blocking layer+semiconductor) as is present in the oxide rectifier.

The authors wish to express their gratitude to Dr. E. A. Coomes and members of the Cathode Research Group for their helpful suggestions and invaluable aid throughout the course of this investigation.

[9] The *R vs. I* curves shown were all obtained with either nickel or platinum probe wires. Tubes were also made with probes of Rh-Pt alloy, pure Fe, pure W, and pure Cu. In these cases and also in the case of some of the nickel and platinum probe tubes the *R vs. I* curves were of the type shown in Fig. 6.

All tubes exhibiting this type of characteristic on either one or both probes were discarded for the following reason: impedance measurements at 1 megacycle, taken between sleeve and probe, showed that the tubes having a peaking *R vs. I* (Fig. 4) characteristic, demonstrated a shunt resistance which fell from megohms at room temperature to hundreds of ohms at 850°C, while the tubes showing a dropping *R vs. I* characteristic (Fig. 6) maintained a shunt resistance of megohms throughout this temperature range. The latter phenomenon was interpreted as meaning that in these cases the probe was electrically insulated from the coating.

[10] N. F. Mott, Proc. Roy. Soc. **A171**, 127 (1939).

Midwest Research Institute—A New Scientific Research Institution

BY GEORGE E. ZIEGLER

Executive Scientist, Midwest Research Institute, Kansas City, Missouri

DURING the past year a new scientific research institution placing emphasis on research in physics and its closely related sciences has come into being in Kansas City, Missouri. The Midwest Research Institute a year ago was just the dream of Middle America's business men; now it is a going scientific institution with a staff of over ninety working on both research for industry and on regional research to benefit the people of Middle America as a whole. The Institute's research program is balanced between physics, with its closely associated engineering sciences, and chemistry, with its many branches. It is the purpose of this article to describe briefly the Midwest Research Institute and to illustrate how its well-coordinated physical research and measurements groups serve as the mainstay for many types of engineering and chemical research, as well as for industrial physics research.

In 1943 a group of public-minded business men saw the need for an outstanding scientific institution of broad base to aid in the region's forthcoming industrial development. They crystallized their vision by calling to a Midwest Research Council meeting leading research men from the Middle Western universities and colleges, as well as state geologists and business people familiar with the research needs and potentialities of the region. Following through on their first step this group of men, under the far-seeing guidance of Mr. Robert L. Mehornay and Mr. J. C. Nichols—business men and civic leaders of the Kansas City Area—contributed over $500,000.00 in 1944 to serve as an initial operating fund for the new institution.

The soundness of the vision of this group of business men made it possible to attract experienced personnel to the Institute for both administrative and laboratory research work. At the present time this same group of business men, now organized as a group of trustees with a board of governors from their own number, has embarked on a much larger fund raising campaign to enable the Institute to increase still further its facilities and to increase significantly its program of regional research so that Middle America will be assured of benefits that can result from research.

PLAN OF ORGANIZATION AND STAFF

The establishment of Midwest Research Institute by its Board of Governors and Trustees as a not-for-profit, scientific institute standing on its own feet gives it a unique opportunity for service. It has the advantage of being able to cooperate with all the universities and colleges throughout the area at the same time it renders research service to industry and government.

FIG. 1. High speed photographic study of chip formation with different cutting tools.

FIG. 2. 120,000-pound tensile testing machine in operation in the engineering mechanics laboratory.

This was demonstrated recently when it sponsored a seminar on high polymers. This two-day seminar was attended by the senior staff members of fourteen universities and twenty-five industrial concerns.

The Midwest Research Institute secured as its president Harold Vagtborg, whose pioneering spirit and vigorous organizational ability brought Armour Research Foundation, Chicago, to its outstanding position among research organizations. The basic plan of operation of the Midwest Research Institute organization provides for a full utilization of his stimulating leadership.

Frank H. Trimble, chairman of the Physics Section, received the Ph.D. degree from the University of Missouri for his work in x-ray diffraction before going to the Armour Research Foundation in Chicago. Here he first supervised extensive research in physical metallurgy and then served as co-chairman of physics research.

The chairmen of Agricultural Chemistry, Inorganic Chemistry, and Organic Chemistry Research are Charles L. Shrewsbury, formerly of Purdue University; George W. Ward, of the National Bureau of Standards; and Carl M. Marberg, formerly of Interchemical Corporation. The Engineering Mechanics staff is under the chairmanship of Martin Goland, formerly of Curtiss-Wright Corporation Research Laboratories, with C. O. Dohrenwend, formerly Chairman of Engineering Mechanics Research at the Armour Research Foundation, as Research Consultant.

The present staff of ninety-two consists of fifty-two research workers, twenty of whom have the Ph.D. degree, seven the master's degree, and twenty-five the bachelor's degree. There are also sixteen laboratory and technical assistants, and twenty-four non-technical employees.

In its general plan of operation the Institute consists of a modern streamlined industrial research organization in which decisions concerning research methods and research expenditures are made by men as close as possible to the actual work. The research group leader on a particular project makes day by day decisions as to what research procedures shall be followed and what equipment procured. The chairman of a section thus can devote his major attention to "quality control" of the research and to looking after the sponsor's interests.

Since Midwest Research Institute is a public service, not-for-profit scientific institution it has heavy responsibilities to the community as a whole. The broad direction of the Institute's program to benefit the people of Middle America, as well as helping American industry solve its specific problems, is a major responsibility of the Institute's president, in addition to those normally incumbent on a chief executive officer.

The author, as Executive Scientist, has a unique set of responsibilities consisting of: (a) The coordination of the research of all sections so that each research problem will be pursued along the lines that currently appear to be most promising, (b) the development of cooperative working relations with the universities and colleges, and (c) the stimulation of professional advancement of the Institute's research staff.

INTERRELATED PHYSICAL TOOLS

Despite the difficulties of war procurement and reconversion delays, the Institute has been able to assemble during its first year a well-rounded

complement of physical tools which permit the Physics Section to carry out a broad based but integrated program of physics research for industry, and to render invaluable aid to metallurgy, engineering, and the various chemical researches.

In developing the Institute's physical facilities and staff, special care has been exercised so that each tool or technique may be used in its range of greatest usefulness. Value and usefulness of individual scientific tools is increased by their integration into planned group application. The plan at Midwest Research Institute is so complete that its description is worth consideration as an illustration of the variety of tools that can converge on a single problem.

For example, equipment to study the appearance of materials includes a latest model Bausch and Lomb research metallograph for opaque objects, or the surface condition of transparent objects; a Leitz polarizing petrographic microscope for studying transparent materials and for carrying out microchemical analyses; as well as a stereoscopic microscope for general studies of form. For those cases where the particle size is too small for ordinary optical equipment the new universal model RCA electron microscope has been installed and is kept in condition for immediate use.

If information is needed concerning the crystal structure of materials, it can be obtained through the use of the General Electric x-ray diffraction unit with its assortment of tubes and newest type cameras. The nature of surfaces can be analyzed by use of the electron microscope operating as an electron diffraction unit. This assemblage of optical, x-ray, and electron optics equipment makes it possible to solve many industrial problems directly, and these tools are indispensable aids to metallurgy and chemistry.

Another important aid to metallurgy and chemistry is a complete Dietert spectrographic analysis unit. Either qualitative or quantitative analyses can be made by the arc or spark method, and the spectrograph has been set up with its camera extending into its own dark room, so that the photographic work can be carried out without delay or inconvenience. The Dietert spectrograph has been supplemented by an ultraviolet Beckman spectrophotometer and a Coleman spectrophotometer. These instruments have proved very useful in glass technology research, as well as for the usual chemical analyses which are so conveniently made by absorption measurements.

The Institute's equipment for physical metallurgy consists of a 30-kilowatt Tocco high frequency generator, a 2-kilowatt Westinghouse 15-megacycle generator, Rockwell and Brinell hardness testers, and a vapocarb heat treating unit, together with quenching equipment. Complete metallurgical specimen preparation, as well as the physical testing equipment which has been primarily secured for physics research in Engineering Mechanics, is also available.

Engineering mechanics laboratory measurements can be carried out for both static and dynamic states. For statics there are Baldwin-Southwark tensile machines of 120,000-pound and of 60,000-pound capacity. There is also a 10,000-pound Dillon unit which is useful for plastics and light alloys. For work in dynamics there are available special high frequency response bridge circuits and impact equipment.

FIG. 3. Hardness testing equipment in metallurgical laboratory.

For certain special impact problems modifications of the Tinius Olsen metallurgical impact tester can be used.

One part of the Physics Section which is of special value to the entire Institute is a complete photographic laboratory and studio. Here photographs of any type can be made, either as part of research data or for reports. Regular studio production type printer, washer, and drier are installed. A liberal supply of all kinds of special photographic film and paper is kept on hand to be available for immediate use. The motion picture equipment includes an Eastman high speed 16-mm camera capable of taking up to 3000 frames per second. The Photographic Laboratory is equipped with an Ozalid machine for quickly making copies of drawings and reports.

The staff and equipment of the Electronics Laboratory have also proved of great value to all other sections of the Institute. The equipment now available includes an assortment of General Radio bridges and meters, as well as various types of oscillators, oscilloscopes, and a recording high frequency response galvanometer and the usual assortment of component parts for building up special electronic circuits.

A physics section in a broad based research organization is in a position to render more assistance to all of the other branches of research than is true of any other section, because of the fundamental nature of physics equipment and techniques. Nevertheless, physics research as such does receive invaluable aid from the other sections. At Midwest Research Institute there is available a complete, fully staffed analytical laboratory so that accurate information can be obtained on the chemical nature of material under investigation. Many times the solution of problems in physics has been made easier through consultation and advice from the chemistry staff concerning the availability of materials or concerning means of making the needed materials out of those available.

Of inestimable service to the Physics Department is the Institute's well-equipped Instrument and Machine Shop. In fact, the Physics Department, including Engineering Mechanics and Metallurgy, is one of the major customers of the shop.

FIG. 4. Projection densitometer being used for spectrographic analysis.

RESEARCH PROJECTS—REGIONAL AND INDUSTRIAL

One regional research project in physics has as its purpose the making available to the industry of Middle America as many physical techniques as possible. For example, one group is becoming proficient in the operation of the electron microscope, so that when an industry calls for some electron microscope photographs it will be possible to render not only a quick service, but an economical one. Similar procedures are being followed for all of the equipment mentioned in the description of facilities. This project is a particularly good one from the viewpoint of the professional standing of the men in the Physics Section because it provides an opportunity for publishable research. The physics staff also actively participates on other regional projects which consist of:

1. Relation of properties of wheat to the baking properties of flour.
2. Improvement of wood properties through chemical treatment.
3. Inexpensive surface hardening treatment for barn and feed lots.
4. Non-fuel uses of petroleum and natural gas.
5. Beneficiation of the marginal cores of the region.

The industrial research of the Institute is carried on in confidence with all patents being fully assigned to the sponsor. Nine industrial projects were completed during the first year and twenty-six are now in progress with a budget of approximately $400,000 for the forthcoming year. Space in this article prohibits a detailed description of the projects now under way. This has been included in the Institute's published annual report.

The whole program of the Midwest Research Institute is proving to be an excellent opportunity for physicists to demonstrate to the satisfaction of all that the arts, skills, and science of an experienced research physicist can properly enter the solution of every industrial research problem.

Here and There

New Appointments

Richard C. Darnell, consulting engineer on instrument design and application, has been appointed by the Department of State, under its cultural cooperation program, to serve in China as a specialist in scientific instruments and laboratory equipment. He will assist in the selection of modern instruments needed to replace those worn out or looted from universities and research organizations. He will remain in China for about six months.

Raymond T. Ellickson, assistant professor of physics at the Polytechnic Institute of Brooklyn, has accepted an appointment as associate professor of physics at Reed College, Portland, Oregon.

James W. McRae, electro-visual engineer for Bell Telephone Laboratories, has been appointed director of radio projects and television research for that organization. Ralph Bown, assistant director of research at Bell Telephone Laboratories since 1944, has been named director of research.

David S. Saxon joined the research staff of Philips Laboratories, Inc., on April 1, 1946, as an associate physicist and is in charge of the section on theoretical physics. Edmund S. Rittner joined Philips' research staff on May 15, 1946, as associate chemist. His work will be carried on in the photo-cell laboratory.

Brooklyn Polytechnic Symposia

A series of eight symposia on "Recent Progress in the Field of High Polymers" will be conducted at the Polytechnic Institute of Brooklyn, October, 1946 through May, 1947.

Awards

Raymond D. Mindlin, associate professor of civil engineering at Columbia University, has recently been awarded the Medal for Merit by order of President Truman for his wartime work in the development of the radio proximity fuse. Professor Mindlin was largely responsible for the mechanical design of the radio tubes in the proximity fuse.

For distinguished work in glass technology, the honorary degree of Doctor of Science was awarded to William C. Taylor, vice president and director of glass technology of Corning Glass Works, at the 110th annual commencement exercises held at Alfred University June 10.

Stevens Institute Fellowships

The Experimental Towing Tank, Stevens Institute of Technology, has announced the establishment of several fellowships for graduates of engineering colleges who are interested in learning the techniques of model tests of ship and flying-boat hulls as well as in acquiring experience in the broader principles of hydrodynamic research in which the Tank is engaged. For information and application forms address Professor John P. Fife, Director of Personnel, Experimental Towing Tank, Stevens Institute of Technology, Hoboken, New Jersey.

Liquids Research Begun at Stevens

Research on the properties of liquids has begun at Stevens Institute of Technology as the result of a grant-in-aid received recently by the college from The Research Corporation. The research concerns the study of liquids in the far ultra-violet section of the spectrum where the air is completely opaque, making it necessary to do the work in a very high vacuum. The liquids being used are mainly melted salts, and the research project will examine what happens internally when solids melt. Results of the experiments made possible by the $4000 grant-in-aid will be published on completion of the research.

Training Program of the Clinton Laboratories

Object

The Clinton Laboratories, which are operated by the Monsanto Chemical Company under contract with the Manhattan District, are planning to conduct a combined training and research program during the fiscal year 1946–47. The purpose of this program is to aid in the dissemination of information, both fundamental and applied, concerning chain-reacting piles and their uses for both science and engineering. The facilities of the Laboratories will be made available to about 35 highly trained scientists and engineers from academic and industrial laboratories who have not had previous experience with piles. Those selected will have an opportunity to attend a

coordinated lecture program on the theory and operation of piles and to participate in the research and development program of the Laboratories. This program includes the following two broad fields:

A. *Fundamental Research in the Fields of Nuclear Physics and Chemistry.* This research will involve both theoretical and experimental work.
B. *Design of Piles.* This program has as its principal objective the extension of the technology of pile development into the important fields of peace-time application.

Organization of Laboratories

The key administrative staff of the Clinton Laboratories is as follows:

Research Director: Professor E. P. Wigner.
(On leave from Princeton University.)
Director of Physics Division: Dr. L. W. Nordheim.
Director of Chemistry Division: Dr. J. R. Coe.
Director of Technical Division: Dr. M. C. Leverett.
Director of Power Pile Division: Dr. C. R. McCullough.
Director of Training Program: Dr. Frederick Seitz.
(On part-time leave from the Carnegie Institute of Technology.)

The Research Divisions of the Laboratories have full-time staffs engaged in the activities of the Laboratories. These staffs include scientists and engineers who have been involved in nucleonics for a number of years. The participants of the training program are expected to work in close cooperation with the full-time staff in order that the Laboratories may function as a well-coordinated unit. Assignments will be made *primarily* on the basis of the interests of the participants; however, the interests of the Laboratories must also be kept in view.

Time

The training program began July 1, 1946, and will extend for the entire fiscal year. The formal lectures will not begin until about September 1, 1946. However, it is highly desirable that the participants arrive as soon after July 1 as possible in order to become familiar with the program of the Laboratories and to become adjusted to participation in it.

Nature of Lecture Program

The lectures will be given by a select group of physicists, chemists, and engineers. The major portion of these will be chosen from the Laboratories' staff, but a substantial fraction will be visiting scientists and engineers who have had extensive experience in the field of nuclear science and engineering. The topics of the lectures will be chosen from the following fields:

A. Fundamental Nuclear Physics.
B. Pile Science (Theory and Operation)
C. Radiochemistry.
D. Engineering Design of Piles.

Housing

The Clinton Laboratories will request living accommodations in Oak Ridge for the participants. These accommodations consist of individual houses, apartments, or dormitory rooms, depending upon individual needs, in the town of Oak Ridge, which is a fully equipped modern community. Transportation is available from Oak Ridge to the Clinton Laboratories. Requests for housing will be handled by Dr. Prescott Sandidge (Address: Box 1991, Knoxville, Tennessee). Moving expenses can be arranged.

Salaries

All participants will be transferred to the payroll of the Clinton Laboratories. Questions concerning salaries will be referred to Dr. Prescott Sandidge. In general a no-gain, no-loss policy will be adopted.

Application for Participation

Such applications should be made to Dr. Frederick Seitz, Department of Physics, Carnegie Institute of Technology, Pittsburgh, 13, Pennsylvania.

As stated above, questions relating to housing and salary will be referred to Dr. Sandidge.

Calendar of Meetings

August

19–20 Mathematical Association of America, Ithaca, New York
20–23 American Mathematical Society, Ithaca, New York

September

9–13 American Chemical Society, Chicago, Illinois
16–20 The Instrument Society of America, Pittsburgh, Pennsylvania
18–21 Illuminating Engineering Society, Quebec, Canada
19–21 American Physical Society, New York, New York
26–28 American Physical Society (Division of High Polymer Physics) and The Fiber Society, Charlottesville, Virginia (Joint Meeting)
30–October 3 American Society of Mechanical Engineers, Boston, Massachusetts

October

3– 5 National Electronics Conference, Inc., Chicago, Illinois
9–11 American Society of Civil Engineers, Kansas City, Missouri
25 American Mathematical Society, New York, New York

November

7– 9 Conference on Electrical Insulation, Division of Engineering and Industrial Research, National Research Council, Baltimore, Maryland
29–30 American Physical Society, Minneapolis, Minnesota

December

2– 6 American Society of Mechanical Engineers, New York, New York
17 Institute of Aeronautical Sciences, New York, New York
26–28 Geological Society of America, Chicago, Illinois

Contributed Original Research

A Method for Preparing Rubber Latex Specimens for the Electron Microscope

R. H. KELSEY* AND E. E. HANSON
Chemical and Physical Research Laboratories, The Firestone Tire and Rubber Company, Akron, Ohio
(Received April 26, 1946)

A new method was developed for preparing natural and synthetic rubber specimens for examination with an electron microscope. The technique consisted of mixing latex with a water solution of polyvinyl alcohol and forming a film from the mixture. Electron micrographs of such specimens showed none of the flattening of particles characteristic of the collodion film method and the micrographs were suitable for direct particle-size measurements.

THE preparation of natural and synthetic rubber latex specimens for examination with an electron microscope is difficult because the individual particles are easily deformed and, under the usual conditions of specimen preparation, the particles tend to agglomerate. Von Ardenne and Beischer[1] and others[2,3] have used a method which consisted of depositing a drop of highly diluted latex on a collodion film and allowing the drop to dry completely. In some instances the drop was withdrawn again into a glass capillary. It was found that in either case the latex particles were flattened at their areas of contact with the collodion film.

The collodion film method was tried in this laboratory with the same poor results observed by Hendricks, Wildman, and McMurdee.[2] Figure 1 is an electron micrograph of a natural rubber latex particle deposited by evaporating latex diluted 200 to 1 on a collodion film. The film has broken and curled to give a profile view of the particle which is observed to be badly flattened at its area of contact with the film. Figure 2 is a typical electron micrograph of natural rubber latex particles deposited on a collodion film. The blurred outlines of the particles are explained by the effect shown in Fig. 1. It was obviously impossible to make good particle size measurements from micrographs of this type. It was found further that severe aggregation of particles usually took place when a drop of the

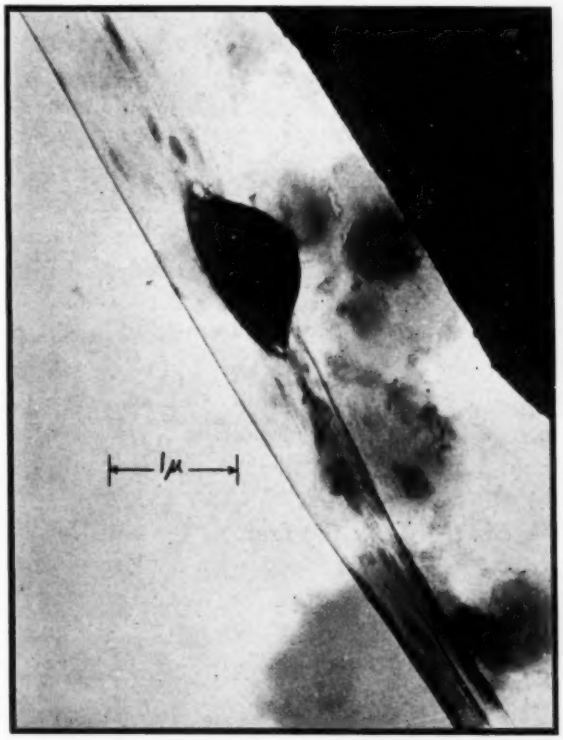

FIG. 1. Natural rubber latex particle. Collodion film broken.

* Present address: Department of Physics, University of Minnesota, Minneapolis, Minnesota.

[1] Von Ardenne and Beischer, "Investigations of the fine structure of high molecular substances with the universal electron microscope," Rubber Chem. and Tech. **14**, 15 (1941).

[2] Hendricks, Wildman, and McMurdee, "Morphology of latex particles as shown by electron micrographs," Ind. Rubber World **110**, 297 (1944).

[3] "Electron microscope studies of rubber latices and pigments," Columbian Carbon Research Laboratories, April, 1944.

diluted latex was dried down. The latex particles which were left behind when the drop was removed with a glass capillary usually were not badly agglomerated, but it was felt that there was some possibility that the latex particles might adhere selectively according to size to the collodion film. An attempt was made to reduce the amount of agglomeration by incorporating in the diluting water various amounts of such wetting or dispersing agents as sodium oleate, orvis paste, aerosol OT, and ammonium caseinate. None of these materials helped very much in reducing the agglomeration of particles. It was also found in this study that very often the latex particles appeared granular around their edges due to foreign material being swept in during the evaporation of the water and crystallizing out upon the surface of the particle. This effect may also be observed in Fig. 1.

The metallic shadow casting technique used by Williams and Wyckoff[4,5] was not tried in this laboratory. However, it is likely that, with this method also, the particles would be flattened at their areas of contact with the glass plate. It is also probable that the particles would have a strong tendency to form aggregates.

In this laboratory, the following approach to the problem was taken: to disperse the latex in a water solution of a film-forming material and to cast a film from it. In this way the latex particles would be completely surrounded by the material of the film and thus the flattening tendency would be greatly reduced. Polyvinyl alcohol, suggested by Mr. R. B. Keller, Jr., proved to be very successful as a water soluble film forming material. From the standpoint of forming strong clear films, the Type *B*, medium viscosity P.V.A.,* proved to be best. The method consists of the following operations: Into each of two 10-ml beakers is placed 1 ml of 0.5 percent water solution of P.V.A. One drop of the latex is placed in the first beaker and the mixture is stirred vigorously with a glass rod. Approximately two drops of this suspension is transferred to the second beaker and the mixture is stirred vigorously. A 200-mesh specimen screen is first dipped in a 0.5 percent solution of aerosol OT, the excess liquid shaken off and the screen then dipped in the latex-P.V.A. suspension. The water component of the film adhering to the specimen screen is allowed to evaporate to dryness and the specimen is placed in the microscope.

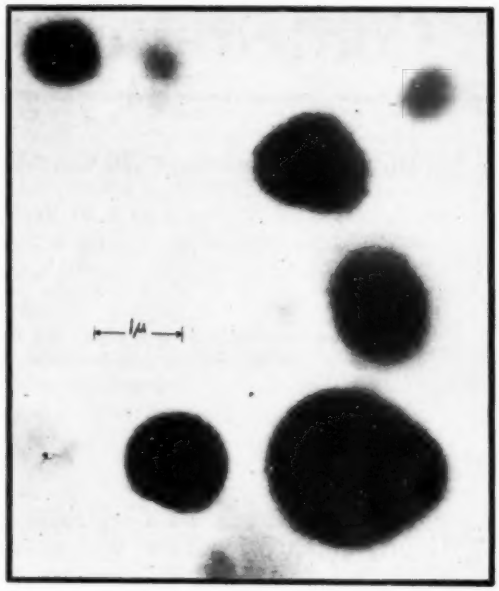

FIG. 2. Natural rubber latex. Collodion film method.

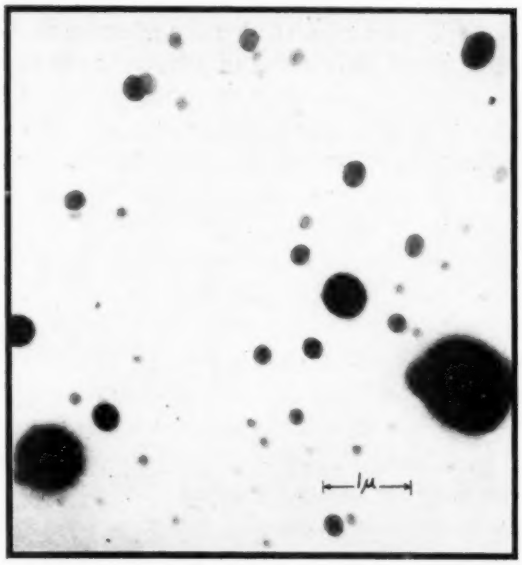

FIG. 3. Natural rubber latex in polyvinyl. Alcohol film.

[4] R. C. Williams and R. W. G. Wyckoff, "The thickness of electron microscopic objects," J. App. Phys. **15**, 712 (1944).

[5] R. C. Williams and R. W. G. Wyckoff, "Applications of metallic shadow casting to microscopy," J. App. Phys. **17**, 23 (1946).

* Supplied by E. I. duPont de Nemours and Company.

FIG. 4. Natural rubber latex. P.V.A. film broken.

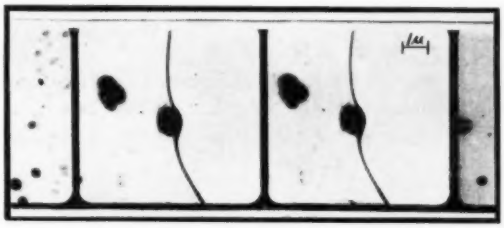

FIG. 5. Stereo electron micrograph of natural rubber latex imbedded in a broken P.V.A. film.

Several "kinks" in the technique are to be noted: The specimen screen was held at its edge with a pair of especially prepared tweezers which could be locked shut with a wire catch. The films of P.V.A. were most quickly dried in a continuously pumped vacuum desiccator with a small air leak for providing air circulation. The use of the wetting agent aerosol proved beneficial in promoting the wetting of the wire mesh with the P.V.A.-latex dispersion. The dilution of the latex had to be varied slightly, of course, depending upon the solids content and the particle size. With a little experience a person can estimate the proper dilution of the latex from the turbidity of the final P.V.A.-latex suspension.

The results obtained by using the P.V.A. technique are indicated in Figs. 3, 4, 5, and 6

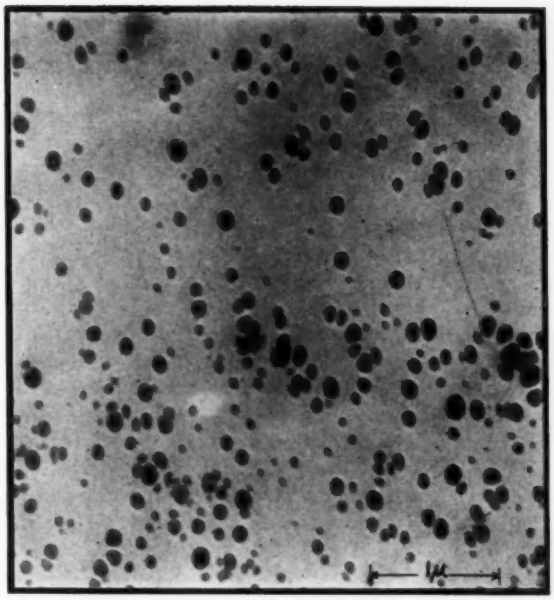

FIG. 6. GR-S type latex in P.V.A. film.

which are micrographs obtained with an RCA Type EMU electron microscope. Figure 3 is a micrograph of natural rubber latex. It is to be noted that the outlines of particles are sharp. Figure 4 is a micrograph of natural rubber latex particles in the edge of a broken P.V.A. film which has curled slightly. Figure 5 is similar to Fig. 4 except that it is a stereo view. There is no evidence of any flattening of the particles. In general, it has been found that whenever the film is stretched, as around a hole in the film, the latex particles tend to elongate in the direction of stretch as is illustrated in Figs. 4 and 5. Figure 6 is a micrograph of a special GR-S type synthetic rubber latex and it illustrates that synthetic rubber latex specimens may also be prepared by the P.V.A. method.

The aggregation of particles is prevented by a violent stirring of the P.V.A.-latex suspension and fewer aggregates occur than with the drying drop method used with collodion film.

It is a pleasure for the authors to acknowledge the interest shown in this problem by Dr. J. H. Dillon and Dr. F. W. Stavely. Thanks are due the Firestone Tire and Rubber Company for releasing this paper for publication.

Perturbation Theory of the Normal Modes for an Exponential *M*-Curve in Non-Standard Propagation of Microwaves†

C. L. PEKERIS*
Columbia University, New York, New York
(Received May 6, 1946)

In this paper a perturbation method is developed for treating non-standard propagation of microwaves beyond the horizon in the case when the deviation of the M-curve from the standard (≡the M-anomaly) can be represented by a term $\alpha e^{-\lambda z}$, where z denotes height in natural units. Here M denotes the modified index of refraction of the air. The method is also applicable to other forms of the M-anomaly which can be derived from an exponential term by differentiation with respect to λ; in fact, in its region of convergence it is formally applicable to the most general type of M-curve, including elevated ducts. The region of practical convergence of the method ranges from highly substandard conditions down to cases where the decrement is a fraction of the standard value. The procedure followed is to express the height-gain function $U_k(z)$ of the kth mode in the non-standard case as a linear combination of the height-gain functions $U_m^0(z)$ of all the modes in the standard case:

$$U_k(z)=\sum_{m=1}^{\infty} A_{km}U_m^0(z). \qquad \text{(a)}$$

The execution of this plan hinges on the possibility of evaluating the quantities

$$\beta_{nm}(\lambda)=\int_0^\infty U_n^0(z)U_m^0(z)e^{-\lambda z}dz. \qquad \text{(b)}$$

It is shown that $\beta_{nm}(\lambda)$ satisfies the differential equation

$$\frac{d\beta_{nm}}{d\lambda}=\frac{1}{2\lambda}+\beta_{nm}(\lambda)\cdot\left[-\frac{1}{2\lambda}+\tfrac{1}{2}(D_m^0+D_n^0)+\frac{\lambda^2}{4}+\frac{1}{4\lambda^2}(D_m^0-D_n^0)^2\right], \qquad \text{(c)}$$

whose solution is

$$\beta_{nm}(\lambda)=\frac{1}{2\sqrt{\lambda}}\exp\left[\frac{\lambda}{2}(D_n^0+D_m^0)+\frac{\lambda^3}{12}-\frac{1}{4\lambda}(D_m^0-D_n^0)^2\right]\cdot\int_0^\lambda\frac{dx}{\sqrt{x}}\exp\left[-\frac{x}{2}(D_m^0+D_n^0)-\frac{x^3}{12}+\frac{1}{4x}(D_n^0-D_m^0)^2\right]. \qquad \text{(d)}$$

Here D_m^0 denotes the characteristic value of the mth mode in the standard case. For large λ the following asymptotic formula holds

$$\beta_{nm}=-\frac{2}{\left[\lambda^3+2\lambda(D_m^0+D_n^0)-2+\frac{1}{\lambda}(D_m^0-D_n^0)^2\right]}+\frac{8\left[3\lambda^3+2\lambda(D_m^0+D_n^0)-\frac{1}{\lambda}(D_m^0-D_n^0)^2\right]}{\left[\lambda^3+2\lambda(D_m^0+D_n^0)-2+\frac{1}{\lambda}(D_m^0-D_n^0)^2\right]^3}. \qquad \text{(e)}$$

Having determined the $\beta_{nm}(\lambda)$ from (d), or by a numerical solution of (c), the characteristic values D_k and the coefficients A_{km} are to be solved from the infinite system of equations

$$\sum_{m=1}^{\infty} A_{km}[(D_k-D_m^0)\delta_{nm}+\alpha\beta_{nm}(\lambda)]=0, \quad n=1, 2, 3, \cdots, \qquad \text{(f)}$$

where δ_{nm} denotes the Kronecker symbol. For this purpose a simple iterative procedure has been developed, which has been found to be rapidly convergent. The A_{km} are normalized by the condition

$$\int_0^\infty U_k^2(z)dz=1=\sum_{m=1}^{\infty} A_{km}^2. \qquad \text{(g)}$$

[The integral $\int_0^\infty U_k^2(z)dz$ diverges when taken along the real axis; it converges, however, and to the same limit, when the path is a radial line in the fourth quadrant of the z plane. In the sequel, whenever an integral is divergent, it will be understood that the path is suitably modified.] One can also expand D_k as a power series in α

$$D_k=D_k^{(0)}+\alpha D_k^{(1)}+\alpha^2 D_k^{(2)}+\cdots,$$
$$D_k^{(1)}=-\beta_{kk}; \quad D_k^{(2)}=e^{i\pi/3}\sum_m\frac{\beta_{mk}^2}{(\tau_m-\tau_k)}, \quad m\neq k.$$

An alternative expression for $D_k^{(2)}$ is given in Eq. (58).

1. INTRODUCTION

IN the theoretical treatment of non-standard propagation of microwaves beyond the horizon by the method of normal modes, one is confronted with the task of solving the equation

$$\frac{d^2U_m}{dh^2}+k^2[y(h)+\Lambda_m]U_m=0, \qquad (1)$$

subject to the condition that $U_m(0)=0$ and that at $h\to\infty$ U_m should represent an upgoing wave only. Here h denotes height in feet,

$$y(h)=N^2(h)-1\equiv 2\times 10^{-6}M(h), \quad k=2\pi/\lambda, \qquad (2)$$

where $N(h)$ denotes the *modified* index of re-

† Publication assisted by the Ernest Kempton Adams Fund for Physical Research of Columbia University, New York, New York.
* On leave of absence from the Massachusetts Institute of Technology. This paper is based on work done at Columbia University under contract with the Office of Scientific Research and Development.

fraction of the air and Λ_m is the characteristic value which is generally complex. It is convenient to introduce natural units of height

$$z=h/H, \quad H=(k^2q)^{-\frac{1}{3}},$$
$$q=\frac{dN^2}{dh}=2.36\times10^{-9}\ \text{cm}^{-1}, \tag{3}$$
$$D_m=\Lambda_m(k/q)^{\frac{2}{3}},$$

whereby Eq. (1) is transformed into

$$\frac{d^2U_m}{dz^2}+[z+f(z)+D_m]U_m=0. \tag{4}$$

The term $f(z)$ in (4) represents the refraction anomaly, and is equal to zero for a standard atmosphere. In the first instance we shall be treating the case where

$$f(z)=\alpha e^{-\lambda z},* \tag{5}$$

and we shall later generalize the treatment to deal with any M-curve represented as a series of Laguerre functions. If the original M-curve is represented by the expression

$$M(h)=bh+ge^{-ch}, \quad b=.036\ \text{ft.}^{-1}, \tag{6}$$

then α and λ are obtained as follows:

$$\alpha=2\times10^{-6}(k/q)^{\frac{2}{3}}g, \quad \lambda=cH. \tag{7}$$

It is to be noted that in contrast to the constants g and c in Eq. (6) which are independent of frequency, the constants α and λ in Eq. (5) are frequency dependent. For a given observed M-curve the constants α and λ will therefore differ with the frequency band used, as will also the height represented by one unit of z.

2. FORMAL SOLUTION OF THE PROBLEM BY THE PERTURBATION METHOD

In order to solve the equation

$$\frac{d^2U_k(z)}{dz^2}+[z+\alpha e^{-\lambda z}+D_k]U_k=0, \tag{8}$$

we seek a solution in the form

$$U_k=\sum_{m=1}^{\infty}A_{km}U_m{}^0(z), \tag{9}$$

where $U_m{}^0(z)$ are the height-gain functions of the mth mode in the standard case, which satisfy the equation

$$d^2U_m{}^0(z)/dz^2+[z+D_m{}^0]U_m{}^0(z)=0, \tag{10}$$
$$\int_0^{\infty}U_m{}^{2(0)}(z)dz=1. \tag{11}$$

The solutions of (10) and (11) are well known,

$$U_m{}^0(z)=C_mu^{\frac{1}{2}}H_{1/3}{}^{(2)}(u), \quad u=\tfrac{2}{3}(z+D_m{}^0)^{\frac{3}{2}}, \tag{12}$$
$$C_m=\left\{e^{i\pi/3}\frac{2}{\sqrt{3}}(\tfrac{3}{2})^{\frac{1}{3}}v_m{}^{\frac{1}{2}}[J_{2/3}(v_m)-J_{-2/3}(v_m)]\right\}^{-1}, \tag{13}$$
$$D_m{}^0=\tau_me^{i2\pi/3}, \quad \tau_m=(3v_m/2)^{\frac{2}{3}}, \tag{14}$$

where

$$J_{1/3}(v_m)+J_{-1/3}(v_m)=0. \tag{15}$$

For small z the power series development of $U_m{}^0(z)$ is useful:

$$U_m{}^0(z)=i\sum_{k=1}A_kz^k, \tag{16}$$
$$A_k=-\frac{1}{k(k-1)}[D_m{}^0A_{k-2}+A_{k-3}], \tag{17}$$
$$U_m{}^0(z)=i[z-(D_m{}^0/6)z^3-z^4/12 +(D_m{}^{2(0)}/120)z^5+(D_m{}^0/120)z^6+\cdots], \tag{18}$$

while for large z one may use the asymptotic expansion of (16)

$$H_{1/3}{}^{(2)}(u)\rightarrow\left(\frac{2}{\pi u}\right)^{\frac{1}{2}}e^{i(-u+5\pi/12)} \times\left[1+\frac{5i}{72u}-\frac{385}{10368u^2}+\cdots\right]. \tag{19}$$

If now the expansion (9) be substituted into (8), we obtain, on making use of (10), the condition

$$\sum_{m=1}^{\infty}A_{km}[(D_k-D_m{}^0)+\alpha e^{-\lambda z}]U_m{}^0(z)=0. \tag{20}$$

On multiplying this equation by $U_n{}^0(z)$, where n is any integer, and integrating from 0 to ∞ we get a system of equations for the determination of D_k and the A_{km}:

$$\sum_{m=1}^{\infty}A_{km}[(D_k-D_m{}^0)\delta_{nm}+\alpha\beta_{nm}(\lambda)]=0, \quad n=1, 2, 3\cdots, \tag{21}$$

* No confusion should arise from the use of λ in (5) and the standard usage of λ to denote wave-length.

$$\beta_{nm}(\lambda)=\int_0^\infty U_m^0(z)\,U_n^0(z)e^{-\lambda z}dz. \tag{22}$$

The characteristic values D_k are then obtained as the roots of the infinite determinant

$$\begin{vmatrix} D_k-D_1^0+\alpha\beta_{11}, & \alpha\beta_{12}, & \alpha\beta_{13}, & \cdots \\ \alpha\beta_{21}, & D_k-D_2^0+\alpha\beta_{22}, & \alpha\beta_{23}, & \cdots \\ \alpha\beta_{31}, & \alpha\beta_{32}, & D_k-D_3^0+\alpha\beta_{33}, & \cdots \\ \cdots, & \cdots, & \cdots, & \cdots \end{vmatrix}=0. \tag{23}$$

Having determined D_k from (23), the A_{km} are obtained by solving the system of linear Eqs. (21).

3. EVALUATION OF $\beta_{nm}(\lambda)$ AS AN INDEFINITE INTEGRAL

The primary task in the perturbation method is the evaluation of the exchange integrals $\beta_{nm}(\lambda)$ defined in Eq. (22). We shall accomplish this by proving that $\beta_{nm}(\lambda)$, as a function of λ, satisfies a differential equation of the first order, for which an explicit solution can be given. For this purpose we shall study the function

$$F(z)\equiv U_n^0(z)\,U_m^0(z), \tag{24}$$

where

$$\ddot{U}_m^0(z)+[z+D_m^0]U_m^0(z)=0, \tag{25}$$

$$\ddot{U}_n^0(z)+[z+D_n^0]U_n^0(z)=0. \tag{26}$$

By multiplying Eq. (25) by $U_n^0(z)$, Eq. (26) by $U_m^0(z)$ and subtracting, we obtain

$$\frac{d}{dz}(\dot{U}_m^0U_n^0-U_m^0\dot{U}_n^0) = -(D_m^0-D_n^0)U_m^0U_n^0, \tag{27}$$

$$\dot{U}_m^0U_n^0-U_m^0\dot{U}_n^0 = -(D_m^0-D_n^0)\int_0^z U_m^0(x)\,U_n^0(x)dx. \tag{28}$$

Now it can be verified by direct substitution that

$$\frac{d^3F}{d^3z}+2\dot{F}(D_n+D_m+2z)+2F = (D_m^0-D_n^0)(\dot{U}_m^0U_n^0-U_m^0U_n^0) = -(D_m^0-D_n^0)^2\int_0^z F(x)dx.* \tag{29}$$

From (29) it follows that

$$F=\frac{d}{dz}\left[(2z+D_m^0+D_n^0)F+\tfrac{1}{2}\frac{d^2F}{d^2z}\right]+\tfrac{1}{2}(D_m^0-D_n^0)^2\int_0^z F(x)dz. \tag{30}$$

We may also note that

$$\frac{d^2F(0)}{d^2z}=2\dot{U}_m^0(0)\dot{U}_n^0(0)=-2, \tag{31}$$

$$\int_0^\infty e^{-\lambda z}\frac{d^2F}{d^2z}dz=e^{-\lambda z}(\dot{F}+\lambda F)\Big|_0^\infty+\lambda^2\int_0^\infty e^{-\lambda z}Fdz=\lambda^2\int_0^\infty e^{-\lambda z}Fdz, \tag{32}$$

$$\int_0^\infty e^{-\lambda z}dz\int_0^z F(x)dx=-\frac{1}{\lambda}e^{-\lambda z}\int_0^z F(x)dx\Big|_0^\infty+\frac{1}{\lambda}\int_0^\infty e^{-\lambda z}F(z)dz=\frac{1}{\lambda}\int_0^\infty e^{-\lambda z}F(z)dz. \tag{33}$$

$$\int_0^\infty e^{-\lambda z}zF(z)dz=-\frac{d}{d\lambda}\int_0^\infty e^{-\lambda z}F(z)dz. \tag{34}$$

* This is the first occasion in the author's experience where use is made of the fact that the product of two functions, each of which is a solution of a distinct second-order ordinary linear differential equation, satisfies a fourth-order linear differential equation. See G. N. Watson, *Theory of Bessel Functions* (The Macmillan Company, New York, 1944), p. 146.

We now substitute Eq. (30) in the integrand of (22) and obtain

$$\beta_{nm}(\lambda)=\int_0^\infty e^{-\lambda z}F(z)dz=\int_0^\infty e^{-\lambda z}dz\left\{\frac{d}{dz}\left[(2z+D_m{}^0+D_n{}^0)F+\tfrac{1}{2}\frac{d^2F}{d^2z}\right]+\tfrac{1}{2}(D_m{}^0-D_n{}^0)^2\int_0^z F(x)dx\right\}$$

$$=\frac{1}{2\lambda}(D_m{}^0-D_n{}^0)^2\int_0^\infty e^{-\lambda z}F(z)dz+\left[(2z+D_n{}^0+D_m{}^0)F+\tfrac{1}{2}\frac{d^2F}{d^2z}\right]e^{-\lambda z}\Big|_0^\infty$$

$$+\lambda\int_0^\infty e^{-\lambda z}\left[(2z+D_n{}^0+D_m{}^0)F+\tfrac{1}{2}\frac{d^2F}{d^2z}\right]dz$$

$$=1+\int_0^\infty e^{-\lambda z}F(z)\left[2\lambda z+\lambda(D_m{}^0+D_n{}^0)+\tfrac{1}{2}\lambda^3+\frac{1}{2\lambda}(D_m{}^0-D_n{}^0)^2\right]dz$$

$$=1-2\lambda\frac{d\beta_{nm}(\lambda)}{d\lambda}+\beta_{nm}(\lambda)\left[\lambda(D_m{}^0+D_n{}^0)+\frac{\lambda^3}{2}+\frac{1}{2\lambda}(D_m{}^0-D_n{}^0)^2\right]. \quad (35)$$

It follows that the exchange integral $\beta_{nm}(\lambda)$ satisfies the first-order differential equation

$$\frac{d\beta_{nm}(\lambda)}{d\lambda}=\frac{1}{2\lambda}+\beta_{nm}(\lambda)\cdot\left[-\frac{1}{2\lambda}+\tfrac{1}{2}(D_m{}^0+D_n{}^0)+\frac{\lambda^2}{4}+\frac{1}{4\lambda^2}(D_m{}^0-D_n{}^0)^2\right].^\dagger \quad (36)$$

The solution of (36) is

$$\beta_{nm}(\lambda)=\frac{1}{2\sqrt{\lambda}}\exp\left[\frac{\lambda}{2}(D_m{}^0+D_n{}^0)+\frac{\lambda^3}{12}-\frac{1}{4\lambda}(D_m{}^0-D_n{}^0)^2\right]$$

$$\cdot\int_0^\lambda\frac{dx}{\sqrt{x}}\exp\left[-\frac{x}{2}(D_m{}^0+D_n{}^0)-\frac{x^3}{12}+\frac{1}{4x}(D_m{}^0-D_n{}^0)^2\right]. \quad (37)$$

4. PROPERTIES OF $\beta_{nm}(\lambda)$

For small λ the solution of the differential Eq. (36) can be started with a power series in λ.

(a). $n\neq m$

$$\beta_{nm}(\lambda)=-\frac{2\lambda e^{i2\pi/3}}{(\tau_m-\tau_n)^2}\sum_{k=0}^\infty C_k e^{i2\pi k/3}\lambda^k, \quad (38)$$

$$\begin{aligned}
&C_0=1, \qquad C_1=6/(\tau_m-\tau_n)^2,\\
&C_2=[10C_1-2(\tau_m+\tau_n)]/(\tau_m-\tau_n)^2,\\
&C_3=[14C_2-2C_1(\tau_m+\tau_n)]/(\tau_m-\tau_n)^2,\\
&C_n=[(4n+2)C_{n-1}-2(\tau_m+\tau_n)C_{n-2}-C_{n-4}]/(\tau_m-\tau_n)^2.
\end{aligned} \quad (39)$$

(b). $n=m$

$$\beta_{mm}=1+B_1\lambda+B_2\lambda^2+\cdots, \quad (40)$$

$$B_1=\tfrac{2}{3}D_m{}^0, \quad B_2=\frac{4}{15}D_m{}^{2(0)}, \quad B_3=\frac{1}{14}+\frac{8}{105}D_m{}^{3(0)}, \quad B_n=\frac{1}{(2n+1)}[2D_m{}^0B_{n-1}+\tfrac{1}{2}B_{n-3}]. \quad (41)$$

† When this paper was first reported at a conference in June, 1945, Dr. W. F. Eberlein commented that he had independently derived Eq. (36) by an application of the theory of the Laplace transform.

For intermediate values of λ one may either use the integral in (37) or one may integrate numerically the differential Eq. (36). The latter procedure was advocated by Professor Hartree.

For large values of λ an asymptotic expansion can be obtained directly from (36) by writing it in the form

$$\beta_{nm}(\lambda)=\frac{-2+4\lambda\dfrac{d\beta_{nm}(\lambda)}{d\lambda}}{\left[\lambda^3+2\lambda(D_m^0+D_n^0)-2+\dfrac{1}{\lambda}(D_m^0-D_n^0)^2\right]}\rightarrow-\frac{2}{\left[\lambda^3+2\lambda(D_m^0+D_n^0)-2+\dfrac{1}{\lambda}(D_m-D_n)^2\right]}$$

$$+\frac{8\left[3\lambda^3+2\lambda(D_m^0+D_n^0)-\dfrac{1}{\lambda}(D_m^0-D_n^0)^2\right]}{\left[\lambda^3+2\lambda(D_m^0+D_n^0)-2+\dfrac{1}{\lambda}(D_m^0-D_n^0)^2\right]^3}. \tag{42}$$

An alternative asymptotic expansion can be derived from (37) by partial integration

$$\beta_{mn}\rightarrow-\frac{2}{\left[\lambda^3+2\lambda(D_m^0+D_n^0)+\dfrac{1}{\lambda}(D_m^0-D_n^0)^2\right]}+\frac{4\left[5\lambda^3+2\lambda(D_m^0+D_n^0)-\dfrac{3}{\lambda}(D_m^0-D_n^0)^2\right]}{\left[\lambda^3+2\lambda(D_m^0+D_n^0)+\dfrac{1}{\lambda}(D_m^0-D_n^0)^2\right]^3}. \tag{43}$$

In doing so one needs to prove that

$$\int_0^\infty\frac{dx}{\sqrt{x}}\exp\left[-\frac{x}{2}(D_m^0+D_n^0)-\frac{x^3}{12}+\frac{1}{4x}(D_m^0-D_n^0)^2\right]\equiv\psi_{nm}=0. \tag{44}$$

We shall state here without proof that

$$\psi_{mm}=\int_0^\infty\frac{dx}{\sqrt{x}}\exp\left[-xD_m^0-\frac{x^3}{12}\right]=\frac{\pi\sqrt{\pi}}{2}(\tfrac{2}{3})^{\frac{1}{3}}h_1(D_m^0)h_2(D_m^0), \tag{45}$$

where h_1 and h_2 are Furry's functions of the first and second kind defined as

$$h_1(x)=(\tfrac{2}{3})^{\frac{1}{3}}x^{\frac{1}{2}}H_{1/3}^{(1)}(\tfrac{2}{3}x^{\frac{3}{2}}), \tag{46}$$

$$h_2(x)=(\tfrac{2}{3})^{\frac{1}{3}}x^{\frac{1}{2}}H_{1/3}^{(2)}(\tfrac{2}{3}x^{\frac{3}{2}}). \tag{47}$$

Since by definition of D_m^0, $h_2(D_m^0)=0$, it follows that $\psi_{mm}=0$. The proof of (44) for $n\neq m$ is left as an exercise to the interested reader.

5. ITERATION METHOD OF SOLVING FOR THE CHARACTERISTIC VALUES D_k AND THE COEFFICIENTS A_{km}

In solving Eqs. (21) and (23), which are of infinite order, one proceeds by first assuming that $A_{km}=0$ for $m>p$, where p is a convenient integer, and then evaluating D_k and A_{km}, $m=1, 2, \cdots, p$. Next, one assumes that $A_{km}=0$ for $m>p+1$ resolves for D_k and the A_{km}, and the accuracy of the results is judged by the agreement between the values in successive approximations. The direct solution of (23) and (21) is, however, a laborious process which rapidly increases in complexity as p exceeds about 4. The following iterative procedure has been found effective and of the same intrinsic simplicity for any value of p.

To begin with, the p equations in (21), being homogeneous, do not determine the absolute values of all the A_{km} but merely the ratios of $(p-1)$ of them to a pth one. The absolute values are then determined from the normalization condition

$$\int_0^\infty U_k^2(z)dz = 1 = \sum_{m=1}^{\infty} A_{km}^2. \tag{g}$$

Let therefore

$$C_{km} = A_{km}/A_{kk}, \quad C_{kk} = 1, \tag{48}$$

and the p equations in (21) are just sufficient to determine the $(p-1)$ constants C_{km} and D_k. We divide the equations in (21) by A_{kk} and pick the kth equation $(n=k)$ to solve for D_k, while the other equations are used to solve for the C_{km}, as is illustrated in the scheme below for the particular case of $k=1$.

$$\frac{D_1}{\alpha} = \frac{D_1^0}{\alpha} - \beta_{11} - C_{12}\beta_{12} - C_{13}\beta_{13} - \cdots, \tag{49}$$

$$\left(\frac{D_1}{\alpha} - \frac{D_2^0}{\alpha} + \beta_{22}\right) C_{12} = -\beta_{12} - C_{13}\beta_{23} - C_{14}\beta_{24} - \cdots, \tag{50}$$

$$\left(\frac{D_1}{\alpha} - \frac{D_3^0}{\alpha} + \beta_{33}\right) C_{13} = -\beta_{13} - C_{12}\beta_{23} - C_{14}\beta_{34} - \cdots, \tag{51}$$

$$\left(\frac{D_1}{\alpha} - \frac{D_4^0}{\alpha} + \beta_{44}\right) C_{14} = -\beta_{14} - C_{12}\beta_{24} - C_{13}\beta_{31} - \cdots. \tag{52}$$

As a first approximation one puts

$$\frac{D_1}{\alpha} = \frac{D_1^0}{\alpha} - \beta_{11}, \tag{53}$$

$$C_{12} = -\beta_{12} \Big/ \left(\frac{D_1}{\alpha} - \frac{D_2^0}{\alpha} + \beta_{22}\right), \tag{54}$$

$$C_{13} = -\beta_{13} \Big/ \left(\frac{D_1}{\alpha} - \frac{D_3^0}{\alpha} + \beta_{33}\right), \text{ etc.,} \tag{55}$$

where the value of D_1/α obtained from (53) is used in (54) and (55). Next, one substitutes these values of the C's in the right-hand sides of Eqs. (49) to (52) and resolves for D_1/α and the C's. This procedure has been found to be rapidly convergent, and is, furthermore, self-correcting in case of arithmetical errors.

6. EXPANSION OF D_k INTO A POWER SERIES IN α

When α is small, it is convenient to expand D_k into the series

$$D_k = D_k^{(0)} + \alpha D_k^{(1)} + \alpha^2 D_k^{(2)} + \cdots. \tag{56}$$

It is known from standard perturbation theory that

$$D_k^{(1)} = -\beta_{kk}; \quad D_k^{(2)} = e^{i\pi/3} \sum_m \frac{\beta_{mk}^2}{(\tau_m - \tau_k)}, \quad m \neq k. \tag{57}$$

It is possible also to derive an alternative expression for $D_k^{(2)}$:

$$D_k^{(2)}(\lambda)=\tfrac{1}{2}\lambda D_k^{(1)}(\lambda)^2+\frac{1}{2\sqrt{\lambda}}\exp\left[D_k^{(0)}\lambda+\frac{\lambda^3}{12}\right]\int_0^\lambda \exp\left[-D_k{}^0x-\frac{x^3}{12}\right]$$
$$\cdot\left[\left(1+\frac{\lambda}{2x}\right)D_k^{(1)}(\lambda+x)+D_k^{(1)}(\lambda)D_k^{(1)}(x)\right]x^{\frac{1}{2}}dx$$
$$=\lambda D_k^{(1)}(\lambda)^2+\frac{1}{4\sqrt{\lambda}}\exp\left[D_k^{(0)}\cdot\lambda+\frac{\lambda^3}{12}\right]\int_0^\lambda\left[D_k^{(1)}(\lambda)+\left(2+\frac{\lambda}{x}\right)D_k^{(1)}(\lambda+x)\right]$$
$$\cdot\exp\left[-D_k{}^0x-\frac{x^3}{12}\right]x^{\frac{1}{2}}dx. \quad (58)$$

Since the former expression is simpler for computational purposes we shall not give here the derivation of (58).

7. APPLICABILITY OF THE PERTURBATION METHOD TO A MORE GENERAL CLASS OF *M*-ANOMALIES

It is possible to apply the results obtained for the case when the M-anomaly is of the form $f(z)=\alpha e^{-\lambda z}$ to more general types of M-anomalies. To begin with, if

$$f(z)=\alpha e^{-\lambda z}+\gamma e^{-\mu z}, \quad (59)$$

then we merely write in Eq. (21) in place of $\alpha\beta_{nm}(\lambda)$, $[\alpha\beta_{nm}(\lambda)+\gamma\beta_{nm}(\mu)]$. Once the $\beta_{nm}(\lambda)$ are computed as functions of λ, there is no additional labor required to deal with an $f(z)$ which consists of a sum of any number of exponential terms. If instead of $f(z)=\alpha e^{-\lambda z}$ we had $f(z)=\alpha z e^{-\lambda z}$, then the corresponding $\beta_{nm}'(\lambda)$ would be

$$\beta_{nm}'(\lambda)=\int_0^\infty U_m{}^0(z)\,U_n{}^0(z)ze^{-\lambda z}dz$$
$$=-\frac{d\beta_{nm}(\lambda)}{d\lambda}. \quad (60)$$

If $\beta_{nm}(\lambda)$ is known, $d\beta_{nm}(\lambda)/d\lambda$ can be computed directly from Eq. (36). When Eq. (36) is integrated numerically, the derivative $d\beta_{nm}(\lambda)/d\lambda$ is computed at each point in any case. Evidently, for $f(z)=\alpha z^k e^{-\lambda z}$, where k is a positive integer,

$$\beta_{nm}'(\lambda)=\int_0^\infty U_m{}^0(z)\,U_n{}^0(z)z^k e^{-\lambda z}dz$$
$$=(-)^k\frac{d^k\beta_{nm}(\lambda)}{d\lambda^k}. \quad (61)$$

By successive differentiation of Eq. (36), it is possible to express any high order derivative of $\beta_{nm}(\lambda)$ in terms of $\beta_{nm}(\lambda)$. From a purely formal point of view we can say therefore that by our method we can treat any M-anomaly by expanding it into a series of Laguerre functions, since these functions involve only terms of the form $z^k e^{-\lambda z}$. It may be pointed out that a single term $z^k e^{-\lambda z}$ vanishes both at the ground and at great height and reaches a maximum at $z=k/\lambda$. Such a single term is therefore suitable to represent an elevated duct.

Tables of $\beta_{nm}(\lambda)$ for n and m ranging from 1 to 6 are available at the Columbia University Division of War Research, Mathematical Physics Group, for $0<\lambda(0.1)<4$ and $0<1/\lambda(.01)<.25$. These tables were computed by Mrs. B. Brown, and Misses D. Weinstock, L. Selig, F. Jones, and E. Herman under the supervision of Miss Alice Osterberg.

Stresses in Cylindrical Glass-Metal Seals with Glass Inside

ALBERT W. HULL
Research Laboratory, General Electric Company, Schenectady, New York
(Received March 28, 1946)

It was shown previously that, when a cylinder of glass is sealed to the outside of a metal rod, the principal stresses in the glass are of opposite sign, so that tensile stresses cannot be avoided except by a perfect match. In this article the stresses are calculated for a solid glass cylinder sealed to the *inside* of a metal cylinder. It is shown that the stresses are *all of the same sign*, so that a moderate mismatch in thermal expansion, with the metal expansion the greater, is allowable and perhaps desirable. Large differences in expansion should be avoided, because of the shearing stresses at the ends.

MANY modern devices use cylindrical seals, in which a cylinder of glass is sealed to the inside surface of a metal cylinder, either with or without a central wire. These devices include microwave tubes, thyratrons, capacitors, and refrigerators. The stresses in such seals are different from those in glass-wire seals. They can be calculated easily from the equations given in an earlier paper.[1]

CALCULATION OF STRESSES

The form of seal is shown in Fig. 1. Let the components of stress be p_r, p_θ, and p_z, in the radial, tangential, and axial directions, respectively. Only the central portion of the seal will be considered, in which the stresses are independent of z, and in which no shearing stresses exist. The equations of the earlier paper, which refer to stresses in the outer cylinder, are:

Radial stress,

$$p_r = -\left[\frac{E_2\delta}{1+\alpha+\alpha\beta R}\right]\left[\frac{a^2}{b^2}-\frac{a^2}{r^2}\right], \qquad (1)$$

Tangential stress,

$$p_\theta = -\left[\frac{E_2\delta}{1+\alpha+\alpha\beta R}\right]\left[\frac{a^2}{b^2}+\frac{a^2}{r^2}\right], \qquad (2)$$

Axial stress,

$$p_z = -\left[\frac{E_2\delta}{1+\alpha+\alpha\beta R}\right]\left[2\sigma\frac{a^2}{b^2}+\frac{1+\alpha+\alpha\beta R}{1+\beta R}\right], \qquad (3)$$

where

E_1 = elasticity (Young's modulus) of internal cylinder,
E_2 = elasticity (Young's modulus) of external cylinder,
σ = Poisson's ratio, assumed equal for metal and glass,
a, b = radii of internal and external cylinders, respectively,
$R = E_2/E_1$, $\alpha = (a^2/b^2)(1-2\sigma)$, $\beta = b^2/a^2 - 1$,
$\delta = (k_2 - k_1)(t - t_0)$,

k_2 and k_1 are the mean contraction coefficients between t_0 and t of the outer cylinder and inner cylinder, respectively,

t is the temperature at which the stress is observed, and

t_0 is the "sealing temperature," i.e., the temperature at which the glass ceases to flow after sealing. δ is, therefore, the difference in total contraction of metal and glass, in cooling from the sealing temperature to the observation temperature (normally room temperature). The stress is defined to be positive when it is tension, negative when compression.

These equations may be modified to represent the stresses of the inner cylinder by making use of three simple relations[2]:

(a) The radial stress is the same for inner and outer cylinders at the boundary $r = a$, and is constant throughout the inner cylinder.

(b) The tangential and radial stresses are equal in the inner cylinder.

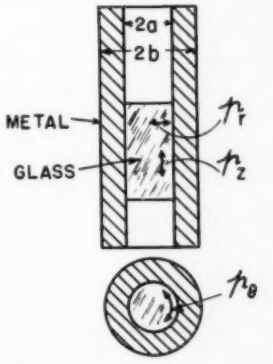

FIG. 1. Cylindrical seal with glass inside. The stress in the central portion can be calculated from expansion data.

[1] A. W. Hull and E. E. Burger, "Glass to metal seals," Physics **5**, 387 (1934).

[2] H. Poritsky, "Analysis of thermal stresses in sealed cylinders," Physics **5**, 406 (1934).

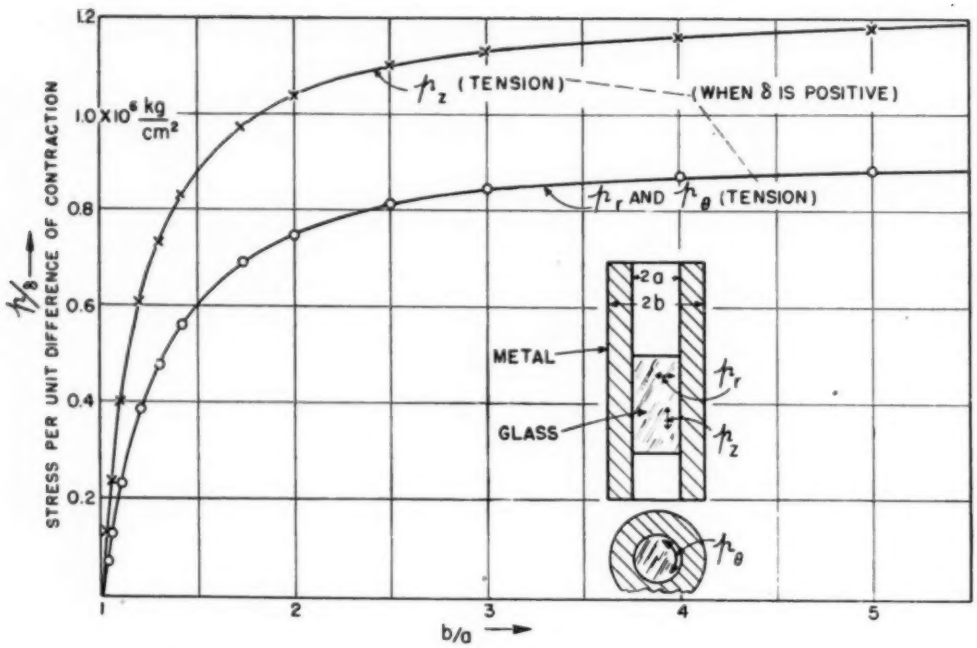

FIG. 2. Stress in internal glass cylinder per unit difference of contraction, δ, between metal and glass ($\delta = \{k_{\text{outer cyl.}} - k_{\text{inner cyl.}}\}\{t - t_0\}$), as function of ratio b/a of metal diameter to glass diameter. When δ is negative, the stresses will be compression.

(c) The total axial stress over any cross section z=constant *of both cylinders* is zero. Hence,

$$p_z(\text{internal}) = -\frac{b^2-a^2}{a^2} p_z(\text{external}).$$

The calculations will be made for an external cylinder of iron, for which $E_2 = 2.05\times10^6$ kg/cm². This is the metal most likely to be used in thick sections, i.e., with large values of b/a. For Fernico ($E_2 = 1.80\times10^6$), with thicknesses ordinarily used ($b/a \leq 1.1$), the radial and tangential stresses are about 2 percent greater than those given here, and the axial stress 4 percent greater; while the maximum difference, even for very thick Fernico tubing, does not exceed 10 percent. The elastic constants used for the calculations are therefore:

$$E_1 \text{ (glass)} = 0.65\times10^6 \text{ kg/cm}^2,$$
$$E_2 \text{ (metal)} = 2.05\times10^6 \text{ kg/cm}^2,$$
$$\sigma_1 = \sigma_2 = 0.30.$$

TABLE I. Stresses in internal glass cylinder per unit difference of contraction δ, between metal and glass, as function of ratio b/a of metal diameter to glass diameter. Positive stresses are tension; negative, compression. When δ is negative, the signs of all stresses are opposite to those given in the table.

b/a	$P_r = P\theta$	P_z
α	+0.91	+1.193
5	+0.882	+1.18
4	+0.872	+1.164
3	+0.845	+1.130
2.5	+ .811	+1.102
2.0	+ .750	+1.040
1.732	+ .691	+0.975
1.414	+ .560	+0.830
1.30	+ .460	+ .735
1.20	+ .388	+ .610
1.10	+ .230	+ .401
1.05	+ .1285	+ .236
1.025	+ .071	+ .1325
1.00	0.000	0.000

The calculated values for the stresses in the inner cylinder are given in Table I and Fig. 2. For comparison, the stresses in external glass cylinders are shown in Fig. 3.[1]

COMPARISON OF INTERNAL AND EXTERNAL SEALS

A comparison of Figs. 2 and 3 reveals one striking difference. *The stresses in internal seals are all of the same sign.* Thus, when the contraction of the metal is greater than that of the glass (δ negative) all the stresses will be negative, i.e., compressions. This is a desirable condition, because glass is strong in compression. However, excessive differences of contraction should be

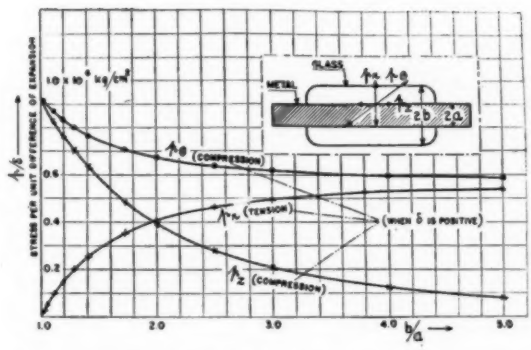

FIG. 3. Stress in cylindrical seal at surface of wire ($r=a$) per unit difference of contraction, δ, between metal and glass, ($\delta=\{k_{\text{outer cyl.}}-k_{\text{inner cyl.}}\}\{t-t_0\}$) as function of ratio b/a of glass diameter to wire diameter. When δ is negative, the signs of stresses are the reverse of those indicated, *viz.* tension in place of compression, and *vice versa*.

avoided, since the shearing stresses at the ends are proportional to the difference in contraction.

With external seals the situation is different. Here the two largest stresses, namely, the radial and the tangential stresses, are of opposite sign, so that there is no safe condition except that of zero stress. For example, a metal which contracts more than the glass will give an axial stress which is a compression, as observed with the quartz wedge testing equipment[3]; and this is sometimes mistaken for a desirable mismatch. Actually, as may be seen in Fig. 3, the tangential stress also is a compression, but the radial stress is tension, tending to break the bond between metal and glass. This bond is the weakest part of the seal; hence this type of stress should be avoided.

INTERNAL SEAL WITH CENTRAL WIRE

When a central wire is added to the internal seal (Fig. 4), one has a combination of the two cases considered above, namely an internal and an external seal. For the central wire seal, in which the glass is external, the only safe condition is a close match to the glass. The external metal cylinder, however, may be mismatched to yield a mild compression of the glass. The values given in Table I and Fig. 2 will apply to this case, with small error, provided the central wire is well matched to the glass.

FIG. 4. Cylindrical seal with central wire.

[3] A. W. Hull and E. E. Burger, Rev. Sci. Inst. **7**, 98 (1936).

Particle Size Determination from X-Ray Line Broadening

L. S. BIRKS AND H. FRIEDMAN
U. S. Naval Research Laboratory, Washington, D. C.

(Received April 8, 1946)

The x-ray line broadening method of determining particle size was compared with direct measurement on electron micrographs. By controlled heating of the carbonate, magnesium oxide particles were prepared from 50 to 1000A in diameter. Particle size calculated from x-ray data taken on a Geiger counter spectrometer agreed to ±10 percent with the microscope measurements. Mechanical mixtures of two different sizes were examined by the x-ray method, but the particle sizes could not be determined unless the two maxima of the distribution curve were completely resolved.

INTRODUCTION

THE broadening of x-ray diffraction lines is one of the most accurate indirect methods of determining particle size for crystallites smaller than 1000A diameter. The theory relating line broadening to particle size was developed by Scherrer,[1] von Laue,[2] and Bragg.[3] It was considered in more detail by Warren,[4] Patterson,[5]

[1] Scherrer, "Bestimmung der Grosse und der inneren Struktur von Kolloidteilchen mittels Rontgenstrahlen," Nach. Gesell. Wiss. Göttingen, Zitzungsber., July 26, 1918 in R. Zsigmondy, *Kolloidchemie* (Otto Spamer, Leipzig, 1920), third edition.

[2] Von Laue, Zeits. f. Krist. **64**, 115 (1926).

[3] W. Bragg, *The Crystalline State* (G. Bell and Sons, London, 1933).

[4] B. E. Warren, "X-ray diffraction study of carbon blacks," J. Chem. Phys. **2**, 551 (1934).

[5] A. L. Patterson, "The diffraction of x-rays by small crystalline particles," Phys. Rev. **56**, 972 (1939).

Jones,[6] Murdock,[7] and others. Warren[8] in particular showed that the size of MgO particles could be determined from x-ray line broadening measurements. In the present paper, the particle size of MgO determined from x-ray line broadening was compared with the size by direct measurement with the electron microscope over the range from 50 to 1000A. Magnesium oxide was chosen for the particle size studies because of the ease with which uniform specimens could be prepared by heating the carbonate.

DIRECT MEASUREMENT WITH THE ELECTRON MICROSCOPE

Magnesium oxide was prepared by heating magnesium carbonate in air. The temperature of conversion was varied from 200°C to 1000°C and heating periods ranged from 2 hours to 12 hours. The electron microscope was calibrated with a grating replica. The replica spacing was determined to ±5 percent using the lines of the mercury spectrum. Nineteen different fields were photographed in the electron microscope and the mean deviation was 1 percent. Each of the oxide specimens was then photographed at the same magnification as the grating replica. Therefore the accuracy of the measured magnification was estimated to be ±5 percent.

Figures 1 through 6 are typical micrographs of the unconverted carbonate and the oxide at various temperatures. Originally the carbonate was in the form of thin flakes of the order of

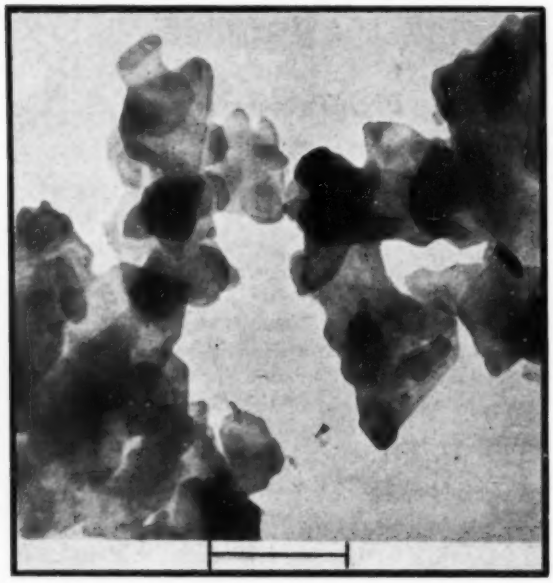

FIG. 1. Commercial magnesium carbonate. Scale indicates one micron.

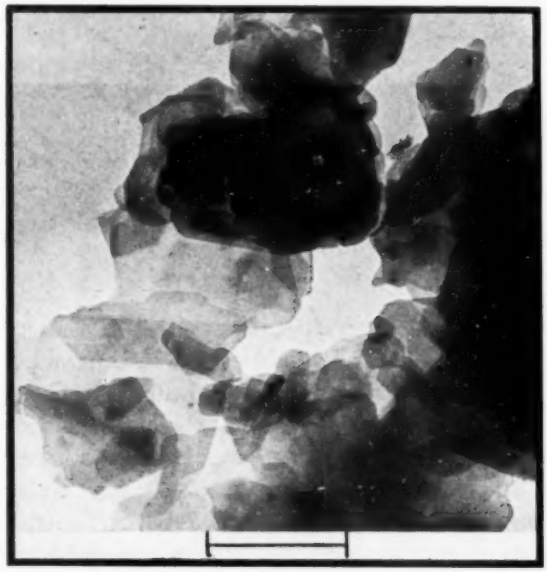

FIG. 2. Magnesium carbonate heated at 200°C for 6 hours. Scale indicates one micron.

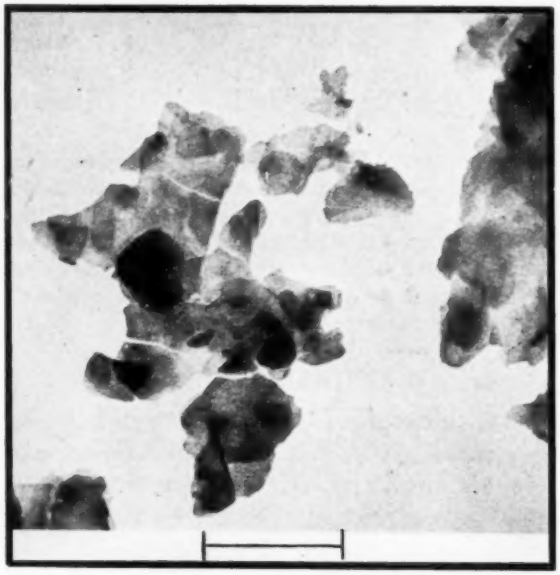

FIG. 3. Magnesium carbonate converted to magnesium oxide at 400°C for 6 hours. Scale indicates one micron.

[6] F. W. Jones, Proc. Roy. Soc. **A166**, 16 (1938).
[7] C. C. Murdock, Phys. Rev. **36**, 8 (1930).
[8] B. E. Warren, J. App. Phys. **12**, 375 (May 1941).

one micron in diameter. After treatment at 200°C no apparent change had taken place. At 400°C however, a definite mosaic appeared in the flakes and it was possible to make a rough estimate of the size of the particles comprising the mosaic. The accuracy of the measurement was not better than ±25 percent. At high temperature the particles were larger and clearly separated although the shape of the original carbonate flakes was still apparent. For each heat treatment, several hundred particles were measured and distribution curves plotted. Each specimen showed a narrow distribution curve with only slight asymmetry. The peak value in

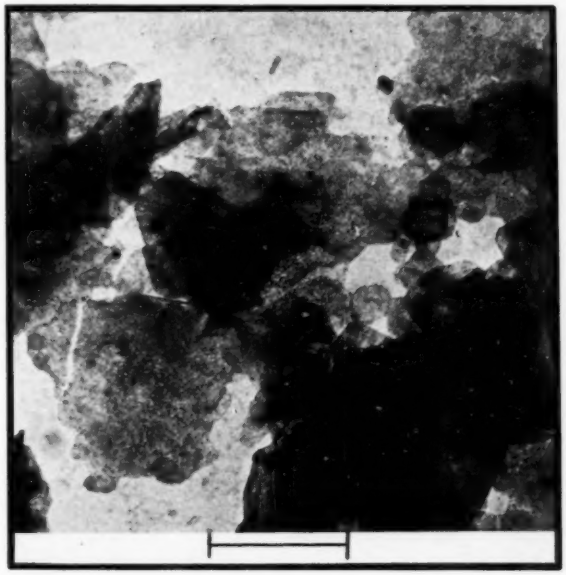

FIG. 4. Magnesium carbonate converted to magnesium oxide at 600°C for 6 hours. Scale indicates one micron.

angstroms plotted against heating period for the various temperatures is shown by the dotted lines in Fig. 7. The sizes range from 50A at 400°C and 2 hours to 1000A at 1000°C and 12 hours. The rate of growth was slow at 400°C but increased rapidly with increasing temperature to a value of approximately 40A per hour at 1000°C. These results are compared below with those obtained by x-ray diffraction.

X-RAY LINE BROADENING

The determination of size by x-ray diffraction makes use of the relation that for particles

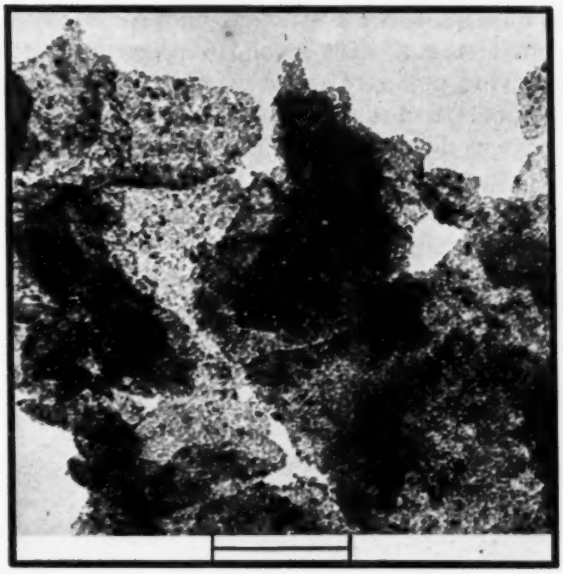

FIG. 5. Magnesium carbonate converted to magnesium oxide at 800°C for 6 hours. Scale indicates one micron.

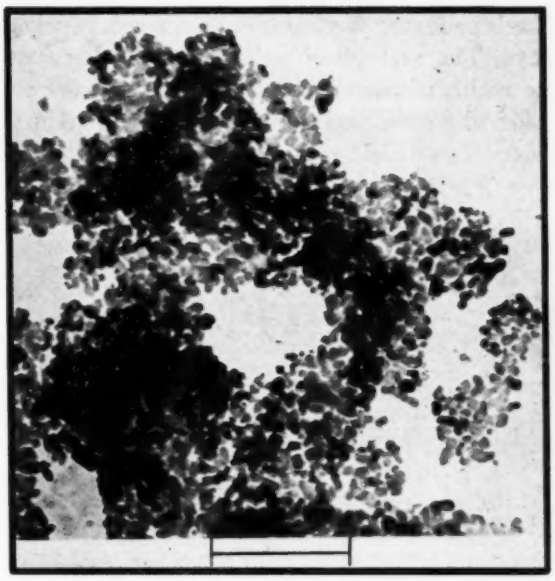

FIG. 6. Magnesium carbonate converted to magnesium oxide at 1000°C for 6 hours. Scale indicates one micron.

smaller than about 1000A the diffraction lines are broadened by an amount depending on the size of the particles. The width of the diffraction lines from large particles are a characteristic of the apparatus and do not depend on the particle size. An analogous effect is found in optical grating spectra; as the number of lines per inch

is increased, the diffraction pattern of visible light becomes sharper and sharper until the resolving power of the measuring apparatus is reached. In x-ray diffraction, planes of atoms correspond to the lines in an optical grating. For the type of x-ray diffraction equipment usually employed, a specimen with particles of the order of 1000A or larger gives the sharpest possible maxima.

The problem of relating the broadening of the line to the size of the particles has been treated by many investigators.[1–8] In general, their methods all lead to an equation of the form,

$$D = K\lambda/B\cos\theta, \tag{1}$$

where

D = diameter of the particle,
K = constant (value given below),
B is the broadening of the line,
λ is the wave-length of the x-radiation, and
θ is the Bragg angle.

The broadening B may be determined in several ways. The method of Scherrer[1] was to measure the width of the diffraction line in radians at a point where the intensity was half the maximum value. Von Laue[2] measured the area under the diffraction line and divided by the maximum intensity. This is known as the integral width method. Recent investigators[5, 6] adopted more rigorous derivations which took into account the shape of the distribution curves for the particles and the direction of measurement in the crystal. The diffraction lines from the MgO specimens in this investigation were symmetrical and their shape closely approximated an error function. The method of width at half maximum was used for all the determinations of broadening. No matter which equation is adopted, B must be corrected for the width of the diffraction line for large particles, known as the instrument width. The correction takes the form,

$$B^2 = B'^2 - b'^2, \tag{2}$$

where B is again the broadening, B' is the width of the line from the small particles, and b' is the instrument width or the width of the line from particles larger than 1000A. The constant K in the equation depends on the method of measuring B and on the assumptions as to the shape of the particle. Scherrer[1] arrived at a value of $K = 0.89$. Patterson[5] obtained a value of $K = 1.11$ when the particles were assumed to be spherical in shape and of cubic structure. From the electron micrographs, the particles treated at 1000°C appeared to be neither strictly spherical nor cubic, although the structure of MgO is cubic. A value of $K = 1$ was adopted as a compromise.

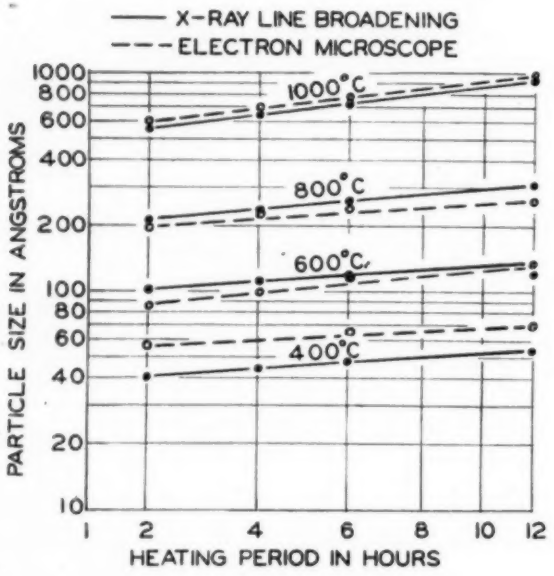

FIG. 7. Particle size in angstroms *versus* heating period in hours for conversion temperatures from 400°C to 1000°C. Solid lines represent results from x-ray line broadening and dotted lines, results from direct measurement on electron micrographs.

The x-ray specimens were prepared by mixing approximately ½ gram of the material with a 2 percent solution of parlodion in amyl acetate. The mixture was smeared on a microscope slide to give a flat surface approximately 1 inch square. The N.R.L. Geiger counter spectrometer[9] was employed with a divergent beam and focusing geometry to give high intensity. The Geiger counter pulses were fed into either a scaling circuit for measuring the intensity at discreet points along the pattern or into a recorder for automatic scanning of the complete pattern.

Each specimen was first scanned and the recorded patterns are shown in Fig. 8. The carbonate pattern contains many lines but they are not sharp or well defined. The pattern for

[9] H. Friedman, Electronics **18**, 132 (April 1945).

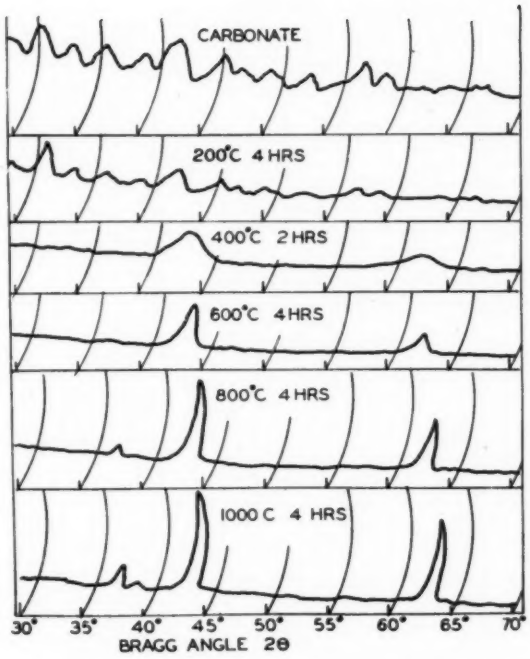

FIG. 8. Automatically recorded x-ray diffraction patterns for magnesium carbonate and magnesium oxide converted at temperatures from 400°C and 1000°C.

200°C is the same as for the untreated carbonate. Close examination reveals that there are no MgO lines present. This confirmed what was observed on the electron micrographs, which showed no change after treatment at 200°C. At 400°C there was no semblance of the carbonate pattern, but two broad halos appeared corresponding in position to the two strongest lines in the MgO pattern. As the temperature was increased, the lines became sharper and more intense until at 1000°C they were almost as sharp as the lines from a powdered quartz crystal. The MgO line at 2θ equals 43° was chosen and the intensity measured at discreet points in this neighborhood by counting for a given time interval. The counts were corrected for non-linearity of Geiger counter response and the lines were plotted as shown in Fig. 9. The width at half-maximum could be measured accurately to $\pm\frac{1}{2}$ minute of arc for the higher temperatures and to ± 2 minutes of arc for the lowest temperatures. The line from quartz at 2θ equals 42.2° was measured to obtain the instrument width used in correcting the broadening.

From the measurements of the width at half-maximum, the diameter of the particles was calculated using Eq. (1). The results are shown as the solid lines in Fig. 7. The agreement between the two methods was ± 10 percent for all particles larger than 100A.

EFFECT OF NON-UNIFORM PARTICLE SIZE

The above data were for specimens whose distribution curves showed a small range of particle size. The following are some data on mechanical mixtures of specimens of two different sizes. The distribution curve for such mixtures has two peaks, one for each of the components. Figure 10 shows the x-ray results for three specimens, *A*, 1000°C, 6 hr.; *B*, 400°C, 12 hr.; and *C*, a 50–50 mixture of *A* and *B*. The line for the 50–50 mixture had the same width at half-maximum as the 1000°C sample indicating the same particle size. However, the peak in-

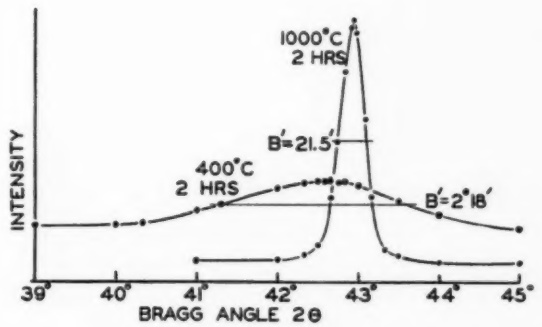

FIG. 9. Typical diffraction lines from magnesium oxide converted from the carbonate at 400°C and 1000°C. The intensity was measured with a Geiger counter at the points shown on the curves.

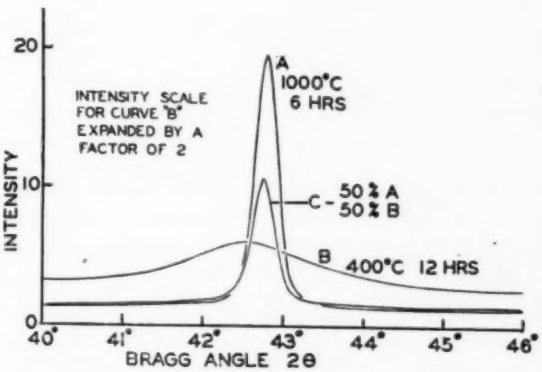

FIG. 10. Effect of a mixture of particles of different sizes. *A* is for particles approximately 700A in diameter and *B* is for particles approximately 50A in diameter. *C* is for a 50–50 mixture by weight of *A* and *B*.

tensity was approximately half as great. Thus the maximum intensity could be used as a qualitative measure of the amount of large size material present.

When the size of the two components was not greatly different so that the peaks of the distribution curves for the two were not resolved, the true particle size could not be determined. Figure 11 shows the x-ray lines for three specimens, *D*, 800°C, 6 hr.; *E*, 600°C, 6 hr.; and *F*, a 50–50 mixture of *D* and *E*. The line from the 50–50 mixture is intermediate in both width and height between the two and a measure of the width gives particle size approximately half-way in between the two.

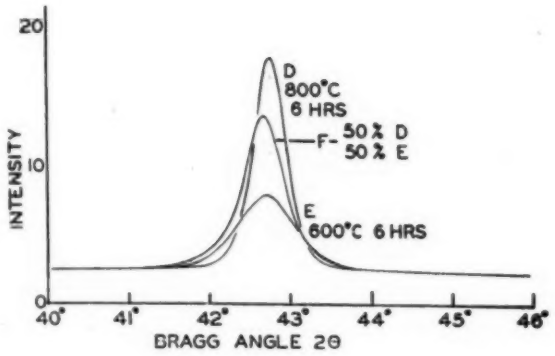

FIG. 11.

SUMMARY

Electron micrographs, at known magnifications, were used as comparison standards for x-ray line broadening determinations. The line broadening was measured with a focusing type of Geiger counter spectrometer. Results by the two methods agreed to ±10 percent except for particles smaller than 100A where the accuracy with which they could be measured on electron micrographs was only of the order of 25 percent.

Although all the x-ray data shown here were for the magnesium oxide line at 43° 2θ, data were also taken for the second strongest line at 62° 2θ and the results agreed to within 10 percent. The material for this paper was condensed from N.R.L. report H-2434 prepared in the summer of 1944.

The Effect of Hydrostatic Pressure on Plastic Flow under Shearing Stress

P. W. BRIDGMAN
The Physics Laboratories, Harvard University, Cambridge, Massachusetts

(Received April 25, 1946)

This paper presents measurements of the forces required to drive a punch into plates of several grades of steel as a function of the distance of penetration, the entire punching operation being conducted in a fluid medium subjected to hydrostatic pressures up to 30,000 kg/cm². Qualitatively, the effects are similar to those already found for the tensile properties of steel subjected to hydrostatic pressure, namely, ductility is greatly increased, and greatly increased distortion is tolerated without fracture. The effects are similar in general character for all the steels experimented on here, but are quantitatively accentuated for the softer steels. At a pressure of 20,000 kg/cm² or more a punch may be driven completely through a plate of mild steel, with no loss of coherence at any stage of the process, and with strain hardening, when expressed in terms of true shearing stress, which may increase by a factor of as much as 3. If the punching operation is suspended at any intermediate stage before complete penetration and afterward completed at atmospheric pressure, very material strengthening will be found as compared to virgin material of the same geometrical configuration. There are certain qualitative differences in the details of the ductility exhibited during the processes of punching and pulling. At intermediate pressures and penetrations the true shearing stress in punching may, under proper circumstances, exhibit maxima, for which there is no analog in the pulling operation. This is to be understood in terms of a difference of geometry, there being greater opportunity for self-healing during the punching operation, and, furthermore, partial deterioration of the coherence of the metal not necessarily leading to complete catastrophe.

INTRODUCTION

A NUMBER of experiments have established the very large effect of pressures up to 30,000 kg/cm² in increasing ductility under tensile stresses.[1] In this paper a study is made of the

[1] P. W. Bridgman, Rev. Mod. Phys. **17**, 3–14, 1945. Eight reports to the Watertown Arsenal, March 1943, through Dec. 1944, numbered No. WAL 111/7, 111/7-1, etc., through 111/7-7.

effect of pressure in increasing the magnitude of the flow which can be tolerated without fracture under the action of shearing stresses. In general, the results are of the same qualitative character as for tensile stress, in that much greater deformations are possible without fracture under pressure than at atmospheric pressure.

THE METHOD

Perhaps the most natural method would be that of twisting a rod. There are, however, great technical difficulties in applying, inside a vessel carrying high hydrostatic pressure, rotations of the magnitude which experiments with simple compressive stresses[2] suggested would be necessary to produce fracture, and no attempt was made to develop this method. Some form of punching seemed indicated by the instrumental limitations. Preliminary experiments were made in which a rod was passed through holes in a cylindrical sleeve and a closely fitting cylindrical core and sheared through by longitudinal displacement of the core within the sleeve. The apparatus was adapted to materials of various strengths by providing holes by which several rods could be sheared simultaneously. There were, however, difficulties in so fitting the specimens to the holes as to start the plastic flow in all specimens simultaneously, and the method was abandoned.

The method finally adopted was the punching of a circular disk; the apparatus is shown in Fig. 1. The specimen to be punched, shown shaded, is compressed tightly between an upper and a lower annular clamp in order to prevent warping when the punch penetrates. The disk to be punched is 0.050 or 0.03 inch thick, depending on its hardness. The two surfaces were ground to parallelism in a surface grinder. The punch was of "Teton" tool steel, left glass hard. The edge of the punch was sharp, and the face flat. The cylindrical side was full diameter for a length of 0.019 inch and then relieved. The die through which the punching is expelled was of the same Teton steel, with sharp edges, and tapered at a double angle of 1° to eliminate friction on the expelled punching in the die. The cylindrical holder for punch, specimen, and die was of a Cr Mo steel, heat treated to Rockwell C hardness 30. All parts were ground and fitted accurately together. The specimen in the holder was mounted in the 30,000 apparatus in the same position as that taken previously by the tension specimens. The force driving the punch was measured with the same "grid" that was used to measure tensile load, the displacement of the punch was measured in the same way as the elongation of the tension specimens, and the whole technique of the experiment was very similar. Since the total motion of the punch from initial contact to complete penetration was less than the total elongation of the tension specimens, the total change of hydrostatic pressure during the course of the punching was less than in the corresponding tension experiment, which is an advantage.

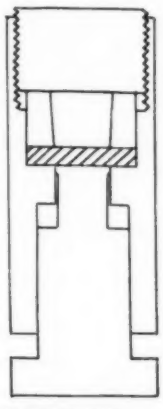

FIG. 1. The punch with specimen, shaded, in position.

The measurements consist in simultaneous measurements of the hydrostatic pressure, the force on the punch, and the displacement of the punch, the latter being measured externally from the displacement of the piston producing the hydrostatic pressure. This latter displacement includes, in addition to the actual penetration of the punch, the elastic distortions of all the intermediate parts, including the punch itself, the transmitting parts within the pressure chamber, and the external piston. These elastic distortions were corrected out of the final result by making a sufficient number of readings before plastic flow began to establish the slope of the line of elastic distortion, and subtracting from the total displacement after plastic flow began an amount proportional to the total load and the slope.

The total load on the punch was converted into shearing stress per unit original area by dividing the total load, after correction for

[2] P. W. Bridgman, J. App. Phys. **14**, 273–283 (1943).

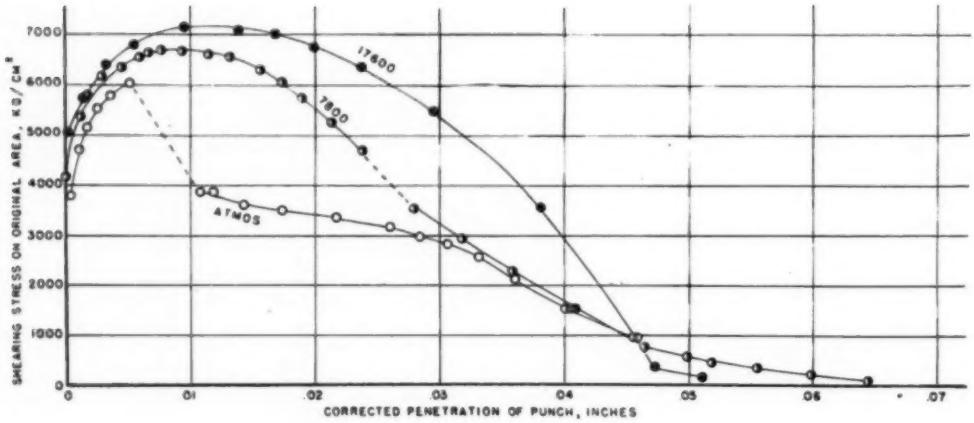

FIG. 2. The experimental data at several different pressures, indicated on the curves, for heat treatment No. 3 of steel No. 4.

friction on the punch, by the area of the sheared region (product of thickness of plate and circumference of punch). This shearing stress on the original area was then converted to "true" shearing stress by multiplying by the ratio of the initial thickness to the running thickness. The "true" shearing stress was finally plotted against the penetration of the punch. The friction on the punch was computed from the readings at the end of the punching process, when the face of the punch had been driven completely through the plate, but the unrelieved sides of the punch were still in contact with the plate. This contact persisted for a displacement of 0.019 inch; during contact the driving force dropped proportionally to the distance still to go. The maximum correction for the friction of the punch was about 10 percent.

It would have been desirable if the "true" shearing stress could have been plotted against the strain, so as to get a strain hardening curve for pure shear. The conditions of plastic flow were not, however, well enough defined to permit any clean cut evaluation of the strain. Ideally the strain might be localized in the thin cylindrical shell included between the diameter of the punch and the diameter of the die. Actually, however, the strain spread out into the surrounding region from this cylindrical shell in a way that would be most difficult to compute. The question was investigated by using punches of different diameters, thus varying the thickness of the cylindrical shell. If a true strain-hardening curve of stress against shearing strain could be obtained by the idealized calculation, then there should be a simple connection between the results obtained with the different punches, the true shearing stress for a certain penetration with one punch being the same as that at a penetration twice as great with a punch of twice the clearance. Three punches were used, with clearances varying from 0.0040 to 0.0008 inch. At the same penetration of the punch the force with the largest clearance was only 3 or 4 percent less than with the smallest clearance. This shows that the plastic flow must be pretty well spread outside the idealized cylindrical shell, and frustrates the attempt to express the results in terms of absolute strains. For this reason these experiments on punching have a more qualitative significance than the tension experiments.

THE MEASUREMENTS

All the final measurements were made with the largest punch, with a clearance of 0.0008 inch. Measurements were made on five grades of steel. The first was a 1045 steel from the Watertown Arsenal in the "as received" condition; tensile data for this will be found in my reports to the Arsenal.[3] The others were two steels, Nos. 2 and 4, which had been used in certain experiments for the N.D.R.C. during the war,[4] in two different heat treatments. The compositions and heat treatments were as follows:

Steel No. 2, C 0.45, Mn 0.83, P 0.016, S 0.035, Si 0.19.
Steel No. 4, C 0.90, Mn 0.47, P 0.015, S 0.036, Si 0.11.
Heat treatment No. 3; annealed at 1900°F for 0.5 hour, giving a coarse grained structure.
Heat treatment No. 9; held at 1800°F for 0.25 hour, quenched into brine, and drawn at 600°F for 1 hour.

[3] In particular, in Report No. WAL 111/7.
[4] These reports have been recently declassified (7/12/46).

. The qualitative nature of the effects is shown in Fig. 2, in which is plotted for heat treatment No. 4 the shearing stress on the original area (which is proportional to the total driving force on the punch) against the corrected penetration of the punch. In this instance the material "breaks" at atmospheric pressure after a penetration of the punch to one-tenth the thickness of the plate. This is indicated by the dotted line in Fig. 2. The force jumps down, and the punch jumps in, the intermediate configurations being unstable and controlled by elastic distortion in the punch itself and the transmitting members. After the break, a force comparable with the maximum is still required to advance the punch, the force gradually dropping off as penetration becomes complete. The first effect of hydrostatic pressure is to suppress the break, displacing it at the same time toward higher penetrations. In Fig. 2, at the next pressure above atmospheric, 7800 kg/cm², only a vestige of the break remains, and it has been displaced from a penetration of 0.005 to 0.025 inch (one-half the thickness of the plate). At the next higher pressure, 17,000, no vestige of the break remains.

On converting total loads into true shearing stresses and correcting for friction, Fig. 2 is transformed into Fig. 3. The secondary rise in the true stress at atmospheric pressure after passing the break is explained by the character of the punching. This is not truly cylindrical, but the exit diameter, in contact with the die, is slightly less than the diameter at the face of the punch, so that the punching has the shape of a truncated cone. After the break, the larger base of the cone has to be forced through a smaller aperture, like forcing a conical rubber stopper the "wrong" way through an aperture, thus accounting for the increase in force. The drop of force when expulsion nears completion is caused by distortion in the thin lip of the plate. With increase of hydrostatic pressure the truncated cone becomes a true cylinder, brightly burnished over its entire external surface, instead of being burnished only over the ring corresponding to the penetration of the punch before the break. The transition between the two conditions is gradual.

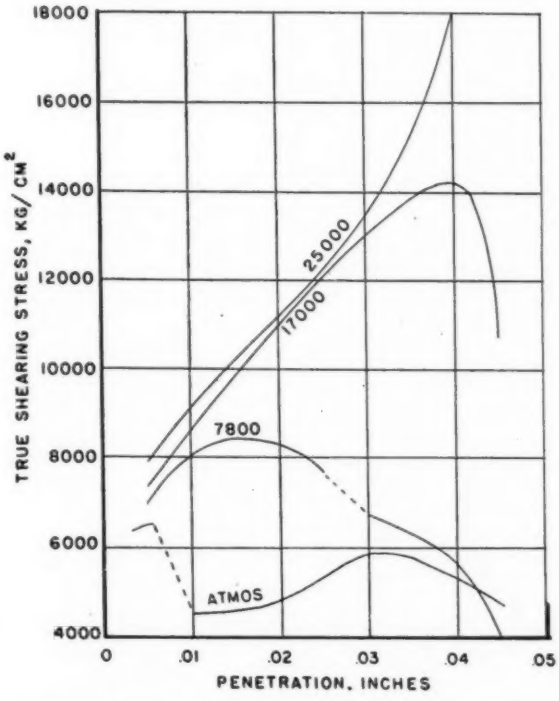

FIG. 3. The "true" shearing stresses corresponding to the data shown in Fig. 2. The original data for the run at 25,000 kg/cm² are not shown in Fig. 2, in order to avoid confusion with the data for 17,600.

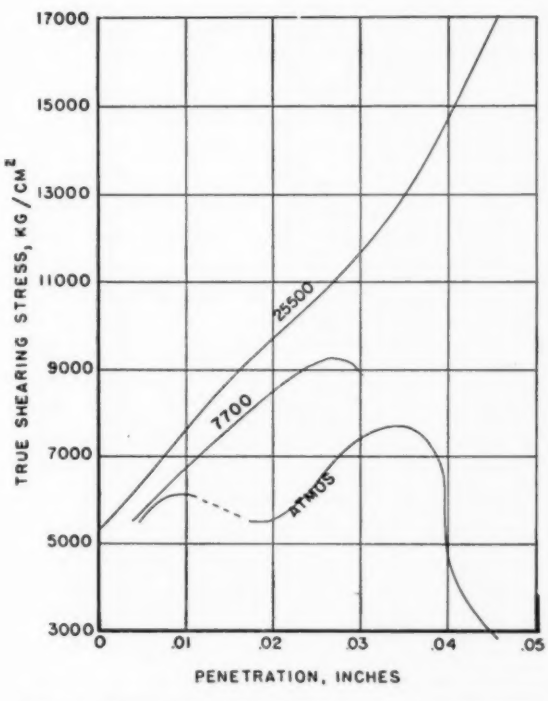

FIG. 4. "True" shearing stress *versus* penetration at several pressures for the 1045 steel, "as received." The heavy line at .05 inch indicates the total thickness of the plate.

In Fig. 3 the true stress at the first pressure above atmospheric, 7800, rises to a maximum and then drops slightly before the vestigial break occurs. That is, there has been some deterioration of the steel after a certain degree of penetration, but no wide open break. At the next pressure, 17,400, strain hardening is approximately linear with the penetration up to a penetration to 0.8 the original thickness. The drop beyond 0.8 represents deterioration, without actual fracture. The upper curve in Fig. 3 is for a pressure of 25,000; the corresponding curve was not drawn in Fig. 2. At this pressure any deterioration is displaced so nearly to complete penetration as to be beyond experimental reach. The upward curvature at the end of this curve is probably real, and corresponds to the fact that the average effective strain increases at an accelerated rate as penetration nears completion.

The Watertown 1045 steel and heat treatment No. 3 for steels No. 2 are much similar. In Fig. 4 is shown true stress *versus* penetration for the 1045 steel, and in Fig. 5 for heat treatment No. 3

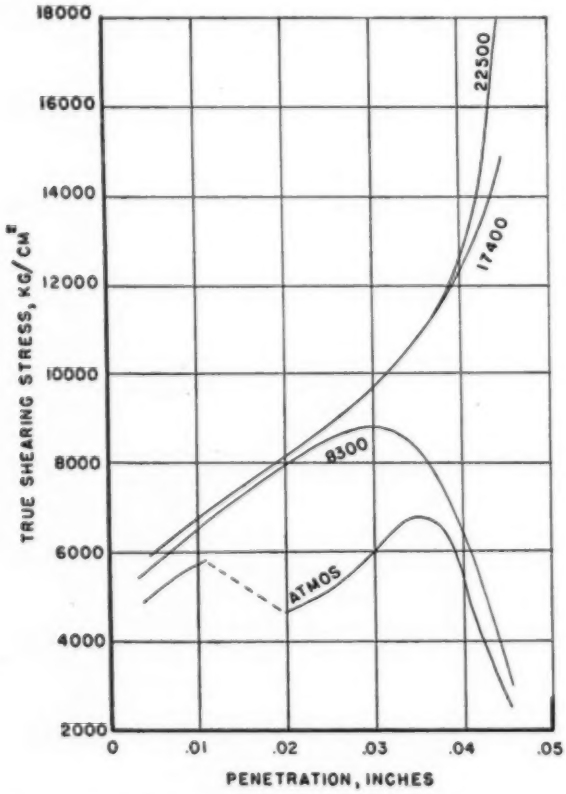

FIG. 5. "True" shearing stress *versus* penetration at several pressures for heat treatment No. 3 of steel No. 2.

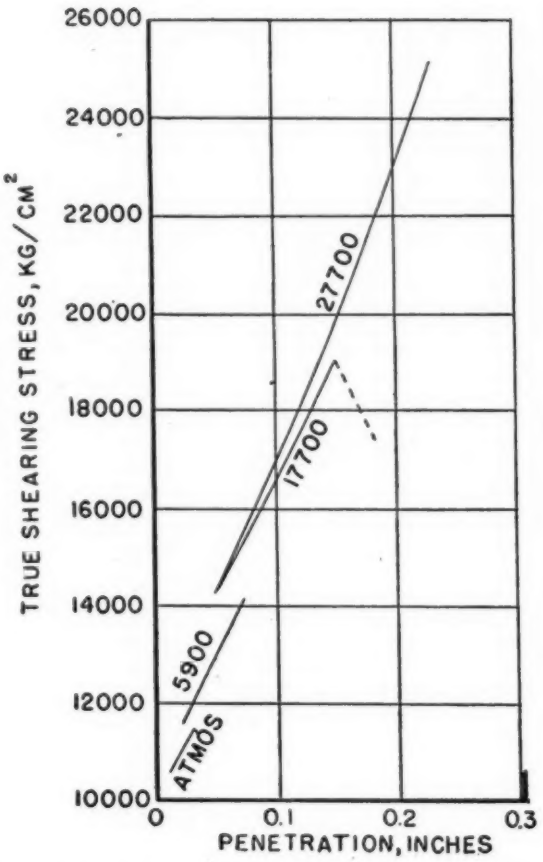

FIG. 6. "True" shearing stress *versus* penetration at several pressures for heat treatment No. 9 of steel No. 2.

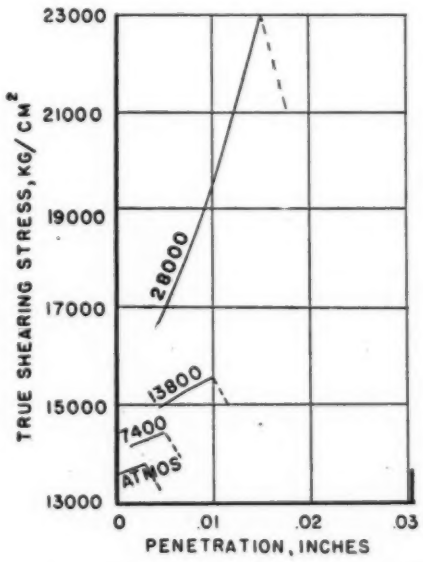

FIG. 7. "True" shearing stress *versus* penetration at several pressures for heat treatment No. 9 of steel No. 4. The total thickness of the plate was .0302 inch.

of steel No. 2. These steels are both softer than No. 4, and the curves for both show upward curvature at the deepest penetrations and the highest pressure. Toward the end of penetration, the strain is increasing more rapidly than in the initial stages, because it has less chance to spread out from the idealized cylindrical shell, and the steels are soft enough not to show the deterioration at high strains shown by No. 4.

Figures 6 and 7 show the results for heat treatment No. 9 on steels No. 2 and No. 4. This heat treatment gives a much harder product, with higher resistance to punching and much less plastic yield when the break does occur. The effects of pressure here are in the same direction qualitatively as for the softer steels, but they do not go nearly so far. The fracture phenomena are not suppressed in the pressure range shown in the figures; however, the penetration of the punch before the break occurs is much increased by pressure. This agrees with the results previously found for tension, namely that the phenomena for the harder steels are qualitatively the same as for the softer steels, but the scale of the effects is changed, a much higher pressure being required for the same plastic flow without fracture in a harder steel as compared with a softer steel.

In order to demonstrate that the punching may be moved bodily through the surrounding metal under pressure without fracture, an experiment was made on the 1045 steel in which the punch was driven 0.9 through the plate at a pressure of 23,000 kg/cm², and then the punching operation was completed at atmospheric pressure, For comparison, another plate was punched at atmospheric pressure which had been machined so as to have in it a depression of the same dimensions as that which had been driven into the plate by the punch under 23,000. At atmospheric pressure the maximum force required to start the punch moving through the prepunched plate was more than 80 percent greater than the maximum force supported by the geometrically similar virgin specimen. This is evidence of considerable strain hardening, and incidentally shows that the prepunched plate could not have had many wide open fractures, if any.

In another similar experiment the punch was pushed 0.4 through the plate at a pressure of 26,000 kg/cm², and the punching operation was then completed at atmospheric pressure. In this case 42 percent more force was required to start the punch moving through the prepunched plate than was needed for a geometrically similar virgin specimen. The prepunched plate behaved in the way usual for strain hardened material in that the maximum penetration of the punch up to the break (calculated from the new zero) was only 0.38 of that for the virgin specimen. The true shearing stress at the maximum penetration under pressure was 8900 kg/cm²; it required 7300 true stress to make flow resume at atmospheric pressure. Some of the difference between these two figures may be caused by a loss of strain hardening by an annealing effect on resting. However, if the total difference between these two figures is ascribed to a specific effect of hydrostatic pressure, it would mean a raising of the plastic flow stress by only 8 percent per 10,000 kg/cm² pressure, and this is slightly less than has been previously found under similar circumstances.

DISCUSSION

The qualitative resemblance of the effects of pressure on plastic flow in tension and in shear has already been commented on. The greatest increase of shearing stress observed is that for the 1045 steel, which shows a maximum increase under 26,000 kg/cm² of something more than threefold. In tension a threefold raising of the flow stress for this steel is produced by a strain of 3.75, or an elongation of 43-fold (second Arsenal report).

In addition to this rough qualitative resemblance there is one significant qualitative difference between the strain-hardening curves for tension and for pure shear. The strain-hardening curve for tension rises linearly with increasing strain until the point of fracture is reached, which occurs abruptly, with no previous warning. The difference between a strain-hardening curve for tension at one pressure and another higher pressure is merely, to a first approximation, that rupture on the second curve is not reached until a higher strain than on the first. In shear, however, the strain-hardening curves for different pressures do not coincide over their entire extent, but, especially at the lower pressures, the

approaching fracture announces itself by a dropping away from the strain-hardening curve for high pressures. In a certain range of pressure the strain-hardening curve may show a maximum. This is evident in Figs. 3–5 on the curves for the first pressure above atmospheric. This would indicate a deterioration of the steel before complete fracture. The physical explanation of the difference between shearing and tension is to be sought in the difference of the stability relations. If an incipient fracture occurs in tension the adjacent parts are immediately removed from the region of atomic interaction and the fracture is catastrophic. On the other hand, when tangential slip of one part on another occurs, the slipping parts are not necessarily removed from atomic contact and cohesion remains to an extent depending on the degree of destruction of the lattice structure. In other words, in tangential slip the phenomenon of self-healing can occur, but it cannot in tension. Hydrostatic pressure keeps the slipping parts in contact, so that the self-healing is more complete the higher the pressure.

Hysteresis and Related Elastic Properties of Tire Cords

HELMUT WAKEHAM AND EDITH HONOLD
Southern Regional Research Laboratory, New Orleans, Louisiana*
(Received May 25, 1946)

A method of evaluating mechanical hysteresis, elastic modulus, elongation, and growth rate of a yarn or cord subjected to cyclic loads in a fatigue test is described. The test is applied to seven typical tire cords—one Nylon, two rayon, and four cotton cords including both high stretch and low stretch cords. Results are presented showing the effect of cycle number, moisture content, temperature, and load range on the elastic properties of each of the cords tested. The influence of cyclic loading on the stress-strain curve is also discussed. It is concluded that moisture content is the dominant factor influencing the elastic properties of tire cords and that the heat produced by mechanical hysteresis of the tire cord contributes appreciably to the heat build-up observed in tires during heavy duty service.

IN a previous publication[1] preliminary data on the mechanical hysteresis of cotton and rayon tire cords were presented. The results of a more extended investigation of the hysteresis and related elastic properties of tire cords are reported in the present paper.

The phenomenon of elastic hysteresis for textile materials has received little attention by previous investigators in the field of textile properties. Barker and Tunstall[2] obtained extension and recovery curves for wool fibers by means of an autographic recording stress-strain apparatus in which the rate of loading and unloading was relatively slow. Later methods of investigation were of the same type and extended over only a few cycles.[3–5] Such published results are of limited applicability, however, because they give little insight into the properties of the material during prolonged use. Whereas exposed fabric, such as wearing apparel, usually can be reliably tested at convenient intervals during its lifetime, the evaluation of the properties of tire cords during service presents a unique problem because the cord is vulcanized in rubber and cannot be removed without destroying the usefulness of the tire. There is need for a testing procedure in which the change in properties during mechanical deterioration of the cord to the point of failure will parallel the changes in actual service.

In a general sense, any test in which the test

* One of the laboratories of the Bureau of Agricultural and Industrial Chemistry, Agricultural Research Administration, U. S. Department of Agriculture.

[1] H. Wakeham, E. Honold, and E. L. Skau, J. App. Phys. **16**, 388 (1945).

[2] S. G. Barker and N. Tunstall, Trans. Faraday Soc. **25**, 103 (1929).

[3] W. F. Busse, E. T. Lessig, D. L. Loughborough, and L. Larrick, J. App. Phys. **13**, 715 (1942).

[4] W. S. Denham and T. Lonsdale, Trans. Faraday Soc. **29**, 305 (1933).

[5] O. Eisenhut and W. Grether, Melliand Textilber. **22**, 122 (1941).

specimen is subjected to cyclic deformation is a fatigue test. Numerous tests of this type for tire cord both in and out of the tire have been described[6,7] in which the time, or number of cycles, to fatigue failure is measured. No doubt the information so derived is extremely useful, especially in control testing, but the research worker interested in improving cord needs to find out also what changes take place in the cord during its deterioration to failure. This phase of the problem seems to have been almost completely overlooked by workers in the tire cord field.

One of the major problems in the design of large heavy-duty truck tires has been the high temperatures built up during service as a result of the imperfect elasticity of the tire. The heat generated is unquestionably related to the elastic hysteresis of the rubber and the tire cord. While rubber hysteresis has received considerable attention by investigators in the rubber industries,[8] relatively little is known of cord hysteresis and the contribution which it makes to the high temperatures observed in tires during service.

It was with these facts in mind that the comparison of elastic properties described below was undertaken.

APPARATUS

When the tension on a cord is progressively increased to a maximum and then lowered again, the elongation for a given load differs, depending upon whether the tension is increasing or decreasing. If percent elongation of the cord is plotted against the increasing and decreasing loads, a loop as shown in Fig. 2 (right-hand side) is obtained. The area within the loop is directly related to energy loss or hysteresis, because of imperfect elasticity of the cord. In the apparatus used the cord is stretched and relaxed in a straight line while the record of the elongation and load are traced on the moving paper of a kymograph. The tracings so obtained are sinusoidal-like curves of different amplitudes from which the hysteresis and other elastic properties may be calculated.

[6] W. H. Bradshaw, A.S.T.M. Bull. 13 (October, 1945).
[7] L. Larrick, Textile World, **95**[5], 107 (1945).
[8] See for example: J. H. Dillon, I. B. Prettyman, and G. L. Hall, J. App. Phys. **15**, 309 (1944). E. T. Lessig, Ind. Eng. Chem. Anal. Ed. **9**, 582 (1937). M. Mooney and R. H. Gerke, Ind. Rubber World, **103**[4], 29 (1941). H. S. Sack, J. Motz, and R. N. Work, J. App. Phys. **15**, 396 (1944).

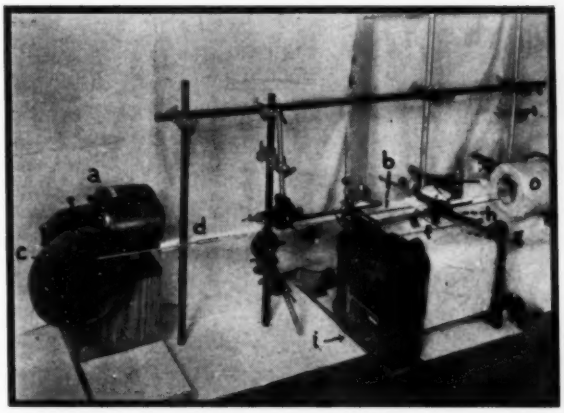

FIG. 1. Mechanical loading and recording apparatus at the left-hand end of the oven. See text for complete description.

In this group of experiments, the cord is tested within a specially constructed oven, as described in the previous paper,[1] but the arrangement of the apparatus beyond each end of the oven (*o*, Fig. 1) has been changed. In series, starting at the left-hand end, there are motor-driven geared eccentric (*a*), a calibrated spring (*b*), the left-hand tie, the cord, the right-hand tie, a connection, and movable brace which permits growth take-up. The eccentric and spring apply the increasing and decreasing load cycle to the cord; a slotted insert (*c*), which moves diametrically across the face of the eccentric and locks into position, permits the adjustment of the stroke to the selected load range. The connection between this pegged insert and the spring is made by means of a rigid bar (*d*) and a heavy wire (*e*). The latter is always in line with the cord, being held in position by frictionless pulleys. At each end of the spring, a recording pen is attached (*f*, *g*). Rigidly and immovably fastened to the framework is a third pen (*h*) which draws a straight line on the kymograph roll to serve as a guide line from which all calculations are made.

The pens rest lightly on paper passing through the kymograph (*i*), and trace the above-mentioned simultaneous curves so that at any instant during a cycle, the distance between the pens is convertible to load and the tracing of the right-hand pen (*g*) permits the calculation of percent elongation of the cord. As a cord is taken through successive cycles, a permanent nonrecoverable stretch occurs, which must be taken

up to keep the pens on the paper while maintaining the selected load range. This is accomplished by an arrangement beyond the right-hand end of the oven (*o*). The right tie extends from the cord through a connector to a ring which slips around the shaft of a movable brace, the position of which is changed as the cord stretches. From suitable measurements on the tie at each end the length of the cord can be calculated.

The apparatus at each end of the oven is mounted on a rigid frame so that the observed motion of the elongation pen accurately represents the stretch in the cord rather than any flexibility or relative motion in the system. The precision of this arrangement was tested by placing a tempered steel wire of B. & S. No. 30 gauge in the position to be occupied by the cord and its ties. The load cycle was applied to the wire and the elongation recorded was found to be closely comparable with that calculated for a steel wire by known values of Young's modulus for steel.

PROCEDURE

The cord, of approximately 100-cm length, is taken through the cycles at a rate of 1 cycle per second. Tracings are made at designated cycle intervals as these are indicated by an automatic counter attached to the apparatus. Temperatures in the tubular oven are controlled and measured in the manner previously described.[1]

The moisture contents of the cords, in percent of their dry weights (frequently referred to as moisture "regains") are found by actual determination of the moisture after each run is completed. The standard procedure for obtaining moisture and oven dry weight is followed throughout.[9] In certain experiments the cords to which the cyclic loads had been applied were later tested for their stress-strain characteristics. Since in such cases it was impossible to determine the moisture directly, the moisture content of another length of the same cord simultaneously contained in the tube was taken as the content of the loaded cord. Check determinations in which the moisture contents of both loaded and dummy cords were determined agreed within the experimental error of an individual measurement.

[9] A.S.T.M. Standards, Part III, D269-42T, p. 1952 (1944).

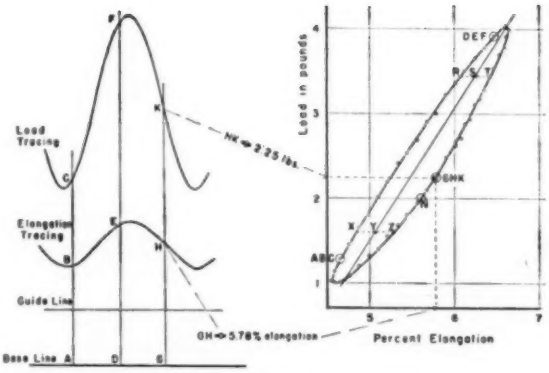

FIG. 2. Method of calculating hysteresis loop on the right from the kymograph tracings on the left. For complete details of this calculation see text.

The moisture content of the cord in the test oven is controlled by preconditioning the cord and by passing conditioned air through the tube while the run is in progress. The apparatus is in a room in which the humidity is controlled to ± 3 percent and cord moisture over the middle of the range is changed by merely adjusting the room humidity. For the dry runs the cord is first dried in a vacuum before insertion into the tubular oven and then kept surrounded by dry air during the run. When it is desired to keep the cord with a definite moisture content at high temperatures the air passed through the tube is conditioned by first being bubbled through water in a constant temperature bath.

At the start of a run, the cord is introduced into the oven, a 4-ounce weight attached, and measurements taken to establish the cord length which is used as a basis of all percent elongation calculations. After all necessary connections and preliminary adjustments are made, the run is started but may be interrupted briefly at any time to make further adjustments as the cord grows in length.

Figure 2 depicts schematically the method of plotting the hysteresis loop from the kymograph tracings. The base line is set parallel to and at a distance above or below the guide line as dictated by the observed length of the cord at a particular cycle. Two transparent right triangles (similar to those used in drafting work) are used to facilitate the measurements. The perpendicular side of the one is ruled in millimeters and that of the other in pound-equivalent distances. By fitting the base of the millimeter triangle against

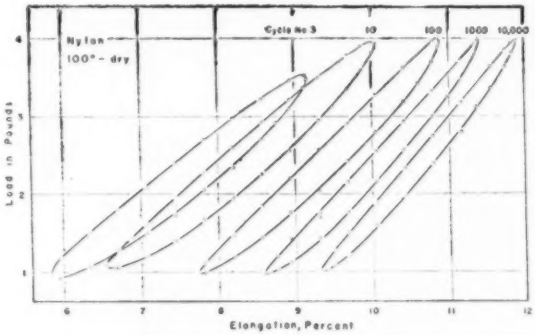

FIG. 3. Typical mechanical hysteresis loops at various cycle numbers for dry Nylon at 100°C.

the base line the distance to the elongation tracing (AB) can be read directly in millimeters and converted into percent elongation. The ruled side of the load triangle is moved along against the millimeter scale to convert the distance between the tracings (BC) to load in pounds. These simultaneous readings are plotted on coordinate paper as shown—thus values from AB and BC are used to plot point ABC, values from DE and EF to plot point DEF, etc. Sufficient pairs of readings are made to permit drawing of the hysteresis loop.

From the hysteresis loop elastic characteristics of the cord are obtained as follows.

Hysteresis

The loops are integrated graphically with a planimeter and converted into inch-pound values per 100 inches of length. Hysteresis may be expressed in any energy units as, for example, calories per centimeter length of cord or calories per gram of cord.

$$1 \text{ inch-pound}/100 \text{ inches} = 1.06\times10^{-4} \text{ calorie/centimeter}.$$

$$\text{Calories/gram} = \frac{(\text{calories/centimeter})\times10^{6}}{\text{grex}}.$$

In the results reported below the hysteresis is expressed in inch-pound per 100 inches because this value is obtained directly from the plots of load in pounds *vs.* percent elongation.

Elastic Modulus

At each of two load levels, arbitrarily chosen, of 0.6 pound from top and bottom of each loop (RT and XZ, respectively), the average of the percent elongation readings is marked (S and Y) and a line drawn through these two points to establish the slope of the loop. Elastic modulus is determined as dynes per square centimeter from the formula derived from Young's modulus:

$$M = t\times\frac{100}{3.1416g^2/4}\times6.895\times10^4,$$

in which t is the tangent value of line SY, g is the gauge or diameter of the cord in inches, and 6.895×10^4 is the factor converting pounds per square inch into dynes per square centimeter.

Percent Elongation

The percent elongation at 2 pounds during the unloading portion of the cycle is arbitrarily chosen to represent the elongation of the cord for that cycle. This corresponds to point N in Fig. 2.

Rate of Growth

This is defined as the increase in cord elongation produced by a tenfold increase in cycle number as, for example, the difference between the elongations for the tenth and for the hundredth cycle.

Hysteresis loops were plotted at selected intervals during the run; i.e., at cycle numbers 3, 6, 10, 30, 100, 300, etc., for 10,000 cycles. Such a series of loops for dry Nylon at 100°C is shown in Fig. 3. Secondary graphs were made of hysteresis, elastic modulus, and elongation, each *vs.* cycle number on a logarithmic scale for convenience in graphing. These are shown in the results described below.

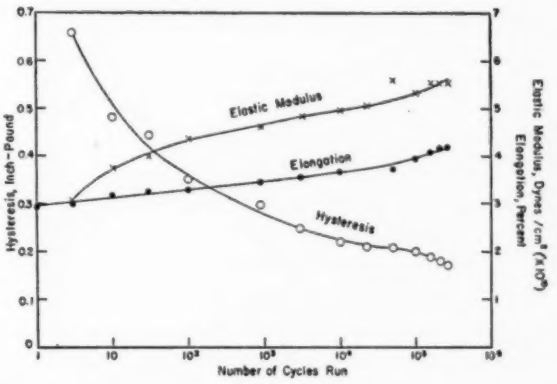

FIG. 4. Hysteresis, elastic modulus, and elongation *vs.* cycle number to point of rupture for dry experimental cotton cord-2 at 145°C.

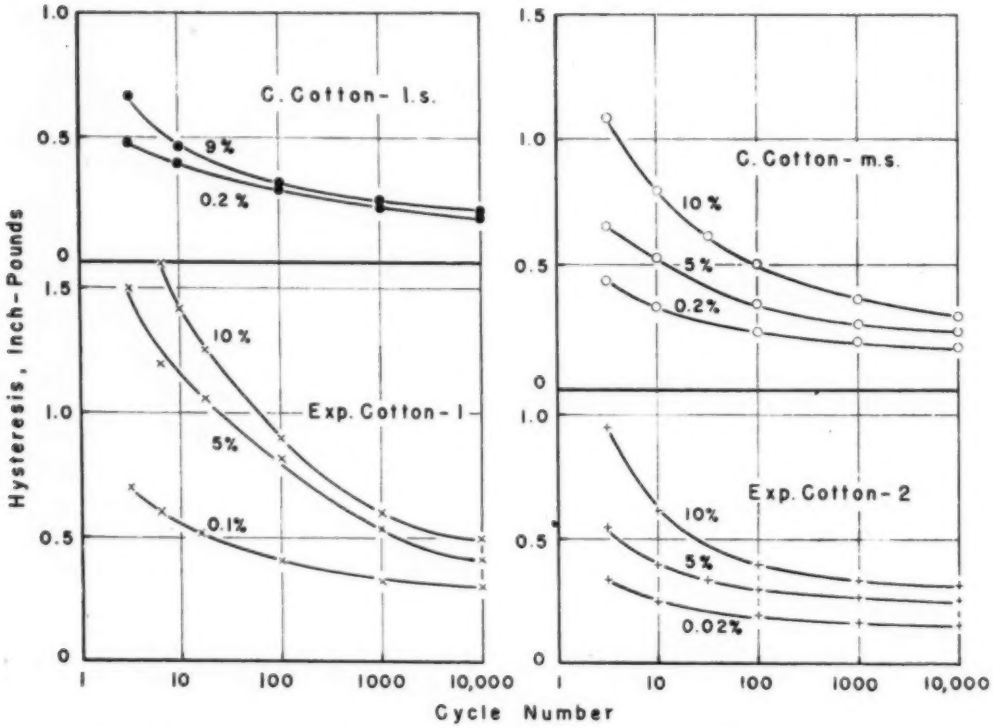

FIG. 5. Hysteresis vs. cycle number at constant moisture and 25°C—cotton cords.

EXPERIMENTAL RESULTS

Seven different cords were chosen for this study: (1) 210/4/2 Nylon; (2) 1100/2 viscose rayon; (3) 2200/2 viscous rayon; (4) 18/4/3 medium stretch cotton; (5) 16/4/3 low stretch cotton; (6) 17/4/3 unstretched experimental cotton; and (7) 17/4/3 stretched experimental cotton. Some physical properties of these cords under A.S.T.M. standard testing conditions[10] are shown in Table I. The two rayon cords have

TABLE I. Some physical properties of tire cords used in study of elastic properties.

Cord designation			Nylon	Rayon		Cotton			
						Commercial		Experimental	
				1	2	Medium stretch	Low stretch	1	2
Gauge			0.016	0.023	0.033	0.031	0.032	0.035	0.031
Construction[a]			210/4/2	1100/2	2200/3	18/4/3	16/4/3	17/4/3	17/4/3
Grex (dry)[b]			1986	2444	5366	4342	5064	4716	4446
Standard conditions	Breaking load	In lb.	25.2	14.2	28.3	20.0	26.7	23.4	24.7
		In g/grex	5.76	2.64	2.39	2.09	2.39	2.25	2.52
	Percent elongation	At 10 lb.	12.4	9.8	6.1	7.0	5.0	14.7	6.2
		At break	22.0	16.6	17.5	12.3	11.2	21.8	11.8
	Moisture, % of dry weight		4	14	14	8	8	8	8
Bone dry	Breaking load	In lb.	25.4	18.0	34.3	17.7	24.8	18.5	22.0
		In g/grex	5.80	3.34	2.90	1.85	2.22	1.78	2.24
	Percent elongation	At 10 lb.	11.8	4.5	3.3	6.0	5.2	10.4	6.0
		At break	22.0	10.8	12.2	8.7	9.1	15.4	9.4

[a] The first figure represents size of single yarns (denier for Nylon and rayon and yarn number for cotton); the second figure represents number of single yarns per ply; and the third figure represents number of plies in the cord.
[b] The grex unit is defined as the weight in grams of 10,000 meters of cord. See A. G. Scroggie, Rayon Text. Mo. 25. 45 (1944).

[10] A.S.T.M. Standards, Part III, D179-42, p. 811 (1944).

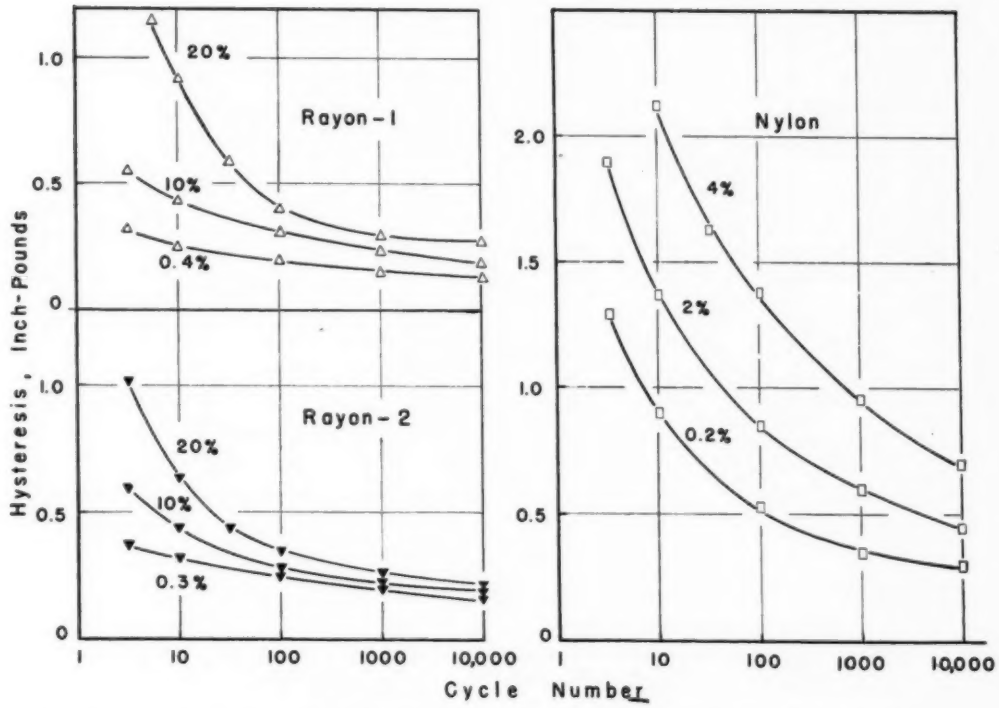

FIG. 6. Hysteresis *vs.* cycle number at constant moisture and 25°C—rayon and Nylon cords.

weight and strength ratios of approximately 2 :1- and comparisons of these two cords when tested at equal load ranges may be expected to demonstrate to some extent the effect of load. The first two cotton cords are samples of commercial cords which have been used as fabric in regular tires. The last two are experimental cords made in this laboratory as part of the research program on cotton tire cords.

The hysteresis and related properties of a tire cord are functions of many variables such as load range, cycle number, cycle frequency, temperature, and moisture content. In much of this investigation the cyclic tension was kept in the range between 1 to 4 pounds. The cycle frequency was standardized at approximately one cycle per second. Even at this rate 3 hours were required to run off 10,000 cycles. Since it was also desired to investigate the variables of temperature and moisture content, it was necessary to limit the number of cycles run in a routine test to approximately 10,000. Continued operation beyond this point gave little additional information as the test described in Section 1 demonstrated.

It was, furthermore, not practicable to make a large enough number of runs under identical conditions with samples from any one cord to obtain anything like a statistical average. Duplicate and triplicate runs were made on numerous samples; and in most cases the deviations between individual curves of duplicate runs were less than the differences found between any two cords. Thus, the results herein presented demonstrate real dissimilarities between the cords studied, although the accuracy with which these have been determined leaves considerable room for improvement.

1. Effect of Cycle Number

As the tire cord is subjected to alternating loads its elastic properties undergo gradual changes. These changes are illustrated in Fig. 4 in which the hysteresis, elastic modulus, and elongation are plotted *vs.* cycle number (on a logarithmic scale) to the point of failure for experimental cotton cord-2. These curves are typical of those obtained for all cotton, rayon, and Nylon cords tested. In all cases hysteresis decreases whereas elastic modulus and elongation increase with continued cyclic loading.

In the work here reported no study has been

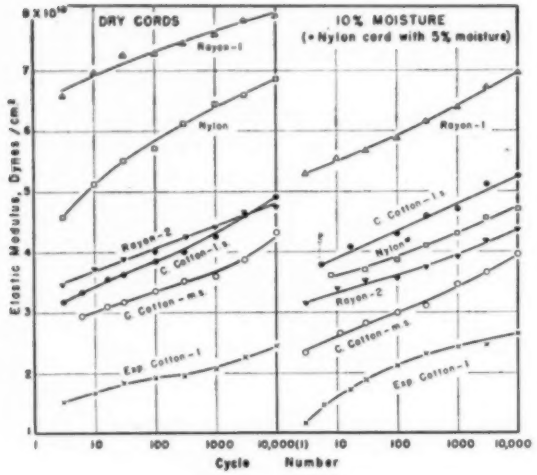

FIG. 7. Elastic modulus *vs.* cycle number at constant moisture and 25°C.

made of cord properties at or immediately prior to rupture. This has not been practicable because of the long time required to break a cord under the rates and magnitudes of cyclic loads imposed by the apparatus used. There seems little doubt, however, that such a study would throw considerable light on the mechanism of fatigue failure of tire cords and other industrial fabrics.

2. Effect of Moisture

Hysteresis at 25°C as a function of cycle number is shown for each tire cord at various moisture contents in Figs. 5 and 6. It is evident that hysteresis in all cases increases with increase in moisture, with much more increase for Nylon than for the other cords. Hysteresis curves for the low stretch commercial cotton cord are almost independent of moisture content—curves obtained with 4, 5, and 8 percent plotted practically on top of those shown. On the basis of comparable moisture contents the rayon hysteresis is less affected by moisture than that for cotton. Any advantage rayon may possess over cotton in this respect, however, is offset somewhat by the greater hygroscopicity of the rayon which is responsible for its higher moisture content under comparable conditions both in the tire and out.[11] After the first hundred cycles the hysteresis of all cotton and rayon cords are of the same order of magnitude with the possible exception of the experimental cotton-1 which is somewhat higher than the others over the whole range.

The effect of moisture on the elastic modulus at 25°C as a function of cycle number is depicted in Fig. 7. As the oscillatory loading treatment progresses the elastic moduli of all cords increase at a fairly uniform rate—approximately 0.4×10^{10} dynes per cm² for each tenfold increase in cycle number. In Fig. 8 the elastic modulus after 10,000 cycles is plotted as a function of moisture. The cottons exhibit different curves from those for the rayons and Nylon in that the modulus is greatest in the vicinity of 4 to 5 percent moisture. One explanation which might be advanced for this phenomenon is that the swelling by water of the less organized cellulose chains in the intermicellar regions results in a better stress distribution—as water is added to the dry state the resistance to deformation and the elastic modulus increases. Continued swelling beyond about 5 percent water content, however, increases the

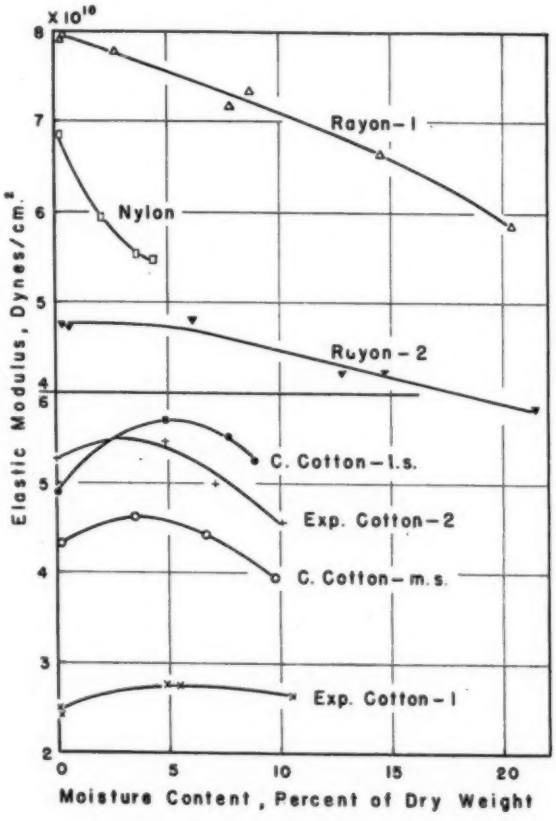

FIG. 8. Elastic modulus *vs.* moisture after 10,000 cycles at 25°C.

[11] H. Wakeham, E. Honold, and H. J. Portas, Ind. Rubber World, **113**, 659 (1946).

distances between chains to the point where the intermolecular forces decrease and less stress is required to produce unit deformation. This latter effect is observed over the whole moisture range for the Nylon and rayon cords.

A comparison of the elastic moduli of the two rayon cords is of interest inasmuch as the 2200/2 rayon is approximately twice the weight and strength of the 1100/2 cord. The heavier cord has a much lower modulus despite the fact that the modulus calculation takes into account the differences in cross-sectional area of the two cords. As was pointed out earlier, the comparison of these two cords with the same applied tension was, in effect, comparable to running one at two different load ranges. The results shown would seem to indicate that for viscose rayon the elastic modulus for reversible deformation is a function of the load range and increases with increasing load over the range studied.

Typical curves of the elongation as a function of imposed load cycle are plotted in Fig. 9 for dry samples of the various cords studied. It is to be noted that these elongations, which are based on the original length of the cord with a 4-ounce tension, are not accurately reproducible because

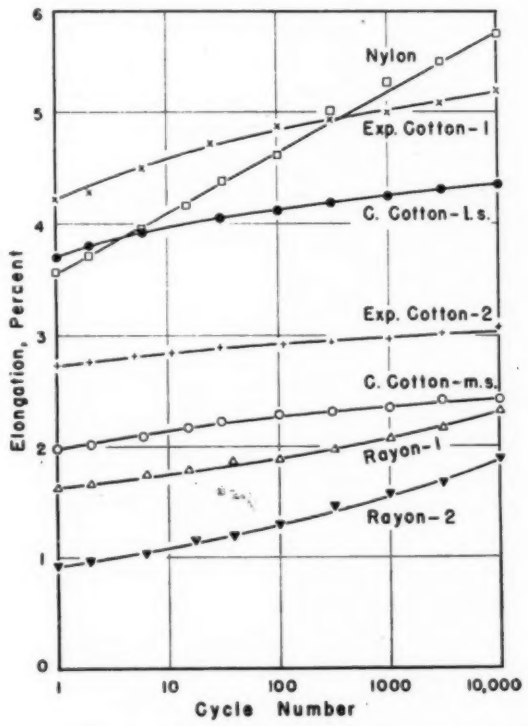

FIG. 9. Elongation *vs.* cycle number for dry cords at 25°C.

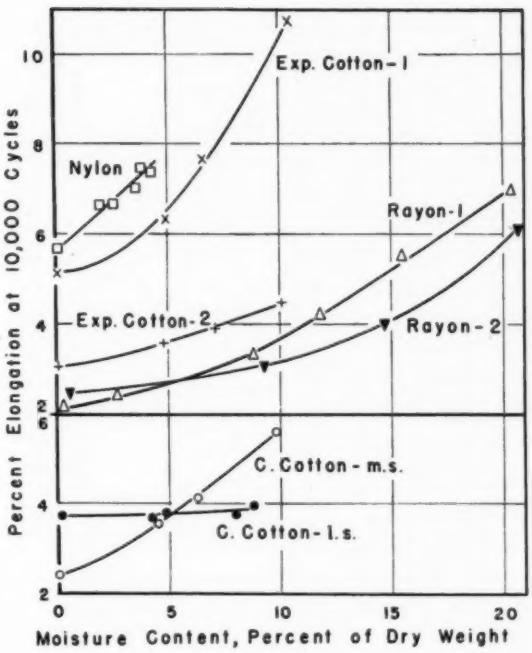

FIG. 10. Total elongation after 10,000 cycles *vs.* moisture at 25°C.

of some unavoidable variations in handling when the cord is inserted into the oven for testing. The slope of the curve, or the rate of growth, is not appreciably affected by this manipulative error and is a significant characteristic of the cord. Slopes of the elongation curves in Fig. 9 are seen to vary considerably for the different cords.

The total elongation observed during the first 10,000 cycles of cyclic loading is a function of moisture content as shown in Fig. 10. All cords exhibit an increase in elongation with increasing moisture. The cottons with a low stretch (Exp. cotton-2 and C. Cotton l.s.) increase much less than the others. In fact, the low stretch commercial cotton does not increase in elongation at all with moisture addition, simulating its hysteresis behavior mentioned in connection with Fig. 5.

In Fig. 11 are depicted the rates of growth as functions of moisture content. The rayons and high stretch experimental cotton-1 are found to be greatly influenced in their growth rates by moisture. This behavior is in line with the hypothesis that in a fiber with considerable intermicellar space the swelling effect of water decreases the intermolecular forces between the

high polymer chains in these spaces. This allows the material to undergo greater creep and exhibit the progressive growth demonstrated in Figs. 9 and 11. Cotton cords which have been subjected to stretch treatments to reduce their elongations are not only more compact in their cord organizations but also, it is believed, more oriented with respect to the cellulose chains in their intermicellar regions. The intermolecular forces are strong enough to reduce the interference by water molecules. Dillon and Prettyman[12] thus found that tenacity and ultimate stretch in a tensile test of low-stretch cotton cords at room temperature are practically independent of moisture contents, whereas considerable effect was observed for the medium-stretch cotton cord.

It is of interest to compare the curves for Nylon in Figs. 10 and 11. The rate of growth in Fig. 11 is independent of moisture; yet, according to Fig. 10, the total elongation observed after 10,000 cycles increases appreciably with moisture increase. Apparently the initial stretch during the first cycle is a function of moisture, but the creep factor with continued loadings is not. This is in agreement with Leaderman's[13] findings on the effect of humidity on creep of Nylon with a static load. The initial deformation observed was considerably greater at the higher humidity than at the lower humidity, but the slopes of the curves at various humidities for deformation *vs.* log time are almost identical.

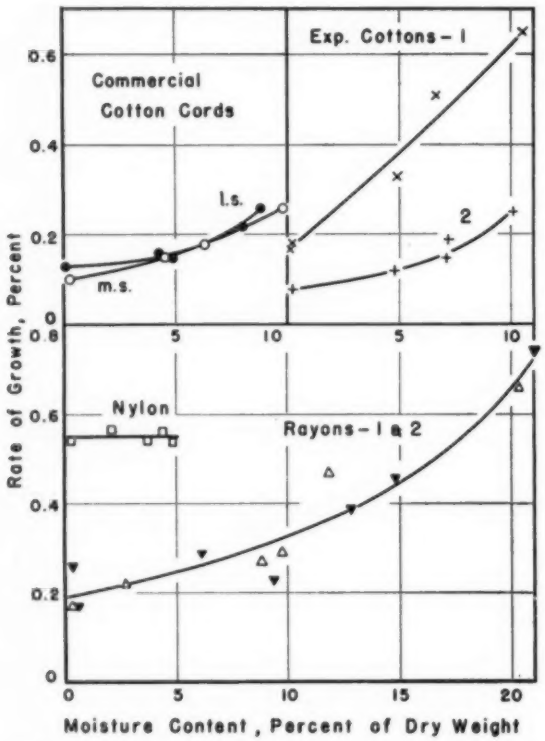

FIG. 11. Rate of growth *vs.* moisture for cords at 25°C.

[12] J. H. Dillon and I. B. Prettyman, J. App. Phys. 16, 159 (1945).

3. Effect of Temperature

The effect of increasing temperature on the elastic properties of the tire cords herein described is, in general, the same as that of increasing moisture content. The magnitude of the effect due to temperature is, however, somewhat smaller than that of moisture over the ranges commonly encountered.

Curves of hysteresis *vs.* cycle number at temperatures of 25°, 65°, and 145°C are plotted for the dry tire cords in Figs. 12 and 13. Measurements were also made at 105° but the curves for these were omitted for the sake of simplicity in the figures—they were, within experimental error, all between those for 65° and 145°C. It is to be noted that the scale of ordinates in Figs. 12 and 13 is considerably magnified over that shown in Figs. 5 and 6. Except in the Nylon tire cord, the temperature effect on the hysteresis curves is actually a small one, and for the dry cotton cords almost negligible, especially after the first ten thousand cycles.

One characteristic of the rayon cord which is indicated by Fig. 13 deserves particular attention. The 65° hysteresis curves of the rayon cords are lower than those for either 25° or 145°, and are also lower than those for 105°C. In fact, the 105° curves were found to be almost superimposed on those for 25° and, therefore, were not plotted. This result indicates that with increasing temperature on the dry rayon cord the hysteresis first decreases somewhat before rising. Whether or not this phenomenon persists much beyond the ten thousand cycle point is not indicated by the data.

The effects of temperature on the elastic modulus are illustrated in Fig. 14. A small or negligible increase in elastic modulus is shown for the commercial cotton cords in going from 25° to 145°. The rayon modulus, on the other

[13] H. Leaderman, *Elastic and Creep Properties of Filamentous Materials and Other High Polymers* (The Textile Foundation, Washington, D. C., 1943) p. 231.

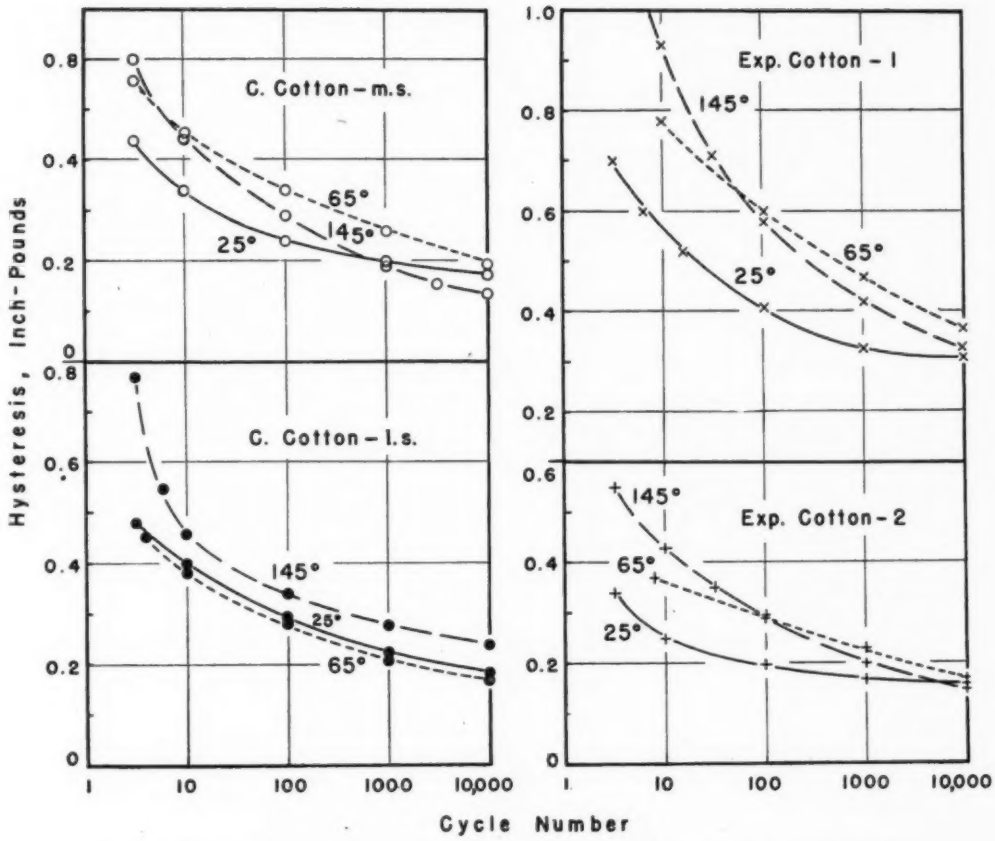

FIG. 12. Hysteresis *vs.* cycle number at constant temperature for dry cotton cords.

hand, drops considerably over the same temperature range, and the Nylon even more so. This greater reversible elongation which the rayon and Nylon cords show at elevated temperatures may be of some advantage in the tire under road conditions where considerable flexing of the tire is required.

In Fig. 15 is plotted the rate of cord growth, or the elongation per tenfold increase in cycle number, *vs.* temperature for all seven cords in a dry condition. The cotton cords have low growth rates which increase more or less regularly with temperature; the growths of the rayon and Nylon are high to begin with and increase more rapidly with higher temperatures. These results are in keeping with the known greater growth of rayon and Nylon tires.

4. Combined Effect of Temperature and Moisture Content

After investigating the effects of the moisture content and temperature variables individually, a thorough survey of the combined effect of these variables did not seem necessary. Since for a given cord increase in either temperature or moisture generally produced similar changes in the elastic properties studied, it seemed logical to expect that increasing both factors simultaneously would merely result in a greater change.

The results shown in Fig. 16 on the medium stretch commercial cotton and the rayon-1 cords justify such an expectation. For the cotton cord, going from 25° and dry cord either to 25° and 3 percent moisture or to 100° and dry cord produces almost identical changes in elastic properties; similarly for the rayon a change either to 25° and 6 percent or to 100° and dry cord results in the same effect. Combining the temperature and moisture increases produces the new curves shown.

In terms of the intermolecular forces between the high polymer chains in the intermicellar

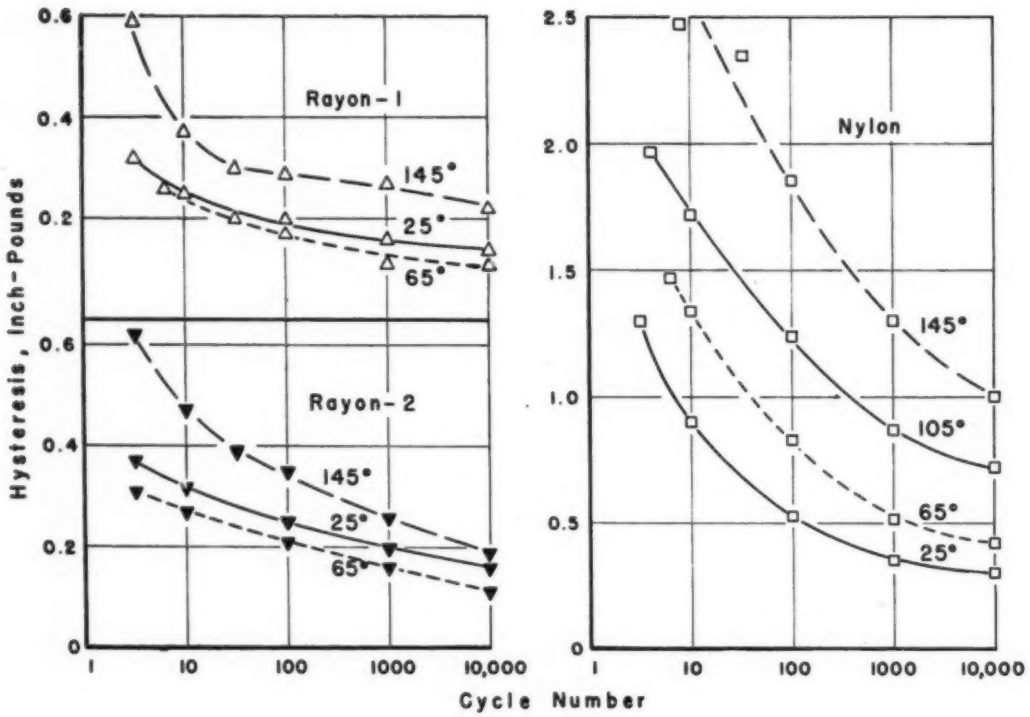

FIG. 13. Hysteresis *vs.* cycle number at constant temperature for dry rayon and Nylon cords.

spaces of the cellulose fiber, the similarity in elastic behavior produced by high temperature and high moisture content is quite reasonable. The explanation has already been advanced that the addition of water molecules to the regions of unoriented chains decreases the intermolecular forces existing between the chains. An increase in temperature would likewise be expected to decrease the same forces and result in greater elongation and growth, and lower elastic modulus.

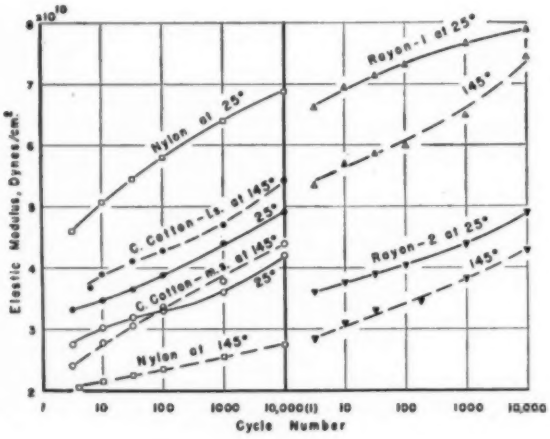

FIG. 14. Elastic modulus *vs.* cycle number at constant temperature.

5. Effect of Load

The results so far reported have all been for cyclic loads over the same range of 1–4 pounds regardless of the cord being tested. It seemed reasonable to expect that the elastic properties of a cord should vary somewhat with the load range chosen for the cycle. An experimental exploration of this effect was possible with the present apparatus using the rayon-1 cord. The load range was reduced to approximately 1.6 pounds (instead of 3 pounds) and runs were made at five mean loads varying between 1.3 and 4.6 pounds. Elastic properties after 1000 cycles *vs.* the mean load are plotted in Fig. 17. It is to be noted from this figure that at low mean loads the hysteresis of the cord rises appreciably to higher values. This result is of practical interest since the average tensions on individual cords in the tire are thought to be fairly low.

In view of this effect of load on the elastic properties of a tire cord, it appeared worth while to make a comparison of these properties when

the load cycle is on a comparable basis—for example, over the same range in grams per grex for each cord. The range 0.1 to 0.4 gram per grex was chosen and runs were made on all cords in the dry condition at 25°C. The values obtained after 1000 cycles, shown in Table II, demonstrate that the properties of these cords when compared on this basis vary widely not only when cords of different types are considered but even when cords of the same group, i.e., cotton, are compared.

6. Effect of Cyclic Loading on the Stress-Strain Curves

In commercial testing much importance as a quality index is attached to the tenacity and elongation of a tire cord as measured by a conventional testing machine. Cords to which the cyclic loading treatment had been applied for 10,000 cycles were tested for their stress-strain curves in such a testing machine and the curves compared with similar ones for untreated samples of the same cord. These are shown in Fig. 18. Since it was necessary to condition all cords to comparable moisture levels before testing, a tension of 0.5 pound was applied to the cord during the conditioning period in order to prevent undue relaxation during this time. Thus, in Fig. 18 there are shown for each cord the stress-strain curves for (1) the conditioned cord directly from the spool; (2) the conditioned cord to which a tension of 0.5 pound had been applied during conditioning; and (3) the conditioned cord which had been subjected to cyclic loading and to which a 0.5-pound load had been applied during conditioning. The resulting curves demonstrate that the cyclic loading process shifts the stress-strain curves to lower strain or elongation values.

DISCUSSION

In the foregoing experiments the hysteresis, elastic modulus, elongation, and rate of growth of several tire cords have been compared under cyclic loads similar to those applied in certain fatigue tests. It has been found that these cord properties vary with cycle number, moisture content, temperature, and load. It is unfortunate that the apparatus used in these experiments does not also permit investigation at higher rates of cyclic loading, as this is very probably an additional factor influencing cord properties. Such a study must be left for future investigations.

The most significant of the variables investigated appears to be the moisture content of the tire cord. The properties of all types of cords measured are affected to a greater or less degree by this factor, probably because the polymeric structure of the fibers is influenced by the added water. Some of the moisture may be thought of as entering into the intermicellar spaces and finding places between the cellulose chains in these regions. There the intermolecular forces of the water molecules are revealed as a viscous drag, increasing the hysteresis of the fiber. The water molecules, furthermore, may decrease somewhat the cohesion between chains permitting greater elastic stretch when a load is applied. Though such an explanation may not be the correct one, it emphasizes the fundamental influence which moisture exerts on tire cord properties and the extent to which moisture should be considered in problems of fabric design and utilization.

It seems reasonable to presume that the fatigue process which the cord undergoes in a tire, if at

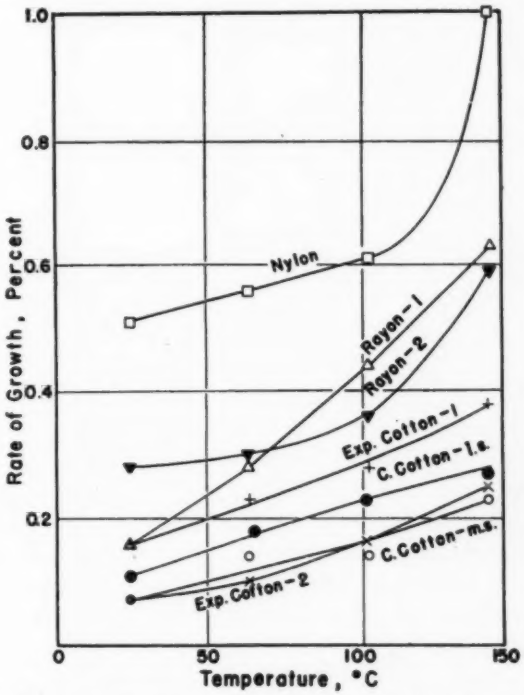

FIG. 15. Rate of growth *vs.* temperature for dry cords.

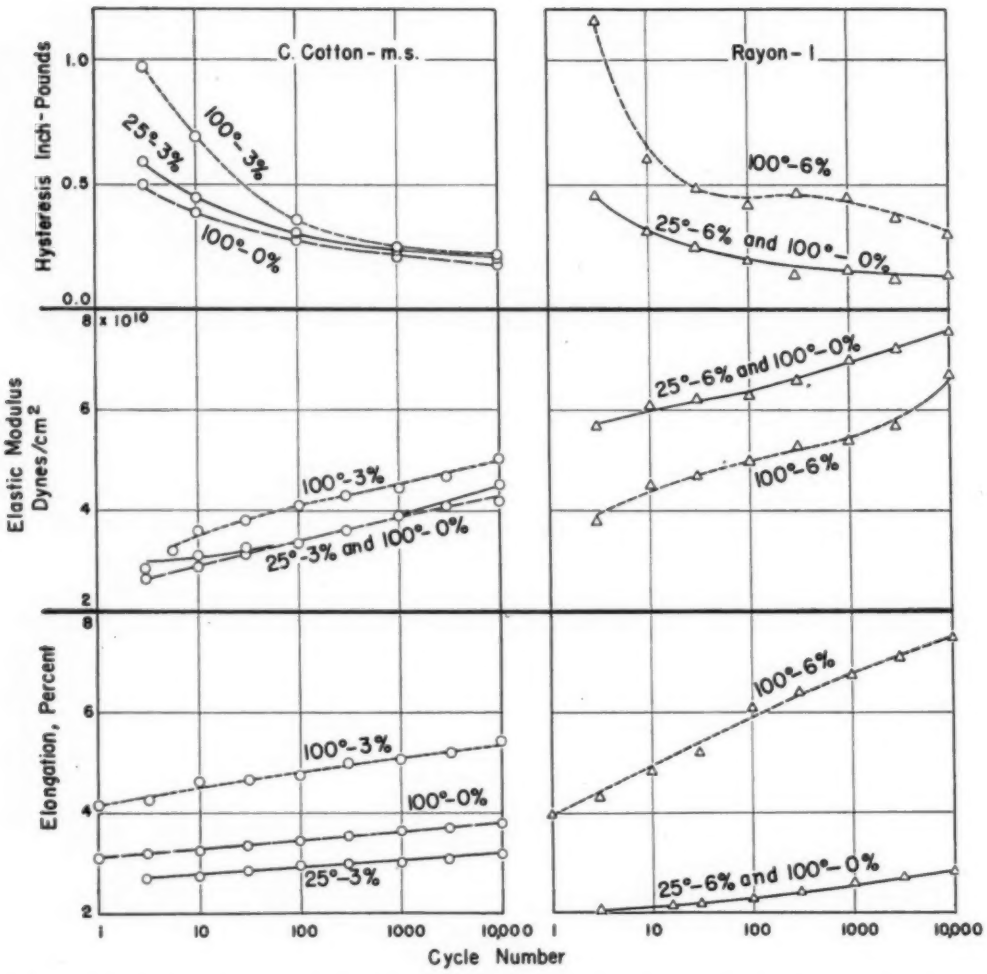

FIG. 16. Effect of temperature and moisture combined. Hysteresis, elastic modulus, and elongation *vs.* cycle number for a cotton and a rayon tire cord.

all similar to that involved in these experiments, is slower than that followed in an accelerated laboratory fatigue test. Certainly the cord in the tire must go through many more load cycles than the few hundred thousand required to produce failure in the laboratory. This difference is probably associated with the fact the cord in the tire is surrounded by rubber. The rubber restricts the motion and deterioration of mechanical properties; and this restricting effect is absent in the cord tested in the laboratory.

How significant hysteresis and elastic modulus of tire cords are in tire performance is, therefore, a problem difficult to evaluate. It seems certain that hysteresis energy of the cord contributes to heat build-up in the tire. The authors in another investigation, for example, have demonstrated

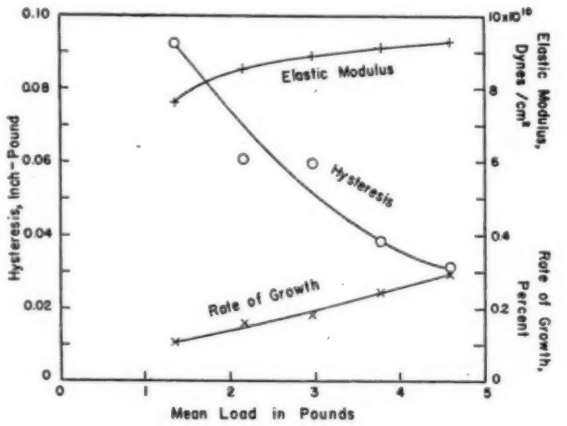

FIG. 17. Effect of load. Hysteresis, elastic modulus, and rate of growth *vs.* mean load for dry rayon-1 at 25°C after 1000 cycles had been run. A load range of 1.6 pounds was maintained for each mean load plotted.

TABLE II. Comparison of elastic properties of tire cords after 1000 cycles (25°C, dry cords, 0.1 to 0.4 g/grex).

Cord	Grex (dry)	Elastic modulus dynes/cm²	Growth rate at 0.2 g/grex	Hysteresis Inch-lb. per 100 inches	Hysteresis Calories per gram
Nylon	1986	6.00×10^{10}	0.247%	0.098	5.25×10^{-3}
Rayon-1	2444	7.66	0.105	0.072	3.10
Rayon-2	5366	4.60	0.215	0.258	5.10
Com. Cotton (m.s.)	4342	3.56	0.073	0.207	5.07
Com. Cotton (l.s.)	5064	5.16	0.130	0.278	5.83
Exp. Cotton-1	4716	2.07	0.170	0.356	8.01
Exp. Cotton-2	4446	4.37	0.086	0.169	4.05

that the torsional hysteresis of tire sections containing cord are higher than the same sections in which the cord structure has been destroyed.[14] But tire heat build-up is determined by so many additional factors involved in tire structure and rubber composition that the part contributed by the cord can only be estimated. A 7.00–20 truck tire, weighing approximately 65 pounds, contains about 12 pounds of cord. Assuming that the average stress cycle of the cord is such that the hysteresis energy loss is approximately 5×10^{-3} cal. per gram of cord (Table II), one may estimate that the fabric produces around 27 cal. of heat per revolution of the tire. At 500 r.p.m., or approximately 50 miles per hour, the cord is generating about 13,500 cal. of heat each minute. Since such a tire has a heat capacity of about 10,000 cal. per degree C, the heat from the cord is sufficient to produce, under adiabatic conditions, a temperature rise of about 1.35°C per minute. This estimate indicates without much question that the elastic hysteresis of the cord fabric makes an appreciable contribution to the high temperatures observed in tires in service.

One might deduce from a consideration of tire design and performance that a low elastic modulus in the tire cord would be desirable. Greater reversible stretch in the cord should produce a tire more homogeneous in elastic properties, with fewer ply and tread separations and increased bruise resistance. Here again, however, it is only possible to surmise a correlation between laboratory testing and tire performance without making tests with actual tires.

[14] H. Wakeham and E. Honold, Ind. Rubber World **113**, 377 (1945).

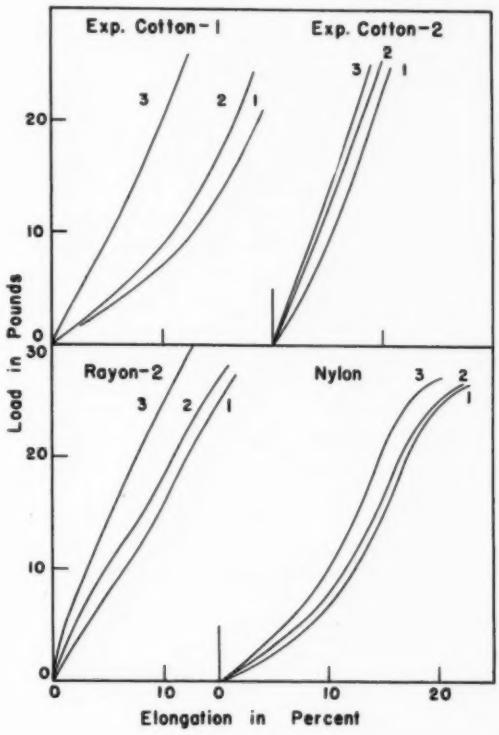

FIG. 18. Stress-strain curves for (1) moisture conditioned cord, (2) cord conditioned with a tension of 0.5 pound, and (3) cord subjected to cyclic loading for 10,000 cycles and conditioned with a tension of 0.5 pound.

ACKNOWLEDGMENT

The authors are grateful to many members of the Southern Regional Research Laboratory staff for their interest and cooperation in this work, and especially to Jacquelyn Souderes and Gene Hassinger for their assistance with many of the calculations.

Letters to the Editor

On the "Power Function"

FIDEL ALSINA FUERTES
Agrupacion Estudiantes de Fisica, Instituto de Fisica, La Plata, Argentina
December 12, 1945

IN a recent note, D. A. Wells[1] sets up a "power function" through which the generalized Lagrangian forces are determined for a wide variety of forces acting on a holonomic system, by the relation

$$Q_k = \partial P / \partial \dot{q}_k$$

(P = power function; $\dot{q}_k$ = time derivative of the generalized coordinate q_k).

When the forces are proportional to the speed of the particles acted upon, P reduces to the dissipative function considered by the late Lord Rayleigh.[2] The purpose of this letter is to show to what extent the P-function widens the field of allowable forces.

Let us consider, for the present, a single particle. For such a simple system, the P-function reads

$$P = \int \sum_{i=1}^{3} F_i d\dot{x}_i \tag{1}$$

(F_i = cartesian component along the i-axis of the force acting on the particle; $\dot{x}_i$ = time-derivative of the i-Cartesian coordinate).

Integration limits, not shown in (1), must be chosen such that

$$\partial P / \partial \dot{x}_i = F_i. \tag{2}$$

P is, according to (1), a function of both upper and lower limits, and perhaps of the integration path. One of the limits is taken constant to obtain (2), and the independence of the integration path is assured when the "conditions of integrability"

$$\partial F_i / \partial \dot{x}_j = \partial F_j / \partial \dot{x}_i \tag{3}$$

are fulfilled. When $F = av^n$, Eq. (3) holds (Wells). When F_i are proportional to $\dot{x}_i$ (Rayleigh), Eq. (3) holds automatically, since both sides are zero.

Let it be now F a force depending on the speed v of the particle in an arbitrary way

$$F = f(v); \tag{4}$$

$f(v)$ may contain, further, coordinates and time. If the direction of F coincides with that of v, it can be easily shown that Eq. (3) holds for any $f(v)$. We have

$$F_i = f(v)\frac{dx_i}{ds} = f(v)\frac{\dot{x}_i}{v} \tag{5}$$

and, taking into account $v^2 = \Sigma \dot{x}_i^2$,

$$\frac{\partial F_i}{\partial \dot{x}_j} = \frac{d}{dv}\left(\frac{f(v)}{v}\right)\frac{\dot{x}_j \dot{x}_i}{v} \tag{6}$$

a relation asserting the validity of (3).

Thus, for single-particle systems, P-functions can be obtained under much more general conditions than allowed by "dissipative functions." In spite of this, it is interesting to remark that anisotropic forces cannot enter in consideration, lest (6) ceases to be symmetrical in i, j. The only case of allowable anisotropy appears when the forces are proportional to the speed, i.e., Rayleigh's case.[3]

Let us proceed now to systems formed by p particles. In order to set up the P-function for the system, we first obtain the $P\nu$-function for each of the p particles and then add up

$$P = \sum_{\nu=1}^{p} P\nu \quad (\nu = 1, 2 \cdots p). \tag{7}$$

The existence of P is restricted by same conditions as above, namely: *forces should be isotropic, directed along the tangents to the trajectories of the particles acted upon, and depending on the speeds, coordinates, and time in an arbitrary way.*

When considering many-particle systems, one is tempted to put simply a new sum sign in (1). By doing so, Eq. (3) would appear

$$\frac{\partial F_{\nu i}}{\partial \dot{x}_{\mu j}} = \frac{\partial F_{\mu j}}{\partial \dot{x}_{\nu i}}$$

and the functions (4) *should be taken independent of the individual particle* in order to satisfy (6). This is a drastic restriction, as it cuts off even simple applications like Example 1 in Wells' article. Besides, it is an unnecessary limitation, since definition (7) does not differ from Wells'. In fact, the expression for P remains

$$P = \sum_{\nu=1}^{p} \int \sum_{i=1}^{3} F_{\nu i} d\dot{x}_{\nu i} \tag{8}$$

with the integrability conditions

$$\frac{\partial F_{\nu i}}{\partial \dot{x}_{\nu j}} = \frac{\partial F_{\nu j}}{\partial \dot{x}_{\nu i}}. \tag{9}$$

It is easy now to find a simpler expression for P. Let us put, according to (4)

$$F_\nu = f_\nu(V_\nu);$$

the i-component of the force acting on the ν-particle reads

$$F_{\nu i} = f_\nu(v_\nu)\frac{\dot{x}_{\nu i}}{v_\nu} \tag{10}$$

and, using (8)

$$P = \sum_{\nu=1}^{p} \int f_\nu(v_\nu)\frac{1}{v_\nu}\left[\sum_{i=1}^{3} \dot{x}_{\nu i} d\dot{x}_{\nu i}\right]. \tag{11}$$

The bracket can be written

$$\sum_{i=1}^{3} \dot{x}_\nu d\dot{x}_{\nu i} = \tfrac{1}{2} d \sum_{i=1}^{3} \dot{x}_{\nu i}^2 = \tfrac{1}{2} dv_\nu^2 = v_\nu dv_\nu \tag{12}$$

and finally

$$P = \sum_{\nu=1}^{p} \int f_\nu(v_\nu) dv_\nu. \tag{13}$$

This expression is obviously independent of the frame of coordinates. The rest of the equations can easily be rewritten in generalized coordinates, if desired.

Since the power-function has been specified, and used, only in relation to $\dot{x}_i$'s (or the $\dot{q}_k$'s), it is evident that it is determined for each system except for an additive arbitrary function of coordinates and/or time

$$P = \sum_{\nu=1}^{p} \int f_\nu(v_\nu) dv_\nu + \varphi(x_i, t).$$

[1] D. A. Wells, J. App. Phys. **16**, 535 (1945).
[2] Lord Rayleigh, in *Collected Papers* (1899), Vol. 1, p. 176.
[3] E. T. Whittaker, *Analytical Dynamics* (1937), p. 231.